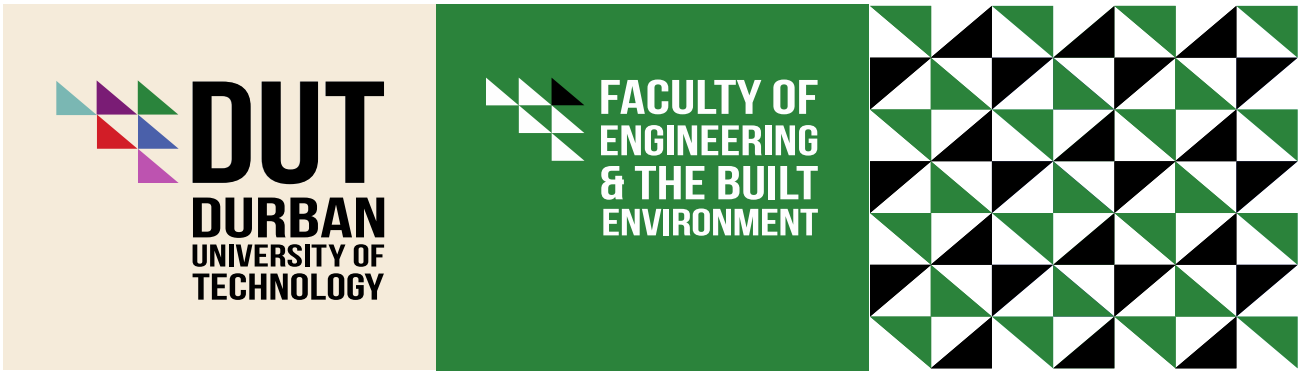

DECOMPOSITION OF METHANE INTO CARBON AND HYDROGEN OVER Ni-Li/CaO CATALYST

A thesis submitted in fulfilment of the academic requirements for the award of the degree of;

MASTER OF ENGINEERING

Durban University of Technology

Faculty of Engineering and the Built Environment,

Department of Chemical Engineering

Ronald Wafula Musamali

November 2017

Supervisor: Dr. Yusuf Isa

Declaration

I, Ronald Wafula Musamali, do hereby declare that this project titled *Catalytic decomposition of methane into carbon and hydrogen over Ni-Li/CaO*, is my own work and that, to the best of my knowledge and belief, it contains no material previously published or written by another person nor material to which substantial extent has been accepted for the award of any degree of any university or institution of higher learning except where due acknowledgement has been made in this text.

Ronald Wafula Musamali

…… ……

Student **Signature**

Dr. Yusuf Isa

…… ……

Supervisor **Signature**

Abstract

Overdependence on fossil-based fuels and their effect on environment is a global concern by energy stake holders. Bulk of present day hydrogen comes from gasification of coal, steam reforming and partial oxidation of hydrocarbons. Steam reforming accounts for over 50% of world hydrogen production despite producing carbonaceous gases which are harmful to the environment and poisonous to both; proton exchange fuel cells and alkaline fuel cells. Natural gas is a preferred feed for hydrogen production, because it is abundantly available on earth. Catalytic decomposition of ammonia can produce clean hydrogen but ammonia itself is an air pollutant. Catalytic decomposition of methane into carbon and hydrogen is an attractive option to producing clean hydrogen because its products are carbon and hydrogen.

In this work, five different catalysts comprising of varying quantities of nickel and lithium, supported on calcium oxide were synthesized by incipient wetness impregnation method and designated according to weight % as; 30%Ni/CaO, 37.5%Ni-12.5%Li/CaO, 25.0%Ni-25.0%Li/CaO, 12.5%Ni-37.5%Li/CaO and 50%Li/CaO. The synthesized catalysts were characterized by (XRD, SEM, BET and TEM) and tested for methane decomposition.

From the XRD patterns of the synthesized catalysts, distinct crystalline phases of CaO and NiO were positively identified in 50%Ni/CaO according to their reference JCPDS files. Introduction of Lithium hydroxides improved the crystalline structure of the Ni/CaO catalyst. SEM analyses of the catalyst material using Image-J software confirmed that all catalyst materials were nanoparticles ranging from 3.09-6.56nm. BET results confirmed that, all the catalysts are mesoporous with pore sizes ranging from 20.1nm to 45.3nm. Introduction of LiOH to Ni/CaO generates mesoporous structures by destructing the lattices of the CaO structure during the formation of Ni-Li/CaO species.

Particle size distribution in TEM analyses revealed that, a higher nickel loading in the catalyst favours the formation of carbon nanotubes while higher lithium hydroxide loading favours the formation of carbon fibres (CF). Low yield of carbon fibres from methane decomposition on unsupported Ni catalyst in 50%Ni/CaO was attributed to the presence of large Ni particles with low index planes which were incapable of dissociating the unreactive methane molecule.

The aim of this work was to synthesize a catalyst for use in decomposition of methane into carbon and hydrogen, that addresses drawbacks of traditional solid metal catalysts such as sintering and coking. From the experimental results, 37.5%Ni-12.5%Li/CaO catalyst recorded 65.7% methane conversion and 38.3%hydrogen yield while 50%Ni/CaO recorded the lowest methane conversion of 60.2% and a hydrogen yield of 35.7% at 650℃. Outstanding performance of the 37.5%Ni-12.5%Li/CaO catalyst is attributed to the incorporation of lithium hydroxide which provided more catalyst active sites and a molten environment for proper dispersion of the nickel metal. The solid 50%Ni/CaO catalyst readily deactivated due to coking unlike the supported molten 37.5%Ni-12.5%Li/CaO catalyst in which methane decomposition reaction took place by both surface reaction and chemisorption.

Dedication.

This study is dedicated to my parents, my dear wife Catherine and my children whom I dearly love.

Acknowledgements

I'm most grateful to my supervisor, Dr. Yusuf Isa for his guidance, encouragement, positive criticism and moral support throughout this project write up and completion.

My thanks are also due to;

- My employer –The Technical University of Kenya, who granted me study leave to carry out my research project at Durban University of Technology.
- Durban University of technology for use of their facilities and financial support in the purchase of chemicals and equipment.
- NRF for financial aid while doing the research project.
- Sinonke Engineering Ltd for fabrication of the custom made stainless steel reactor.

Finally, my heartfelt thanks goes to my fellow chemical engineering postgraduate students (class of 2016) who helped me get orientation to the Durban University of Technology.

Table of contents

List of figures

List of tables

List of abbreviations

AC	Activated Carbon
AFC	Acid fuel cell
B.E.T	Brunauer-Emmett-teller
CB	Carbon Black
CMD	Catalytic decomposition of methane
CNT	Carbon nanotube
DFT	Density function theory
FC	Filamentous Carbon
MCFC	Molten carbonate fuel cell
MWCNT	Multi walled carbon nanotube
PEMFC	Polymer electrolyte membrane fuel cell
PEM	Proton Exchange Membrane
SEM	Scanning electron microscopy
SMR	Steam methane reforming
SWCNT	Single walled carbon nanotube
TEM	Transmission electron microscopy
XRD	X-ray diffraction

List of chemical formulas

Chemical formula	**English name**
C	carbon
CaO	calcium Oxide
$Ca(OH)_2$	calcium hydroxide
CH_4	methane
CO_2	carbon dioxide
CO	carbon monoxide
Co	cobalt
Fe	iron
H_2	hydrogen
H_2O	water
K	potassium
Li	lithium
$LiOH.H_2O$	lithium hydroxide monohydrate
MgO	magnesium oxide
Mo	molybdenum
Ni	nickel
$Ni(NO_3)_2.6H_20$	nickel nitrate hexahydrate
O_2	oxygen

List of symbols

Symbol	Meaning
≥	greater or equal to
≤	less or equal to
W	Weight (g)
T	temperature (℃)
t	time (h)
F	flow rate
$\Delta H°r$	Standard enthalpy of reaction
$\Delta G°$ (T)	Gibbs energy
K_p	equilibrium constant
R_u	gas constant (8.314J/mol).
p_{CH4}	partial pressure of methane
p_{H_2}	partial pressure of hydrogen
θ	theta (angle of diffraction)
nm	nanometer (10^{-9}m)
Å	angstrom (10^{-10}m)

CHAPTER 1. INTRODUCTION

1.1Background and problem statement

1.1.1 Introduction

Hydrogen is a colorless and odorless gas which accounts for 75% of the universe mass. It is widely used as a fuel in fuel cells such as the proton exchange membrane (Elitzur *et al.* 2016). Various methods namely; steam reforming, gasification of coal, reforming of biogas, partial oxidation and water pyrolysis are used to produce hydrogen gas (Luo and Feng 2016). Carbon monoxide and carbon dioxide gases are associated with these hydrogen production methods, hence the need to embrace another method for producing pure hydrogen (Moury *et al.* 2015).

Catalytic decomposition of methane is the preferred method of producing high purity hydrogen which is free form carbonaceous compounds (Keipi *et al.* 2016).These carbonaceous compounds pollute the environment and accounts for 90% of the total global warming system (Rahman and Khondaker 2012). To mitigate CO_2 emission, two methods are employed; sequestration of CO_2 produced by a Steam methane reforming hydrogen plant and thermal catalytic decomposition of methane(Suleman *et al.* 2016)

1.1.2 Methane Decomposition Fundamentals.

The mechanism of methane decomposition starts with dissociative adsorption of methane molecule on the carbon surface (Bayat *et al.* 2016), as described by the following reaction;

$$(CH_4) \rightarrow (CH_3)a + (H)a \quad (1)$$

This is followed by a series of stepwise dissociation reactions leading to elemental carbon and hydrogen:

$$(CH_3)a \rightarrow (CH_2)a + (H)a \quad (2)$$

$$(CH_2)a \rightarrow (CH)a + (H)a \quad (3)$$

$$(CH)a \rightarrow (C)a + (H)a \quad (4)$$

$$n(C)\,a \rightarrow 1/n(\,Cn)c \quad (5)$$

$$2(H)a \rightarrow (H_2)g \quad (6)$$

Where: subscripts (a), (c) and (g) denote adsorbed, crystalline and gaseous species respectively.

1.1.3 Nickel based catalysts

Solid nickel catalysts (Kuchtanin *et al.* 2016) are widely studied for their use in decomposition of methane and other hydrocarbons because of high carbon filament (CF) yield. The structure and texture of filamentous carbon depends on the catalyst used as reported by (Salipira *et al.* 2016). Despite wide application on industrial scale, solid metal catalysts readily deactivate due cocking and sintering (Baiker 1987).

Carbon filaments formation and yields on co-precipitated Ni-alumina and Ni-Cu-alumina catalysts (Takenaka *et al.* 2004) were studied and the results showed, that the amount of CF formed per gram of the catalyst increases with increasing Ni content in the Ni-alumina catalyst. However, the CF yield was found to be radically lower for pure Ni powder.

Low CF yield (Li *et al.* 2016) from methane decomposition on unsupported Ni catalyst has been attributed to the presence of large Ni particles (50-100nm) with low index planes. The low index planes are incapable of dissociating the unreactive methane molecule. In a reaction of this nature, the total amount of CF formed was dependent on the reduction temperature as well as the reaction temperature. Carbon filaments yield increases with increase in temperature though, the higher the temperature the higher the rate of catalyst deactivation. Data on activation energies of CMD reaction on nickel based catalysts are as shown in table 1-1 below *(Ashik et al. 2015b).*

Table 1-1 Activation energies of Nickel based catalysts reported in literature.

Catalyst name	Activation energy (kJ/mol)	Reference
Ni	65.4	*(Wang and Lua 2014),*
Ni	59	(Snoeck *et al.* 1997)
Ni	59	(Wang *et al.* 2009)
Ni(111)	53.9	(Zavarukhin and Kuvshinov 2004)
Ni-Al	64.6	(Kvande *et al.* 2008)
Ni/SO_2	29.5	(Fukada *et al.* 2004)
Ni/SO_2	90	(Chesnokov and Chichkan 2009)
Ni-Co-Cu	67.5	*(Wang and Lua 2014),*
Ni/TiO_2	60	(Chai *et al.* 2007b)
Ni/ZeoliteY	61.77	(Nasir Uddin *et al.* 2014).
Ni-Cu-Mg	50.4	(Borghei *et al.* 2010)
Ni/Al_2O_3-CaO	88	(Bai *et al.* 2007)

Molten metals of transition elements have been extensively studied and found to have some catalytic power (Cho *et al.* 2011). Catalytic activities of various metals and semi-metals with meting point -39℃ to 660℃ have been studied in detail (Zhan *et al.* 2014). The study of cobalt based catalysts on supported carbon material have been reported by (Fu and Li 2015). However, none of their literature describes supported molten metal catalysts. Studies on catalytic properties of lithium was studied in detail by (Nithyadharseni *et al.* 2015).

The primary objective of this research is to develop a supported molten metal catalyst with a porous inert support such that more reactions occur on a large exposed surface area resulting in 3 to 4 orders of magnitude, thus increasing the rates of reaction at 650℃ (Keipi *et al.* 2016; Ping *et al.* 2016). In this present work, the supported molten metal catalyst was prepared and

characterized in the laboratory according to procedures previously done by (Lee *et al.* 2016) using calcium oxide as a porous support (Ho *et al.* 2014).

1.2 Problem Statement

Solid mono and bimetallic catalysts for use in methane decomposition undergo deactivation and have limited selectivity and due to sintering and coking by deposited carbon on their active sites.

1.3 Research Aims

The main aim of this study is to develop a stable and efficient supported molten metal catalyst which can be used to decompose methane into carbon and pure CO_2-free hydrogen.

1.3.1 Research objectives

- ✓ To establish a phenomenon that the catalytic life of solid nickel catalyst can be enhanced if used together with a molten metal in porous calcium oxide support.
- ✓ To achieve high catalytic activity per unit mass of the molten metal catalyst due to complete dispersion owing to thinness of catalyst micro-crystallites.
- ✓ To reduce deactivation due to coking and sintering which are common in solid metal catalysts.

1.3.2 Research Approach: Experimental

Work in this project commences with extensive literature review on the status of global energy today with emphasis on renewable energy. Aspects of environmental pollution and development of green energy were investigated. Much attention was paid in development of alternative sources of energy to reduce overdependence on fossil fuels whose reserves are fast dwindling. Based on the shortcomings of most hydrogen producing technologies like steam reforming of hydrocarbon which emit CO_2 in the atmosphere, there is need to develop a method which would decompose methane into carbon and hydrogen with less or little CO_2 emission into the atmosphere. Since traditional solid metal catalysts like nickel are limited in performance due to coking and sintering, there is need to address these shortcomings by developing a supported molten metal catalyst in which, the decomposition reaction proceeds by chemisorption and surface reaction.

To synthesize a supported molten metal catalyst, five different catalysts in different ratios by weight were prepared as follows; 50%Ni/CaO, 37.5%/Ni-12.5%Li/CaO, 25%Ni-25%Li/CaO,

12.5Ni%-37.5%Li/CaO and 50%Li/CaO. The method of preparation was incipient wetness impregnation, followed by drying and reduction under a H_2/N_2 environment. The synthesized catalysts were then characterized by XRD, SEM, BET and then used in a packed bed stainless steel reactor to decompose methane at 550℃, 600℃, and 650℃ and 700℃. The spent catalyst was later characterized by TEM to study the shape and size of deposited carbon.

Gaseous products of catalytic decomposition, including unreacted methane from the packed bed reactor were analyzed using a Shimadzu -2014 gas chromatograph. Deposited carbon on the catalyst was determined by weighing the catalyst before and after the reaction to establish microscopic weight changes of the spent catalyst.

1.4 Thesis outline

This Thesis is structured as follows;

Declaration.

This is a declaration that this project is my own work, thoughts and ideas.

Abstract.

In this section, catalytic decomposition of methane is introduced, shortcomings of the present study brought to the fore, purpose of research stated, research outline given and the methodology to be followed is clearly stated.

Dedication.

Special mention to the people who directly or indirectly affect my life on day to day basis is documented here.

Acknowledgement.

All the people who contributed in one way or another in conducting this research are hereby acknowledged.

Table of contents

Contents of every page in heading and sub headings in the project is listed here

List of figures.

Figures representing information in the study are listed here.

List of tables

Tables containing detailed information in the study are listed here.

List of abbreviations and acronyms

Abbreviations for long words and definition of chemical symbols using letters are listed here.

List of symbols

List of commonly used symbols and their meaning as used in this project are put here

Chapter1. Introduction

In this chapter, background information on catalytic decomposition of methane, problem statement, contributions of the study, research aims and objectives, research questions, hypothesis, scope and reasons for the study are given.

Chapter 2. Literature review

This chapter highlights readings and citations of other people's work on catalytic decomposition of methane into carbon and hydrogen using metallic and non-metallic catalysts, catalyst life, chemical reaction fundamentals in a reactor and an evaluation of potential markets for decomposition products.

Chapter 3. Research Methodology

This chapter specifies research design, population and sample, data collection and analysis, procedure on catalyst preparation and characterization, choice of experimental method, experiment design and procedure on measurement of variables.

Chapter 4. Results and Discussions

In this chapter, findings/results from the experimental work done are discussed and relationships between variables clearly shown.

Recommendations

Limitations of the study and further research in this area that needs to be done by interested researchers is documented here.

Conclusion

In this section, generalizations from the experimental results, limitations of the study as well as project feasibility are clearly shown.

References.

In this section, all sources of reference material are listed.

Appendix.

In this section, very detailed information like; Graphs and analysis charts for catalyst characterization, calculations, tables, are put.

CHAPTER 2. LITERATURE REVIEW

2.1 Introduction

Overdependence on fossil-based fuels to meet energy demands and increasing environmental concerns have stimulated an exploration into the development of alternative renewable energy sources. Burning fossil fuels emit nitrogen dioxide and carbonaceous compounds which leads to environmental degradation (Jones *et al.* 2001; Nicoletti *et al.* 2015).

It has been reported (Nikolaidis and Poullikkas 2017), that a bigger proportion of current global hydrogen comes from steam reforming and partial oxidation of hydrocarbons and gasification of coal. The major drawback of these hydrogen producing technologies is emission of carbonaceous compounds which require a separate purging process. During the hydrogen purification stage, carbon dioxide (CO_2) is produced which contribute to global warming and acid rain (de_Richter *et al.* 2016). Natural gas is a preferred source of raw material for producing hydrogen (Faramawy *et al.* 2016), because it is abundantly available on earth and could be produced from biological processes such as fermentation. Natural gas comprises of methane, small hydrocarbons and other elements such as sulphur. Steam reforming accounts for over 50% of world hydrogen production despite producing harmful CO and CO_2 which poison proton exchange fuel cells and alkaline fuel cells (Wang *et al.* 2016). It is worth noting that hydrogen purification methods employed to capture CO and CO_2 are expensive and energy and material intensive.

Water electrolysis is also another method commonly used to produce pure hydrogen, but the yields are very low and hence, not economical. Ammonia decomposition using a suitable catalyst is also a viable option of producing pure hydrogen (Meng *et al.* 2015) but, ammonia catalyst pollutes the environment and is poisonous to proton exchange fuel cells (Pendyala *et al.* 2016). Table 2-1 below shows a list of most viable hydrogen production technologies (Nikolaidis and Poullikkas 2017), their efficiency, advantages and disadvantages. From the table, despite biomass gasification being a promising technology, its efficiency is hard to quantify due to tar formation and varying hydrogen content.

Table 2-1 Hydrogen production technologies.

Process	Efficiency (%)	Major advantages	Major disadvantages
Steam reforming	74-85	Developed technology	CO_2 by product, depend on fossil fuels
Partial oxidation	60-75	Proven technology	CO_2 b product, depend on fossil fuels
Auto thermal reforming	60-75	Proven technology	CO_2 bye product, depend on fossil fuels
Hydrocarbon pyrolysis	-	No emissions	Carbon bye product, depend on fossil fuels
Biomass pyrolysis	35-50	Abundant and cheap	Tar formation and varying H_2 content
Biomass gasification	-	Abundant and cheap	Tar formation and varying H_2 content
Bio photolysis	10	O_2 as by product	Low H_2 yield
Dark fermentation	60-80	Waste recycling	Low H_2 rates and yield
Photo fermentation	0.1	Waste recycling	Low H_2 rates and yield
Electrolysis	40-60	Proven technology	Low overall efficiency, high capital costs
Thermolysis	20-45	O_2 as by product	Corrosion problems
Photo-electrolysis	0.06	No emissions	Low conversion efficiency

Today, methane catalytic decomposition (CMD) reaction is an alternative method to produce both clean hydrogen and carbon nanomaterial due to its process simplicity. Carbon nanomaterials produced are directly used in a direct carbon fuel cell (DCFC) (Liu *et al.* 2010) and pure hydrogen is used in a Polymer electrolyte membrane fuel cell (PEMFC) (Muradov and Veziroğlu 2005). Considering high demand for a high purity hydrogen, many viable technologies based on CMD reaction have been explored. A promising method is step-wise reforming in which deposited carbon is continuously removed from the spent catalyst (Choudhary *et al.* 2002). In CMD reaction, low temperatures favour low carbon coverage on the catalyst surface, thus making catalyst regeneration with steam, oxygen and carbon dioxide easy. Use of carbon based catalysts such as carbon black, activated carbon, ordered mesoporous carbon, carbon nanofilaments (CNFs) and carbon graphite in a CMD reaction, require high activation energy and high temperatures as opposed to use of metal-based catalysts (Kim *et al.* 2004) where reactor surface area (Dunker *et al.* 2006) and presence of defects in graphene layers (Serrano *et al.* 2010) plays an important role.

To reduce catalyst deactivation by deposited carbon, the reaction kinetics of hydrocarbon decomposition on metal catalysts have been done extensively. Methanation, steam reforming of

hydrocarbons and other processes employing metal catalysts (Vogelaar *et al.* 2010) have been used. Accumulation of deposited carbon in these processes blocks the active sites of the catalyst, covers pore holes of the support and diminishes the mechanical strength of the catalyst. This leads to the formation of; carbon whiskers, fibrous carbon and carbon filaments. The formation of carbon nanotubes and in particular, single walled carbon nanotubes (SWCNTs) have been extensively studied and found to have mechanical, chemical, structural, electrical and electrochemical properties (Salipira *et al.* 2016).

2.1.1 Status of the energy globally

Currently, more mature and reliable energies are on the rise and steadily competing the conventional energy sources. In 2012, renewable energy provided an estimated 19% of the global energy consumption with a steady increase to 23.7 % in 2014 (Hussain *et al.* 2017). From figure 2-1 below, among the various renewable energy sources, hydro power commands a huge share at 16.6% of the total 22.7%, while the wind, bio power and solar power share are;3.7%, 2.0% and 1.2% respectively (Hussain *et al.* 2017). Emerging renewable resources are concentrated solar photovoltaic, marine, enhanced geothermal and others contributed to only 0.4% respectively.

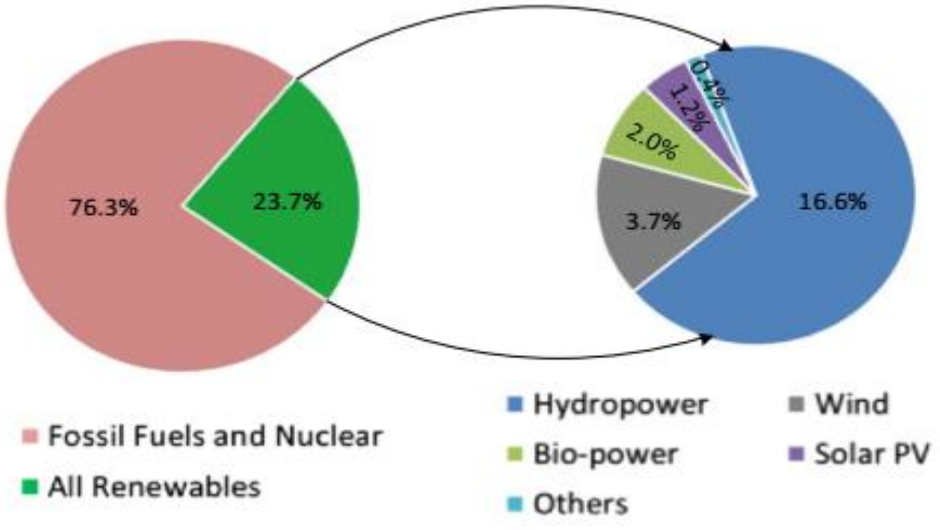

Fig 2-1 Estimated renewable energy share of Global Energy in 2015.

(Adapted from (Hussain *et al.* 2017).

According to the global status report (GSR) on renewable energy in 2016 (Hussain *et al.* 2017), the most tremendous growth in sustainable energy occurred in the power sector with global capacity exceeding1560GW (including small hydro power). A survey of investment in the energy sector in 2015 is summarized in fig 2-2 (Hussain *et al.* 2017). In total,40billion USD was invested by global investors in the renewable energy sector in 2004. An increase in investment was observed up to 279billion USD in 2011; but after 2011, it started to twindle. This reduction is attributed to cutting costs especially for solar photovoltaic (PV), whose installation was high irrespective of the reduction in dollar investment.

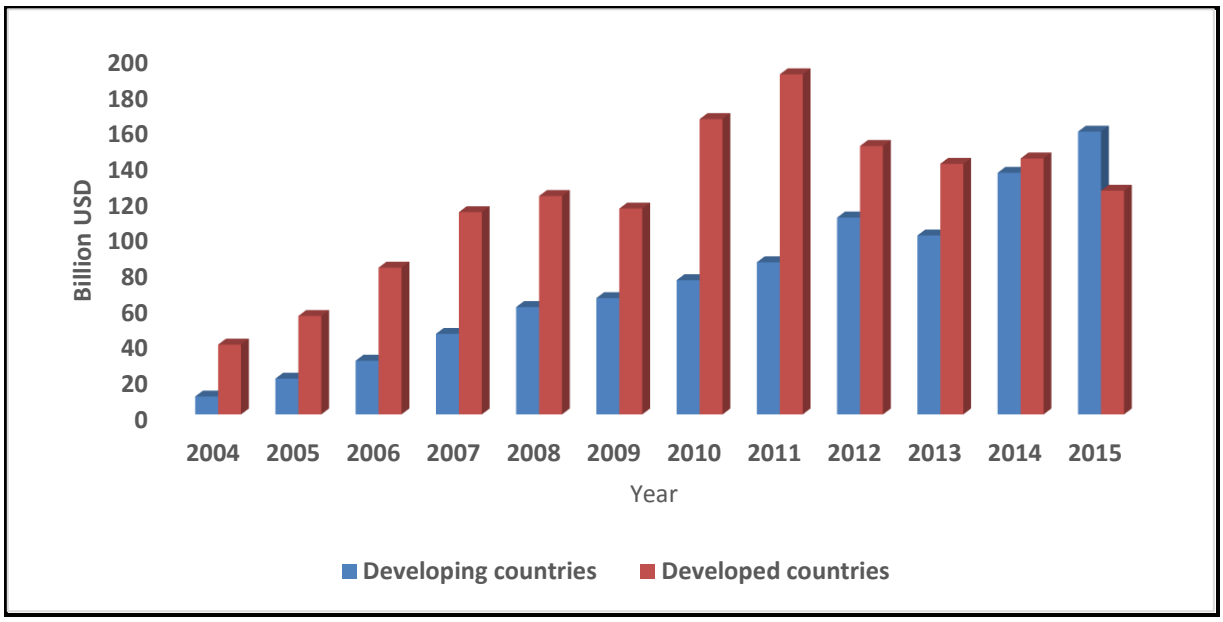

Fig 2-2 Developed and developing countries investment in renewable energies in billion USD; (Adapted from (Hussain *et al.* 2017)

Based on GSR-2016, in terms of total installed renewable power capacity, China, United States, Brazil, Canada and Germany remain top countries. China, United States and Germany were the top countries for non-hydrogen capacity followed by; Spain, Italy and India. From an investment perspective, Mauritania, Honduras, Uruguay, Morocco and Jamaica were among leading countries for investment in new renewable power and fuels.

2.1.2 Fuels and fuel types

Energy sources are classified into three main categories namely; fossil fuels, nuclear energy resources and renewable energy sources. Renewable sources can be used to produce energy

again and again without depletion. Presently, renewable energy sources supply about 23.7% of the global energy demand, which was 2% in 1998 including two exajoules of modern biomass and two exajoules of all other renewable energy sources (Panwar *et al.* 2011). Mainstream renewable energy technologies are solar energy, wind energy, geothermal energy, biofuels, biomass energy and hydropower.

2.1.2.1 Wind energy

Extraction of wind power using modern turbines is increasingly becoming an established global technique. Wind energy is renewable, sustainable, cost-effective and eco-friendly (Mahela and Shaik 2016). Since wind energy doesn't use water, it is more attractive than thermal power plants that uses a lot of water especially in hot and dry areas (Bilgili *et al.* 2015). It is believed that this type of energy would be the second most widespread source of electricity generation after hydropower in the near future (Dragomir *et al.* 2016). In 2015, 63,013MW of wind power was established worldwide, which is 1.8% more than what was produced in 2014 (Allouhi *et al.* 2017). The integral part of a wind energy plant is a turbine which converts mechanical energy associated with wind into chemical energy. The flow pattern of wind is very essential for understanding and assessing the performance of wind turbines. The speed of wind and its frequency varies from one location to another. Wind farms are usually set up in areas where wind is frequent, consistent and at high speed. The characteristics of wind are first studied and recorded to give valuable information which can be used to design and manage wind energy plants.

2.1.2.2 Solar energy

The conversion of concentrated solar energy into a sustainable thermal energy or electricity is an important factor to consider when exploring this technology. Solar energy systems such as solar collector or receiver, solar chimney, solar pond, solar still, solar thermal energy storage, solar heat exchanger and solar heaters are perfect technologies used to convert the solar energy for human use. The only challenge associated with these solar energy appliances is their low efficiency. To improve their efficiencies, some researchers have adopted different techniques to improve the efficiency of these techniques.

Advanced coating materials and large area holographic films have been used to improve optical energy efficiency of the solar system. Some researchers have also used nanofluids for different

solar stills. The loses in solar cells have been studied by (Dhankhar *et al.* 2014) while (Gawande *et al.* 2014) reviewed the influence of roughness geometries on heat transfer improvement in solar thermal systems. Heat transfer characteristics in a solar system can be improved by using porous materials having a solid matrix with inner connected void. Generally, porous materials can be used to achieve different targets in solar energy systems containing adsorption materials, thermal energy storage materials, insulation materials, evaporation materials, heat transfer and augmentation materials.

2.1.2.3 Geothermal energy

Geothermal energy originates from the heat generated and stored in the mantle and the core of the earth where deep vaults let water to these heat sources and the rising hot water generates a thermal reservoir which can reach temperatures of ≥ 350℃ (Malafeh and Sharp 2015). This type of energy is considered as clean, reliable and safe (Nakomcic-Smaragdakis *et al.* 2012). Based on the temperatures of the reservoir fluid, the geothermal energy resource can be classified as; low, medium and high enthalpy resources (Lee 2001). In most cases, geothermal energy is used for heating and for electricity generation. Hot mineral springs have been used for bathing, cooking and heating. Domestically, geothermal energy is used to heat buildings through district heating systems while on industrial scale, geothermal energy is used for food dehydration, milk pasteurization and gold mining.

Electricity generation in geothermal power plants require water or steam at higher temperature (150-370℃). Constant temperature near the earth's surface is picked up by geothermal pumps for direct utilization into buildings and homes. Geothermal energy can also be used directly without converting it into electrical energy. Some of the non-electric utilization of geothermal power are; agriculture applications, aquaculture applications, heat pumps, industrial processes, space heating and cooling, swimming, bathing and balneology while low, medium and high temperature geothermal resources can be used directly (Yazici 2016). It is estimated that 84% of the installed capacity worldwide in 2005 was used in district heating. In this type of geothermal utilization, China, France, Iceland and Turkey were the leaders in district heating; whereas, Italy, Japan, Russia and the United States were major users in individual home heating sector (Kyriakis and Younger 2016).

2.1.2.4 Biomass

Biomass energy is derived from plant and animal material such as; wood from natural forests, waste from agricultural and forestry processes and industrial processes and human or animal waste (Atilgan and Azapagic 2015). The energy released from biomass is green and renewable, thus utilizing this form of energy does not add greenhouse gases into the atmosphere. Biomass is the only renewable source of carbon and can be converted into solid, liquid and gaseous fuels. Biomass resources can be classified as modern or traditional. Modern biomass refers to the use of biomass energy on large scale. In this category, we have; wood and agricultural residues, urban wastes and biofuels such as biogas and energy crops. On the other hand, use of biomass energy on small scale especially in developing countries constitute traditional biomass. It includes; firewood and charcoal for domestic use, rice husks, plant residues and waste from animals (Kyriakopoulos and Arabatzis 2016).

Woody biomass is the accumulated mass, above and underground wood and leaves of living and dead woody shrubs and trees. The major component of woody mass is carbohydrates and lignin produced through the photosynthetic processes (Ntona *et al.* 2015). Woody biomass can be used to generate electricity, produce biofuel, biochemicals such as adhesives, solvents, plastics, inks and lubricants. High energy costs, uncertainty about energy supplies, dependence on foreign energy sources and concern about global climate change and air quality makes renewable energy alternatives such as those from biomass more reliable.

The direct use of biomass entails; burning wood and cooking while indirect use involves converting it into a liquid or gaseous fuel such as alcohol from sugar cane or biogas from animal waste using converting technologies. Upon combustion, the net energy released ranges from 8MJ/Kg for green wood to 20 MJ/Kg for dry plant matter to 55MJ/Kg for methane in comparison to 27MJ/Kg that comes from coal. Most biomass fired-electricity generators use wood and waste materials of forestry and agricultural processes. It has been reported that biomass contributes 35% of primary energy consumption in developing countries, raising the world total to 14% of primary consumption (Toklu 2017).

2.1.2.5 Biofuels

Biofuel is the bioenergy produced from biomass. Since biomass is readily available, a lot of research is being done in this area to make it an efficient alternative to replace nonrenewable

fuels (Cherubini and Strømman 2011). Biofuels are preferred over petroleum because; they can easily be extracted from biomass, they are easily extracted due to their biodegradability, they can be combusted based on the carbon cycle and are environment friendly. The biofuels produced from biomass are solid, liquid and gaseous fuels and can further be classified as first, second and third-class generation fuels based on the chemical composition of biomass.

The first-generation biofuels include biodiesel and vegetable oils produced from plants while the second-generation biofuels comprise of bioethanol and bio hydrogen produced from agricultural by-products and energy plants. The third-generation biofuels include; biogas, bioethanol and biobutanol and are produced from marine resources, sea weed and cyanobacteria. Proper use of these renewable resources leads to reduction in emissions of greenhouse gases (GHG) and reduction in environmental pollutions (Cherubini and Strømman 2011). Recently (Gaurav *et al.* 2017), bio refineries or biomass refineries have been reported to produce the required energy for electricity generation, fuels such as liquid biofuels and chemicals such as platform hydrocarbons with less ecological effects. Simultaneous production of bioethanol and biomethanol from sugar cane juice is economically attractive where hydro power is cheaply available. To avoid over dependence on conventional energy like petroleum, natural gas and coal, there is need to explore other environment friendly energy sources like biofuels (Gaurav *et al.* 2017).

2.1.2.6 Hydro

Hydro power is harnessing of energy from flowing rivers to convert it into useful mechanical energy (Jawahar and Michael 2017), thereby generating electricity using a generator. A hydro power generating system is classified as micro if it's plant has a generating capacity within 100Kw. These are small sources that may be used to supply power to small communities who are not connected to the main grid. River water passes through the forebay and reaches the turbine which converts hydraulic power into mechanical energy. The mechanical energy is subsequently converted into electrical energy by a generator. The hydraulic system comprises of a valve control system which regulates the flow of water into the turbine. Maximum power is usually achieved when the control valve is fully opened. The mechanical power in terms of a rotating shaft is send to the electrical unit which comprises of a synchronized generator connected to a shaft to produce useful electrical power.

Turbines are classified according to head as follows; low head (up to 40m-propeller and Kapla Turbine), medium head (40-100m-Francis, Pump as Turbine, Cross flow and Pelton wheel) and high head (>100m-Turgo and Pelton wheel). Many Pico hydro plants are situated in forest ranges and in remote areas and the main challenge faced by these plants is inadequate supply of turbines and high cost (Jawahar and Michael 2017).

2.1.2.7 Emerging renewable and sustainable energy technologies

Apart from mainstream renewable energy resources (wind, hydro power, solar, biomass, biofuels and geothermal energy), other renewable energy technologies have emerged in the last decade attracting the attention of researchers (Llorente García *et al.* 2011). Commercialization of most of these technologies is still limited but some are economically viable (Moriarty and Honnery 2007). Some of these technologies include; marine energy, concentrated solar (photovoltaic), enhanced geothermal energy, cellulosic ethanol and artificial photosynthesis.

Marine energy or ocean energy is a very attractive renewable energy resource. The technique consists of wave energy, tidal power, tidal currents, salinity and temperature gradients. This type of energy is very consistent and predictable. The potential of wave energy is compared to nuclear energy and the energy stored in these vast oceans in the form of heat, tides, waves and currents is enough to meet world's energy demand many times over. Several technologies and methods are applied for extracting energy from the oceans. The five major technologies applied for extracting energy from the oceans are; wave energy (wave power), tidal energy, tidal currents, salinity and temperature gradients (Hussain *et al.* 2017).

Concentrated solar power (photovoltaics) is a technology used for generating electricity using heat produced by concentrating it on a small area. In this technology, mirrors or lenses are used to reflect sunlight into a receiver where a primary circuit (thermal energy carrier collects the heat which is either used directly or indirectly using a secondary circuit to generate electricity using a turbine. As compared to wind and photovoltaics, concentrated solar power with thermal storage provides a higher capacity factor and distribution (Ummadisingu and Soni 2011).

Enhanced geothermal energy (EGE) does not depend on occurrence of geothermal reservoirs. The reservoirs for extracting the geothermal energy are engineered thus, making its availability to occur anywhere. Major advantages of this energy are; extended lifetime, increased

productivity, sitting flexibility, expanded resources, sizing flexibility and environment friendly. The resource of EGE is huge but not equally distributed. In active tectonic regions, a temperature of ≥150℃ at the depth of 6km is common but confined to those resources (Aljundi 2011).

Cellulosic ethanol is produced from processing of ethanol. It is a complicated process compared to just producing ethanol from sugarcane or corn starch. Research at the University of California-Berkeley indicated that on a life-cycle basis, cellulosic ethanol has the potential of lowering greenhouse gases emission by 90%, relative to the conventional petroleum-based gasoline (Hussain *et al.* 2017). The challenges faced by this technology are either in the formation of commercial level plants or in the technical aspects of the process.

Artificial photosynthesis is where energy transduction is achieved by making use of semiconductors, which can absorb sunlight and generate an electron-hole pair (Wang *et al.* 2014). The energy of this electron-hole pair must be sufficient to carry out the electrochemical oxidation of water to convert it into oxygen and reduction of protons and CO_2 to convert them into chemical fuels. The energy required to split a water molecule into hydrogen and oxygen is 1.23V and reduction of CO_2 for the formation of methane is 1.4-1.6V. Two materials with smaller band gaps are used to absorb a greater portion of the solar spectrum. Artificial photosynthesis is an attractive way of harvesting and using solar energy for fulfilling the energy needs of modern generation (Hussain *et al.* 2017).

2.2 Hydrogen production methods

Hydrogen being an abundant element on earth is found in various substances such as water, biomass, hydrogen sulfide and fossil fuels. Primary sources of hydrogen are classified as; electrochemical, thermal, photonic and biochemical.

2.2.1 Electrolysis

Water electrolysis is the simplest industrial process for producing hydrogen of high purity. The novelty of the process is based on the mobility of electrons which are excited by an electric current passing through a water bath. In this method, solid oxide Electrolyzers and alkaline polymer membranes are vital hydrogen producing equipments. For an electrolytic cell to be efficient, its energies must be sufficient for the reaction to take place. In some cases, the use of a catalysts is employed to improve the intensity and rate of the electrolytic reactions.

One of the limitations of electrolysis process is the use of platinum catalyst which is very expensive. Electrolyzers like proton exchange membranes (PEM) require pure, desalinated and demineralized water before the actual electrolysis process to prevent evolution of chlorine. Desalination of water is done by the ion-selective membranes (Dincer and Acar 2015) .Use of magnesium as a catalyst is done to support oxygen evolution reaction as opposed to chlorine evolution (Ni *et al.* 2006b).

2.2.2 Plasma arc decomposition

Plasma occurs when electrons become excited and change into atomic species after matter has been ionized. These excited electrons produce electrical current of high voltage by particles being electrically charged. Dissociation of methane into hydrogen and carbon is because of this thermal reaction. During the reaction, carbon settles at the bottom as soot and hydrogen is collected in gaseous form. This plasma reaction was done by (Fulcheri *et al.* 2002) in a thermal plasma reactor. In this method, plasma gas is let into two of the three electrodes while methane gas is introduced from the upper part of the reactor. This decomposition process is regarded as high temperature pyrolysis (Dincer and Acar 2015) and can be used to lower cost of producing hydrogen by 5% in comparison to SMR.

2.2.3 Water Thermolysis

This is a single step dissociation of water which can be represented by the following equation;

$$H_2O \xrightarrow{heat} H_2 + \frac{1}{2}O_2 \qquad (7)$$

A heat source of about 2500K to 3000K is required to achieve a reasonable degree of dissociation of 64% at 1bar and 300K as reported by (Dincer and Acar 2015). The only challenge associated with water thermolysis is the separation of hydrogen and oxygen. The experiment on thermolysis of water carried out by (Baykara 2004) reported a 90% conversion of the equilibrium at a residence time of 1ms and at 2500K. To avoid hydrogen and oxygen recombining, palladium membrane is used to achieve maximum separation.

2.2.4 Thermochemical water splitting

Splitting of water cycles thermochemically is advantageous since no catalyst is required to drive the chemical reaction and apart from water, all other reagents used in the reaction can be

effectively recovered. This method does not require O_2-H_2 separation membranes and occurs at moderate reaction temperatures (600K-1200K) and with negligible electric heat requirement.

Reactions of thermally driven S-I cycles can be written as;

$$H_2SO_4 \rightarrow H_2O+SO_3 \quad (8)$$

The resultant gases are steam and sulfur trioxide which are then heated to 800-900℃ Decomposition of SO_3 proceeds thermally to oxygen and Sulphur dioxide.

$$SO_3 \xrightarrow{heat\ (800-900)℃} \frac{1}{2}O_2 + SO_2 \quad (9)$$

After separation from O_2, SO_2 reacts exothermally with iodine and water at low temperatures spontaneously.

$$SO_2 + I_2+2H_2O \rightarrow 2HI + H_2SO_4 \quad (10)$$

Finally, the hydrogen iodide thermally decomposes into hydrogen at temperatures around 425-450℃,

$$2HI \xrightarrow{heat\ (425-450)℃} H_2+I_2 \quad (11)$$

There are no side reactions in this process but it requires high thermal energy to achieve a substantial hydrogen conversion (Dincer and Acar 2015).

2.2.5 Biomass gasification

Common biomass materials are wood, saw dust and sugarcane. When using biomass as a raw material, the moisture content should be kept low either by gasification using steam or drying in the sun. Gasification reaction is done on biomass to produce hydrogen according to the following reaction;

$$CxHy + xH_2O \xrightarrow{high\ temperature\ heat} (\frac{y}{2} +x)\ H_2+xCO \quad (12)$$

Common reactors used in biomass gasification are; fixed bed, movable bed and fluidized bed reactors and the process can be either thermal or auto thermal depending on the amount of heat used in the reaction.

2.2.6 Coal gasification

Coal is an economically viable reserve for hydrogen production. During gasification, coal is partly oxidized with steam and oxygen in high pressure and high temperature reactors. The products of coal gasification are hydrogen, carbon monoxide mixed with steam (syngas) and carbon dioxide. The CO/H_2 mixture is subjected to further processing through shift reaction to increase the yield of hydrogen.

In some cases, the flue gas is processed and cleaned to recover elemental sulfur while the CO/H_2 can be processed further for electricity generation and for use in gas turbines. The main challenge of coal gasification process is the emission of CO_2 into the atmosphere and its capture is a tedious and expensive process. Economically, the raw materials for coal gasification process are low while the capital costs for the plant are very high.

2.2.7 Dark fermentation

When stored biochemical energy in organic matter is converted into other forms of energy either in the presence of light or in the absence of light, the process is called dark fermentation (Dincer and Acar 2015). This process is usually carried out in bioreactors which are easier to construct and less expensive as opposed to photo-fermentation which requires solar energy. The advantages of this method are; the ability to produce hydrogen from organic waste which would otherwise have been wasted and the raw materials are cheap and easily available.

It has been reported that hydrogen production from water diluted with olive oil shows a maximum yield of 640g of hydrogen per ton of oil bulb and 77g of hydrogen per kg of glucose (Das and Veziroglu 2008).

The major challenge of dark fermentation method or anaerobic digestion is low hydrogen production relative to capital investment.

2.2.8 Fossil fuel reforming

The main fossil fuel reforming methods used to produce hydrogen are; steam reforming, partial oxidation and auto thermal reforming. Apart from hydrogen being produced as the main product, CO and CO_2 are produced at the end of the reforming process. Reforming of steam do require an external heat source, but the reaction can proceed in the absence of oxygen. This process

takes place at low temperatures and can yield a higher hydrogen to carbon monoxide ratio as opposed to auto thermal reforming and partial oxidation.

Products of partial oxidation of hydrocarbons are hydrogen, carbon dioxide, carbon monoxide and heat. The heat generated in this process is used to drive the combustion stage. Partial oxidation method is not easily affected by sulfur than steam and auto thermal reforming.

A pure oxygen in feed and absence of an external heat are basic requirements of partial oxidation and auto thermal reforming. This oxygen requirement makes these processes very complex and expensive since additional oxygen separation units are required. Steam reforming is the least expensive and common method to produce hydrogen as compared to other hydrogen producing technologies. The only challenge associated with steam reforming is production of carbon dioxide and carbon monoxide which require further purification steps to obtain pure hydrogen. Table 2-2 shows a comparisons of selected hydrogen production methods and their approximate cost of investment (Dincer and Acar 2015).

Table 2-2 Comparisons of selected hydrogen production methods.

Method	Energy Efficiency	Exergy Efficiency	Cost	SCC	GWP	AP
Electrolysis	5.3	2.5	7.34	3.33	3.33	8.86
Plasma arc decomposition	7.0	3.2	9.18	0.83	0.83	5.14
Thermolysis	5.0	4.0	6.12	7.5	7.5	7.43
Thermochemical water splitting	4.2	3.0	8.06	9.17	9.17	9.43
Biomass conversion	5.6	4.5	8.10	6.67	6.67	2.00
Biomass reforming	3.9	2.8	7.93	6.25	6.25	0.86
PV electrolysis	1.24	0.7	4.5	7.5	7.5	7.71
Photo catalysis	0.2	0.1	5.19	9.58	9.58	9.71
Photo electrochemical method	0.7	0.15	0.00	9.58	9.58	9.71
Dark fermentation	1.3	1.1	7.52	9.58	9.58	9.71
High temperature electrolysis	2.9	2.6	5.54	7.92	7.92	8.57
Hybrid thermochemical cycles	5.3	4.8	7.41	9.43	9.43	9.02
Coal gasification	6.3	4.6	9.11	0.00	0.00	1.31
Fossil fuel reforming	8.3	4.6	9.28	2.5	2.5	5.71
Bio photolysis	1.4	1.3	7.27	7.5	7.5	9.71
Photo fermentation	1.5	1.4	7.61	9.58	9.58	9.71
Artificial photosynthesis	0.9	0.8	7.54	9.58	9.58	9.71
Photo electrolysis	0.78	0.34	7.09	8.33	8.33	9.71
(Zero-emissions and cost,100% efficiency)	10.0	10.0	10.0	10.0	10.0	10.0

2.3 Problems facing methane use and drive towards decomposition

Despite fossil fuels being a potential source of raw material for hydrogen production, there are serious environmental concerns such as; emission of greenhouse gases, pollution of air, degradation of land for human and wildlife use, contamination of water reservoirs and possible cause of Earthquakes. Natural gas is a fossil fuel, though the greenhouse emissions from its combustion are much lower than those from coal (Alcheikhhamdon and Hoorfar 2016).

Natural gas emits about 40-60% less carbon dioxide when efficiently combusted in a new power plant compared to emissions from a conventional coal plant. Based on flue gas emissions, natural gas also emits 15-20% less heat-trapping gases than gasoline in a vehicle combustion engine. Drilling and extraction of natural gas leads to methane leaks which is 34 times stronger

than CO_2 at trapping heat over a 100-year period and 86 times stronger over 20 years. Natural gas does not produce nitrogen oxides upon combustion, which are precursors to smog, but less than that produced from gasoline and diesel in motor vehicles. It has been reported that in every 10,000 U.S homes using natural gas power instead of coal avoids annual emissions of 1,900 tons nitrogen dioxide, 3900tons of SO_2 and 5200tons of particulates (Alcheikhhamdon and Hoorfar 2016). Efforts to reduce these emissions translate into public health benefits like less Asthma, bronchitis, lung cancer and heart diseases. In areas where drilling occurs, there is an increase in concentrations of hazardous air pollutants and particulate matter into the atmosphere.

Construction and land disturbance caused by oil and gas drilling can alter land use and harm local ecosystem by causing erosion and fragmentation of wildlife habits, increased risk of aquatic pollution from chemical spills and depletion of surface waters because of lowering ground water levels. There are possibilities of radioactive materials, methane and other underground gases which can leak into drinking water supplies from improperly cased wells. Though methane doesn't pose serious health effects but its accumulation in large quantities may pose flammability risks.

Hydrogen production from methane is relatively high compared to other feed stocks (Salam and Abdullah 2017). Decomposition of methane as a viable option for producing pure hydrogen, requires higher temperature to break the C-H bond in a methane molecule (Abbas and Baker 2011). Hence, there is a need to develop an advanced approach that can reduce the cost and energy required in methane decomposition. The approach in this case is catalytic decomposition of methane, in which a catalyst is used to lower the decomposition temperature.

2.4 Catalyst systems for the methane decomposition

Catalysis is a process in which the rate of reaction is enhanced by a relatively small amount of a different substance (catalyst) that does not undergo any permanent change itself. Catalysts reduce the energy which is necessary for the reaction to proceed along the reaction pathway. A catalyst offers a new reaction pathway and concentrates the reactants at the surface. A very strong acid site could protonate a paraffin forming a penta-coordinated carbocation (carbonium ion), which decomposes into hydrogen/alkane and a carbonium ion. To achieve lower reaction temperature in methane decomposition, a suitable catalyst is used.

Higher reaction temperatures could increase conversion rate of methane to hydrogen but at the expense of catalyst deactivation which is more pronounced at higher temperatures (Amin *et al.* 2011). Carbon based catalysts are widely used in methane decomposition but they readily deactivate (Abbas and Baker 2011). Substantial progress in CMD processes have been achieved by use of metal-based catalysts. The CMD process begins with dissociative adsorption of methane on a catalyst surface, followed by successive dissociation to produce elemental hydrogen and carbon. The reaction barrier for the decomposition process is in the range of 3.83-4.48eV. Carbon based catalyst have an energy barrier of (1.65-2.17) eV at 600-900℃ while metal based catalysts have energy barrier in the range of (0.54-1.8) eV (Kim *et al.* 2004). It is therefore essential to design a catalyst with high catalytic activity, stability at low temperature and low activation energy. The performance and stability of a catalyst depends on the type of the catalyst support. Most common supports such as SiO_2, Al_2O_3, TiO_2 and CeO_2 enhances chemical reactivity of the metal catalyst for different catalytic reactions (Ruiz *et al.* 2007). Alumina has been recognized as an acid-type catalyst due to its good thermal stability, textural properties and surface sorption behavior through proton-affinity distribution. The acidity of the support promotes the CMD reaction and the catalyst becomes more refractory and stable in sintering and coke formation due to interaction between metals and supports (Salam and Abdullah 2017).

2.4.1 Supported metal catalysts

These are heterogeneous catalysts in which, the support polarizes the metals and subsequently alters their properties. Depending on intensity and interaction, MSI alters dispersion and mobility of the catalyst thus promoting methane conversion and hydrogen yield (Li *et al.* 2011). Some of the factors which influence the catalyst performance are; particle size, electronic state of the catalyst, dispersion of metal particles, texture, pore size (Salmones *et al.* 2009), catalyst composition (Pinilla *et al.* 2010), catalyst preparation method (Chen *et al.* 2005), and the rinsing solvent (Zhang *et al.* 2011b).

2.4.1.1 The active phase

Decomposition of methane can be realized at temperatures of more than 1473K without a catalyst due its strong C-H bond which is about (440kJ/mol at 298K). In CMD reaction, various metal and non-metal catalysts have been used singularly or in combination to enhance their

activity and selectivity (Takenaka *et al.* 2001). Owing to its stability, activity and high carbon yield, nickel is mostly used in CMD reactions. Highly active metal catalysts such as; cobalt, iron, zinc and nickel have partially filled outer electron orbitals, hence readiness to accept electrons. Some metal oxides such as magnesium oxide (MgO) are very active especially when supported on copper, Molybdenum or Tungsten.

2.4.1.2 The promoter

To achieve both high methane conversion and pure hydrogen, CMD reaction being endothermic, is suitably operated at high temperatures. To utilize some catalysts such as Ni/Al_2O_3 which have optimum reaction temperatures irrespective of their composition, it is only prudent to dope it with another catalytically active chemical to get much needed conversion. From literature (Li *et al.* 1998), it has been reported that doping copper into Ni/Al_2O_3 promotes the production of CNFs and hydrogen by altering the optimum reaction temperature to a higher temperature. When a metal catalyst undergoes doping, its improvement in performance is enhanced by delaying its deactivation rate. Researchers found very promising results with the doping of the Raney-type catalyst (Cunha *et al.* 2009b) with copper and doping of a $Ni\text{-}Cu/Al_2O_3$ catalyst (Chesnokov and Chichkan 2009) with iron to improve the stability.

For both the CMD and methanation reactions (Qian *et al.* 2003), alkaline metal oxides are harmful to transition metal oxides when used in combination. From previous studies growth of SWCNTs can be improved when metals such as molybdenum, platinum and ruthenium are used as dopants in combination with active metals. Small additions of molybdenum ($\leq$ 1.0wt %) causes a significant increase in resistance to coking of the nickel catalyst for steam reforming or CO_2 reforming of hydrocarbons (Kępiński *et al.* 2000).

2.4.1.3 The support

The role played by supports in catalysis cannot be under estimated (Li *et al.* 1997). Nickel catalyst is stable and active (Takenaka *et al.* 2001), but its performance can improve to high magnitudes when supported on; Al_2O_3, MgO and SiO_2,Al_2O_3. Substantial catalytic activity is also exhibited by metal oxides like; TiO_3, MgO and SiO_2-MgO. Catalytic activity of Perovskite structured oxides have been investigated and tried for use as CMD catalysts (Kuras *et al.* 2008). Mesoporous CNFs with large surface area (100-300m^2/g) have also been used as supports for

nickel catalyst. Very good quality carbon nanomaterial have been achieved by use of Zeolites as potential supports in the CMD reaction (Guevara *et al.* 2010).

In order to achieve highly dispersed surface area for the catalyst and promote the growth of SWCNTs, several substrates such as Al_2O_3, MgO or SiO_2 are used (Ni *et al.* 2006a). Magnesium oxide supported catalysts are efficient in carbon nanomaterial synthesis because of easy catalyst regeneration from the carbon unlike, Al_2O_3 or SiO_2 supported materials. Porous MgO prepared by thermal decomposition of its salts $Mg(NO_3)_2$ and $MgCO_3$ is an excellent material for growth of SWCNTs. More active sites can be achieved when a Fe/MgO is calcined at 1173K for 10h to give a solid solution structure of small diameter SWCNTs and DWCNTs.

2.4.1.4 Metal-support interaction

The bonding strength between a metal catalyst and its support constitutes a phenomenon called metal-support-interaction (MSI) which affects the removal of metal oxides and metal distribution in the overall catalyst system. When the MSI is strong, it is difficult to reduce the precursor oxide and create room for metal catalyst dispersion which consequently changes the electronic and crystalline state of the metal particle, hence limiting its effectiveness.

When the MSI is weak, the metal catalyst particle is blown up by the growing carbon nanomaterial. This continues to promote the growth of carbon nanomaterial at the tip, while a strong metal support interaction leads to growth at the base of the metal catalyst. In a CMD reaction, a large proportion of SWCNTs do not have metal particles attached to them except only few of them having metal appendages at their ends. There are two movements of metal particles reported in literature; jump movement by charged new layers and smooth movement which forms graphite layers (Chen *et al.* 2001). In CMD reaction, particle size of the catalyst is crucial in a sense that beyond a certain range, it will not influence the growth of carbon nanomaterial. At low temperatures the particles are usually in crystalline form but depict the characteristics of a quasi-liquid state at high temperatures (Chen *et al.* 2001).

2.4.2 Non-supported metal catalysts

The rate of reaction over unsupported monometallic catalysts increases as follows; Ni>Co>Ru>Rh-Pt> Re>Ir-Pd> Cu>W>Fe>Mo (Jin *et al.* 2013). Major focus has been

placed on; Ni, Co and Fe because they are relatively available, cheap, active and stable (Cunha *et al.* 2009a).

Frequent aggregation of nickel particles and carbon encapsulation poisons the unsupported nickel catalyst at reaction temperatures above 600℃ (Zapata *et al.* 2010). Iron catalysts have continuously shown more activity at high temperatures (Takenaka *et al.* 2004), although they produce thin walled carbon nanotubes of the lowest value (Ermakova and Ermakov 2002). On the other hand, use of Cu, leads to low yields of carbon nanomaterial and hydrogen, whilst; Rubidium, Rhodium and Platinum produce insignificant results in CMD reactions. Since most of these unsupported metals are magnetic, it is easier to regenerate them from deposited carbon after the reaction.

2.4.3 Carbonaceous catalysts

At the onset of CMD reaction, hydrogen yield is very high but gradually decreases with time due to catalyst deactivation caused by carbonaceous compounds blocking the active sites of the catalyst. Formation of carbide also contributes to deactivation especially when metal catalysts are used.

The above drawbacks of solid metal catalysts can be overcome by use of carbonaceous catalysts which are stable, no carbide formation, high fuel flexibility, high temperature resistance, less expensive and not easily poisoned by sulphur compounds and other metals and they take longer time to deactivate as compared to metal catalysts (Malaika and Kozłowski 2009). Carbon can be used both as a catalyst and as a support (Dufour *et al.* 2008). Use of carbon catalyst in CMD reaction has been embraced because the produced carbon can further catalyse the process and catalyst regeneration step is not required. Most commonly used carbon catalysts are; activated carbon AC (Moliner *et al.* 2005),carbon black CB (Lee *et al.* 2004a), coal chars (Dufour *et al.* 2008), acetylene black, glassy-carbon, diamond powder and soot (Muradov 2001a), MWCNTs, CNTs and graphite (Guil-Lopez *et al.* 2011) and carbon materials with monolithic honeycomb design (Gatica *et al.* 2013). When using AC,CB,CNF and ordered mesoporous carbon in CMD reaction, high activation energy (143-236kJ/mol) and temperatures (800-100℃) are prerequisites for the process (Kim *et al.* 2004).

Methane decomposition over carbonaceous catalysts starts when a methane molecule dissociates, followed by multiple chain reactions which leads to hydrogen and carbon nanomaterial. At the start, methane molecule interacts with chemically reactive carbon crystallites to overcome the C-H bond energy forming new carbon-carbon bonds in a hexagonal shape. The new carbon phase forms due to the formation of carbon nuclei and growth of carbon nanomaterial. Carbon black is most stable because of easy reach by methane molecules but it is less active (Suelves *et al.* 2007).

2.4.3.1 Metal doping of carbon catalysts

A comprehensive approach to modify carbon catalysts has been adopted by researchers in previous studies on catalysis (Zhang *et al.* 2013). Furthermore, high temperatures favour reduction of carbon supported on most metal catalysts during pre-treatment (Jin *et al.* 2013). Reduction of metal oxides helps to omit the extra hydrogen reducing step, hence making their synthesis easier. Research in this area by (Muradov *et al.* 2005), show that, the presence of small metallic impurities in carbon influences its performance in the CMD processes. Presence of metal particles in carbon makes it turn amorphous leading to the development of more active sites

Experimental trials done on nanocarbon black (NCB) and activated carbon reveals that incorporating metals like cobalt and nickel in their matrix increases their activity. According to Chen (Chen *et al.* 2009a), higher conversion of Co/NCB and Ni/NCB is either by Ni and Co metal particles taking the role of breaking down a methane molecule at the onset of methane decomposition to generate radicals on the surface of nickel or cobalt and then subsequent migration of the radicals to the surface of NCB and eventual breakdown into hydrogen and carbon nanomaterial. Also, performance of nickel and cobalt are better than that of NCB in CMD reaction. Addition of SiO_2 to activated carbon improves its surface area and pore volume. This enhances their performance than that of plain activated carbon resulting in activation of 30% and 27% respectively at 850℃ (Zhang *et al.* 2011a).

2.4.3.2 Performance of metal and carbon catalysts on comparison

Moderate operating environment is desired to produce better CNFs although high temperatures and pressure are needed to give appreciable quantities of hydrogen (Abbas and Wan Daud 2010). In CMD processes where a metal catalyst has been used, removal of carbon nanomaterial

without damaging the catalyst is a delicate procedure but in CMD processes where carbonaceous catalysts have been used, catalyst regeneration is not required (Guil-Lopez *et al.* 2011). The performance of both metal-based catalysts and carbon-based catalysts vary widely even though, they all undergo deactivation at varying rates.

From the most studied groups, carbon black deactivates slowly as compared to others because it has ordered graphene layers with more particle-particle spacing (Serrano *et al.* 2009). Metal catalysts produce very reactive carbon nanotubes (Muradov *et al.* 2006), carbon filaments (Lee *et al.* 2004b) together with molecular sieve-like carbon nanomaterial (de la Casa-Lillo *et al.* 2002),but carbonaceous catalysts produce disordered carbon of different shapes. Iron catalyst can withstand higher reaction temperatures (Ashik *et al.* 2015a) in comparison with other catalysts.

2.4.4 Metal Oxide supported catalysts

2.4.4.1 Li/MgO

The synthesis of lithium magnesium oxide doped catalyst (Wu *et al.* 2016) has been widely used in converting methane into ethylene. However, the catalyst has several shortcomings such as low ethylene yield and lack of stability due to lithium losses which leads to rapid catalyst deactivation especially at high temperatures (Karakaya and Kee 2016). Irrespective of intensive research in this area, the stability and structural morphology of this catalyst remains unclear.

2.4.4.2 $Mn/Na_2WO_4/SiO_2$

From literature (Karakaya and Kee 2016) reviewed the structure of the $Mn/Na_2WO_4/SiO_2$ catalyst. From their findings, they observed that the hydrogen yield was 23% when $Mn/Na_2WO_4/SiO_2$ catalyst was used in a PBR at 800℃ and this type of catalyst is more stable especially when used in combination with other catalysts. The problem with this catalyst lies in its preparation method which requires sophistication to couple together the metal oxides.

In this type of combination, every metal plays a role, i.e. Mn is responsible for the active phase and Na^{2+} responsible for controlling the oxidation of methane while W is claimed to control the catalyst stability. Better performance of catalysts in this category is realized at very high temperatures and usually, a yield of more than 25% is always achieved.

2.4.4.3 La_2O_3

La_2O_3 catalyst has been widely used in CMD reactions either singularly or in combination (Fakeeha *et al.* 2016). Doping the catalyst with alkali earth metals such as magnesium, strontium and calcium improves its catalytic power to realize a yield of 17% at 800℃ in a packed bed reactor. Despite not being as active and selective as Sr/La_2O_3, much improvement in stability has been reported when it is coupled with Calcium oxide. Selectivities of as high as 60% and 9% yield at 740℃ have been achieved in PBR. The major problem associated with this catalyst is that, it shows less stability and activity in CMD reaction, although the yield is significant. The presence of CO_2 at over 650℃ affects the stability of the La_2O_3 catalyst. Under these conditions, La_2O_3 reacts to form a dixymonocarbonate structure which is unstable at high temperature.

2.4.4.4 Fe_2O_3

Iron based catalysts form a significant proportion of catalyst sources for CMD reactions (Su *et al.* 2015). They are mostly desired for high methane conversion of up to 60% at temperatures of over 700℃ though their yield is as low as 5%. Complete oxidation of methane at high temperatures is responsible for this low yield. At elevated temperatures, iron forms $\propto$-Fe-O_3 phase and the oxygen in the lattice promotes the complete oxidation of methane. When steam is contacted with a mixture of methane and oxygen, the carbon selectivity increases to up to 70% at 850℃. Iron based catalysts, despite not being selective; they function better under non-oxidative conditions.

2.4.4.5 Ni-Co/Al_2O_3

According to (Frusteri *et al.* 2011), Ni-Co- Al_2O_3 is a suitable catalyst for a double-cyclic step which involves both CMD and catalyst recovery by combustion leaving the catalyst un-affected. This is because, Ni/Co exhibit a strong MSI together with Al_2O_3 support, hence inhibiting carbon deposition paving way only for carbon filament formation. The particles of cobalt strongly interact with Al_2O_3 support to the form $CoAl_2O_4$ catalyst which gives a higher metal dispersion, thus limiting catalyst agglomeration (Chai *et al.* 2007a). Hydrogen production goes up as reaction temperature increases with total disregard to the quantity Co catalyst loaded.

2.5 Process parameters influencing catalyst activity

The stability and activity of a catalyst in a CMD process is influenced by; partial pressure, space velocity and reaction temperature (Nasir Uddin *et al.* 2014). The initial yield of hydrogen is high

but gradually decreases due to loss of catalyst life. When metal catalysts are used, the catalyst activity increases only up to a certain level before deactivation sets in (Saraswat and Pant 2011). Experimentally, Ni/CuAl catalyst maintains its initial activity at low temperature of between 550℃ to 650℃ with a gradual increase of hydrogen yield from 20% to 31 vol% (Suelves *et al.* 2009). At elevated temperatures, the catalyst losses its ability to function properly because of sintering and formation of amorphous carbon. In studies of catalyst deactivation, pressure and temperature are the major factors promoting the formation of hydrogen.

According to (Wang and Lua 2014), the mean order of reaction is 0.63 and the mean activation energy in CMD reaction using monometallic nickel is 65.4 kJ/mol respectively. Increasing the partial pressure, increases hydrogen yield but also increases catalyst deactivation. As can be seen From Table 2-3 below, an increase in temperature promotes conversion up to 800℃ (Suelves *et al.* 2009; Ashik *et al.* 2015a).

Table 2-3 Effect of reaction temperature in MCD process over NiCuAl catalyst at

(WHSV: 120$g^{-1}_{cat}h^{-1}$)

T (℃)	r_{oCH4}(mmol/min.g_{cat})	X_{CH4}%	C_{dep}(g/g_{Cat})	r_c(g_c/g_{cat}.h^{-1})
550	10.02	34.0	16.4	6.56
600	12.96	52.1	21.3	8.51
650	16.25	64.2	26.0	10.40
700	34.27	79.3	46.8	20.03
750	47.60	85.0	39.0	14.18
800	45.95	91.5	15.6	16.22

2.5.1 Reactor Heating sources

Most commonly used reactors in CMD reaction are; flow reactors, fluidized bed reactors, and fixed bed reactors. Catalytic reactions are usually synthesized in fixed bed reactors (FBRs) and fluidised (FLBRs) while non-catalytic reactions are carried out in flow reactors. Heating media for catalytic reactors are electrical furnaces and microwave ovens whereas plasma and solar have been used in non-catalytic reactions.

Recently, special type of reactors called honey comb monoliths and liquid metal reactors have been explored as possible alternatives to FBR and FLBR due to their characteristic low pressure drop. Currently, runaway temperatures in these type of reactors do limit their use on commercial scale (Salmones *et al.* 2009). Liquid metal reactors are also used in CMD reactions due to their adequate heat transfer between liquid metal and methane gas (Shin *et al.* 2017). Operating CMD reactions at over 1000℃ poses a danger of carbon clogging to the reactor (Chen *et al.* 2005) and promotes carbon deposition. Metal catalyst regeneration can be done but this represents an additional process step which is energy intensive.

2.5.2 Reactor surface area

In many studies, the surface area of the reactor has influence on the kinetics of the CMD reaction in terms of yield. Previously, methane catalytic reactions were done in metallic reactors made of stainless steel and copper, but attempts are being made to commercialize the use of inert materials like quartz, Pyrex and various forms of alumina. When a CMD reaction is carried out at around 600℃ in the presence of oxygen and silica, up to 4.5% of methane is converted into formaldehyde (CH_2O). Glass and quartz reactor walls exhibit the formation of CH_2O at elevated temperatures due to the formation of methane coupling products, especially ethylene due to indicative generation of methyl radicals on their surfaces. Both heterogeneous and homogeneous catalytic oxidation of methane at 600-700℃ showed that, the reaction occurs on the surface and in bulk, with the heterogeneous reaction of alumina being much more intense than on silica.

An increase in internal surface area of a quartz reactor (Vella *et al.* 2010) by introducing quartz or Pyrex packing increases the initiation temperatures and as a result, there is increased residence time of the mixture in the reactor. This effect increases with a decrease in the size of the packing balls. More activity of pure SiO_2 in the conversion of methane to formaldehyde was observed with the selectivity of formaldehyde being lower, when the SiO_2 surface was coated with a metal oxide catalyst (Arena *et al.* 2009). Therefore, catalytic oxidation of methane continues with the formation of methoxide (CH_3OM) on the active site of the catalyst. Partial oxidation of methane on SiO_2 surface, was further analysed by semi-empirical methods (Ding *et al.* 2015) which showed that activation of methane by lattice oxygen in strained siloxane bonds was characterized by a high activation energy and hence, thermodynamically not desired.

2.5.3 Effect of methane residence time

Kinetic parameters documented in literature are used to determine the efficiency of methane decomposition process especially in terms of residence time.

The rate equation describing the process is;

$$r = \mathrm{K}P^{m}{}_{CH4} \tag{13}$$

Where P_{CH4} is the partial pressure of methane at atmospheric pressure, m is the reaction order (-1) and K is the rate constant for the reaction (Ermakova and Ermakov 2002)

From Arrhenius equation;

$$K = \mathrm{A}.e^{-E_a/R_u T} \tag{14}$$

Where A, is the frequency factor, $T$is the temperature (K), $E_a$is the activation energy in KJ/mol) and R_u,is the gas constant. In this case, the determination of the reaction rate is done by putting into consideration both the forward and reverse reaction steps;

$$r = \frac{dN}{dt} = K_{foward}.P^{m}{}_{CH4} - K_{reverse}.\ P^{n}{}_{H2} \tag{15}$$

Where N, is the amount of feed in (mol),t is the time in (s), the rate constant (K_{foward}), is calculated from equation (15) and n,is the reaction order for the reverse reaction which is near unity, while $K_{reverse}$,is calculated from equation (15) and taken as zero in most cases.

To calculate residence time of methane in a reactor, useful experimental data can be obtained from (Hornés *et al.* 2012) for unsupported nickel catalyst and from (Ermakova and Ermakov 2002) for activated carbon. The effect of residence time is studied by assuming that constant reaction rates are equal with reaction rates without considering catalyst deactivation. From Table 2-4 below (Ashik *et al.* 2015a), the rate of methane conversion decreases as the space velocity increases. This can be attributed to reduction of contact time between the reactants and the catalyst.

Table 2-4 Effect of space velocity for MCD reaction over NiCuAl catalyst at(T:700℃)

WHSPV ($1g^{-1}_{cat}h^{-1}$)	r_o(mmol/min.g_{cat})	X_{CH4}(%)	C_{dep}(g/g_{Cat})	r_c($g_c/g_{cat}.h^{-1}$)
24	10.38	54.61	45.8	7.02
60	15.01	31.36	39.0	15.60
120	34.27	31.2	46.8	20.06
240	58.31	20.09	64.6	25.84
480	79.95	11.63	84.0	33.60
1200	134.74	8.77	141.0	56.40

2.6 Catalyst life

2.6.1 Common catalyst preparation methods.

The methods of catalyst preparation are many and as such each individual catalyst may be produced via different routes. In each route, successive steps are involved in the catalyst preparation. Most catalysts (supported metal-oxides) are prepared by successive impregnation, drying, calcination and final activation while zeolite catalysts are prepared by precipitation of the gel, crystallization, washing, ion exchange and finally drying. Important stages in catalyst preparation are; pretreatment of the primary solid (1st precursor) by either impregnation or precipitation or crystallization for zeolites, processing of the primary solid by heat treatment and activation of the catalyst precursor by reduction of metal oxides to metal (hydrogenation), formation of sulfides (hydrodesulphurization) and deammoniation of (acidic zeolites).

2.6.1.1 Impregnation

In this method, a solid is contacted with a liquid containing the components to be deposited on the surface. During impregnation, many processes such as; selective adsorption of species (charged or not charged) by coulomb's force, van dar Waals forces, ion exchange between the charged surface and the electrolyte, polymerization of the species (ions or molecules) attached to the surface and partial dissolution of the surface of the solid takes place. Impregnation can be done through different methods such as;

- ✓ Impregnation by soaking or with excess solution in which excess liquid is eliminated by washing or draining. This technique works well where ion-solid interactions are involved.
- ✓ Dry or pore volume impregnation in which the required components are introduced in the volume corresponding to the support pore volume.
- ✓ Incipient wetness impregnation in which the amount of the solution is determined to correspond to the pore volume of the solute, beyond which, the catalyst begins to appear wet.
- ✓ Another method is deposition by selective reaction with the surface of the support in which the carrier is left to contact with an excess solution for a definite time and the excess liquid is removed by a dipping technique.
- ✓ Impregnation by percolation in which the precursor is sorbed or ion exchanged by percolation of the impregnating solution through a porous bed.
- ✓ Co-impregnation entails introduction of two or more components in a single step.
- ✓ Successive impregnation is where two or several components are introduced one after another in a sequence.

2.6.1.2 Precipitation and co-precipitation.

This method comprises of two distinct steps namely; nucleation and growth. Nucleation demands that the system is far from equilibrium (high super saturation or high solubility for ionic species). The new phase develops as conditions approach the equilibrium state. A phase involving two or more components; where one component is contained in an anion and the second component is in a cation then, the precipitated mixture will have a near fixed composition. If both are anions or cations, the nature of the reaction with a common anion or cation of the precipitate, the solubility constants and the super saturation values will all be different, and the property of the precipitate will change after some time. Low super saturation leads to poorly dispersed solids and highly dispersed solids are thermodynamically unstable and tend to lose stability. Special maturation (or ageing) step is carried out at the end of precipitation if specific effect is required. There are various precipitation and co-precipitation procedures, the simplest method being drop-wise addition of the solution rich in the desired chemical substance to the precipitating solution and vice versa.

The most widely used catalyst preparation procedures are; impregnation and co-precipitation (Abbas and Wan Daud 2010). A lot of water is required in the above methods for catalyst preparation steps (washing and filtering) which require more energy and time to accomplish. A comparative study of both impregnation and co-precipitation on fusion of metallic nitrates was done by (Suelves *et al.* 2006) and (Echegoyen *et al.* 2007). Based on the results obtained, they concluded that the decomposition rate of methane without catalyst deactivation remained the same in an 8-hour reaction period. Stability and activity of NiO-Al_2O_3-SiO_2 catalysts made by co-precipitation method have been reported by (Ashok *et al.* 2008) .

Catalysts for use in CMD reactions are prepared by different methods such as deposition precipitation (Ermakova *et al.* 2000), impregnation(Li *et al.* 2006), reverse impregnation (Suelves *et al.* 2006), mechanochemical activation (Chesnokov and Chichkan 2009) and fusion reverse impregnation (Suelves *et al.* 2006). Catalyst particle size, phase distribution and metal support interaction (MSI) influence the performance of the catalyst. Generally, catalysts prepared by impregnation and deposition-precipitation are suitable for low metal loading of catalyst (e.g. $<$20wt %) and have a weak metal support interaction.

Suitable catalysts specially for thin diameter MWCNTs and SWCNTs are prepared using Sol-gel method (Piao *et al.* 2002). For high carbon and hydrogen yield requiring a high metal loading catalyst, this method can also be used. In most catalyst preparation methods, a Feitknecht compound (FC) is widely used as a precursor to facilitate the formation of a precipitate which is uniform in surface area.

When calcined samples of nickel are reduced to metals from their respective metal oxides, nickel particles nucleate on the surface of the nickel oxide, while aluminium ions form alumina medium upon diffusion. To get a good catalyst (Chen *et al.* 2009b), an FC precursor of Ni/A_2O_3 is usually calcined at high temperature. High metal loading nickel catalysts are usually prepared by reverse impregnation method (Abd Hamid *et al.* 2017) by first synthesizing NiO through precipitation and then drying and calcining at high temperature. The synthesis of bulk Raney catalyst from metal alloys of; Fe, Co and Ni is done by draining out aluminium with NaOH solution at room temperature before use in methane decomposition process. Excellent results were achieved when Cu-Ni Raney-metal was thermally treated *in situ* at 873K in making Raney catalyst (Cunha *et al.* 2009b).

2.6.2 Catalyst deactivation

Products of CMD reaction are basically carbon and hydrogen. Carbon slowly accumulates on the catalyst surface forming graphite material which block active sites of the catalyst and hence, making them inactive (Forzatti and Lietti 1999). The deposited carbon nanomaterial contains impure graphite-like carbons which destroy structure of the catalyst when they increase in volume. It was reported by (Zhang and Amiridis 1998), that a small quantity of carbon ,i.e.10mg of carbon can deactivate 1g of catalyst. In large scale production, the process is controlled to avoid accumulation of carbon on catalyst surface (Chari *et al.* 2013).

Encapsulation of the metal particles within the hollow carbon fibres also contributes to catalyst deactivation (Zavarukhin and Kuvshinov 2004). Since nickel act as the active component in a catalyst system, a catalyst with high nickel content deactivates faster than that with lower nickel content due to the low accessibility of the nickel particles located inside the pores which are quickly obstructed by the deposited carbon nanomaterial. The effect of sulphur poisoning of Rh-Al_2O_3 catalyst was studied by adding up to 30ppm of either SO_2 or H_2S to methane feed at between 800-900℃ (Mancino *et al.* 2016). The yield of H_2 and CO was affected to a point where sulphur poisoning reached a saturation level for contents of ≥10ppm.

2.6.3 Catalyst regeneration

Continuous accumulation of coke on the catalyst active sites curtails its catalytic activity. Other than coking by carbon nanomaterial, sintering also affects the catalyst activity. Accumulation of carbon nanomaterial on the catalyst surface cannot be avoided as it is a by-product of methane decomposition; hence regeneration of encapsulated carbon at high temperatures is the only solution for an efficient CMD reaction. The main methods employed for catalyst regeneration are combustion and gasification of the deposited carbon nanomaterial. For combustion, Oxygen is used (Villacampa *et al.* 2003) and for gasification, steam is used (Aiello *et al.* 2000) or Carbon dioxide (Suelves *et al.* 2006). The above regeneration reactions can be represented using the following equations;

$C + O_2 \rightarrow CO_2$ ΔH_{1073}= -394.7 kJ/mol (16)

$C + H_2O \rightarrow CO_2 + H_2$ ΔH_{1073}= 135.9 kJ/mol (17)

$C + CO_2 \rightarrow 2CO$ ΔH_{298}= 171 kJ/mol (18)

2.6.3.1 Catalyst regeneration by gasification

Metallic catalysts and carbonaceous catalysts can be regenerated but at different conditions. Gasification is preferred because it inhibits further oxidation, heat shocks and increases hydrogen yield from steam. From previous studies involving 3.4 moles of hydrogen produced from a methane molecule, 1.4 extra moles of hydrogen was achieved during gasification by steam (Zhang and Amiridis 1998). The quantity of carbon yield in gasification process is less than that obtained during the decomposition process. A study of the relationship between surface area and converted carbon (Liu *et al.*), reveals that higher O_2 groups are found on the lower surface area after the regeneration process followed by low carbon accumulation and higher conversion rates.

In the work of (Choudhary *et al.* 2001), CMD experiments were performed in two fixed bed reactors at 500℃ using nickel/metal oxide and nickel/zeolite catalysts followed by catalyst regeneration. Based on the results obtained 82:100 carbon to catalyst in grams after 6hrs were obtained and 95% of the coked catalyst was re removed by steam.

2.6.3.2 Catalyst regeneration by combustion

Burning deposited carbon with oxygen eliminates deposited carbon formed on the catalyst more efficiently when compared to gasification. This method is desired because the process heat promotes continuous methane decomposition and is much faster as opposed to gasification. Catalysts with low metal weight % loading are easy to regenerate using combustion method (Cunha *et al.* 2009b) because low MSI promotes carbon accumulation at the backside of the metal catalyst particle.

Catalyst recovery is best achieved at high temperatures as demonstrated by (Saraswat and Pant 2013) in their work to recover Ni-Cu/SiO_2 from spent catalyst by passing O_2 with N_2 in a volumetric ratio of 1:3 at 550℃ . A decrease in catalyst activity from a value of 88% to 80% was experienced when the reaction temperature was lowered from 550℃ to 500℃ because carbon only deposited on catalyst face which is more exposed to gasification.

2.6.3.3 Catalyst regeneration by partial regeneration

This method is employed to avoid the problems of sintering of the catalyst and eventual poisoning during the recovery process. Since oxidizing the formed carbon nanomaterial is very

complex, partial regeneration method is usually employed to oxidize, the encapsulated carbon hence, carbon filaments continue to grow to sustain the metallic particle on the filament's edge from where carbon nanomaterial accumulates.

At this point therefore, the catalyst life is retained several times leaving the main filament un-affected. Other than, full gasification, gasifying a fraction of the accumulated nanocarbon is a viable option to maintain catalyst life.

2.7 Catalytic methane decomposition fundamentals

2.7.1 Overview

Catalytic decomposition of methane occurs in a series of steps. Some key reaction steps in CMD reaction involve; activation of methane molecule, nucleation of carbon nanomaterial and finally growth of carbon nanomaterial. A methane molecule adsorbs dissociatively on the metal surface into hydrogen and carbon atoms.

2.7.2 Activation of methane on metal surface

According to (Snoeck *et al.* 1997),when a methane molecule decomposes, detachment of the first hydrogen atom is considered as the rate determining step of the CMD reaction. Based on density function theory (DFT) calculations (Watwe *et al.* 2000), it was found that dissociation of the first methane molecule on nickel (111) had an activation energy of 127kJ/mol after the electrons were completely polarized. From several studies (Carstens and Bell 1996) especially of SiO_2 and Al_2O_3 supported on Ru nanoparticles, the results showed a yield apparent sticking coefficient (100-1000) times lower than that reported by (Egeberg *et al.* 2002) for methane on Rubidium (0001) on the face of the crystal.

Methane decomposition over carbonaceous catalysts starts when a methane molecule dissociates, followed by multiple chain reactions which leads to hydrogen and carbon nanomaterial. At the start, methane molecule interacts with chemically reactive carbon crystallites to overcome the C-H bond energy forming new carbon-carbon bonds in a hexagonal shape. The new carbon phase forms because of formation of carbon nuclei and growth of carbon nanomaterial. Carbon black is most stable because of easy reach by methane molecules but it is less active (Suelves *et al.* 2007).

2.7.3 Common catalytic methane decomposition methods.

Common methane decomposition methods are; partial oxidation, steam methane reforming and catalytic decomposition of methane.

2.7.3.1 Partial Oxidation

Catalytic partial oxidation of methane is an attractive method in economic and in technical aspects (Acar and Dincer 2014). In this method, the reaction takes place accompanied by release of process heat. The produced heat can be re-used in other process stages hence making it less-energy and capital-intensive and the lower H_2/CO ratio of 2 achieved in this process is more favorable with respect to downstream processes such as the synthesis of methanol. Methane can be converted into syngas directly or indirectly (Meher Kotay and Das 2008). In indirect pattern, a fraction of methane feed is combusted with CO_2 and H_2O in the oxygen atmosphere and balance methane interacts with CO_2 and water to produce CO and hydrogen. Catalytic partial oxidation of methane takes place according to the equations below;

$$CH_4 + 2O_2 = CO_2 + 2H_2O \quad (19)$$

$$CH_4 + H_2O \leftrightarrow CO + 3H_2 \quad (20)$$

$$CH_4 + CO_2 \leftrightarrow 2CO + 2H_2 \quad (21)$$

In this method, methane and other higher hydrocarbons can be converted into syngas at short contact times. This has been done using structured catalysts comprising of ceramic and metal foil honey combs (Lemus and Martínez Duart 2010), gauzes, foams (Tanksale *et al.* 2010) and microchannel plates (Levin and Chahine 2010).

2.7.3.2 Steam methane reforming

In this method, natural gas is first heated in coils which are in the waste heat section of the reformer and then sulfur is removed over a zinc oxide catalyst. Steam that is generated in the process is added to process mixture (steam and natural gas) to further pre-heat the feed before entering the tubular reformer. The process of converting hydrocarbons to hydrogen, carbon monoxide and carbon dioxide at equilibrium takes place over a nickel based reforming catalyst. Hydrogen production from steam reforming (SMR) takes place according to equation (22) (Saito *et al.* 2017) below;

$CH_4 + H_2O \rightarrow CO + 3H_2$ (22)

The reformer exit products are usually cooled before entering the shift converter where temperature shift takes. More hydrogen is produced over a shift catalyst by turning carbon monoxide and steam to carbon dioxide and hydrogen. The shifted gas is further cooled to room temperature before entering the pressure swing adsorption (PSA) unit. Pure hydrogen is obtained and the flue gas from the PSA section is used in the reformer as a fuel supplement with natural gas. It has been reported (Nikolaidis and Poullikkas 2017) , that hydrogen from steam reforming of hydrocarbons constitutes bulk of present day hydrogen.

2.7.3.3 Catalytic decomposition of methane.

In catalytic decomposition of methane (Shinkarev *et al.* 2010), a methane molecule decomposes into gaseous hydrogen, carbon and traces of higher hydrocarbons such as benzene,toluene,naphthalene and C_2 aromatics. The main products of the decomposition reaction are given in the equation below;

$CH_4 \rightarrow C+2H_2 \quad \Delta H°r = +74.9KJ/mol$ (23)

$\Delta H°r$ is the reaction enthalpy at a reference temperature of 298K. By considering the equilibrium composition of the gas mixture, the maximum conversion at a certain temperature can be calculated. According to (Villacampa *et al.* 2003), Gibbs energy is temperature dependent.

$\Delta G°\ (T) = 89658.88-102.27T- 0.00428T^2- 2499358.99T^{-1}$ (24)

Equation (24) above is applicable with the assumption that graphite indeed forms on the face of the catalyst particle. Gibbs energy can also be expressed in terms of equilibrium constant K_p;

$\Delta G_R\ (T)=\Delta G°(T) +R_u(T)\ln K_p$ (25)

Where T is the reaction temperature in (K) and R_u is the gas constant (8.314J/molK). At equilibrium, Gibbs energy tends to zero. In CMD reactions, the equilibrium constant is also a function of the partial pressure of methane (p_{CH4}) and partial pressure of hydrogen (p_{H_2}) at atmospheric pressure.

Since fossil fuels generate greenhouse gases such as CO_2 and methane that cause global warming (Castaldo *et al.* 2015) other sources of energy are being exploited (Ghandehariun *et al.* 2016) to reduce emission of these pollutants into the atmosphere. In these new methods, greenhouse gases are being used as feedstock for partial oxidation, steam reforming and dry reforming. Present day hydrogen is produced from fossil fuels and one attractive route is catalytic decomposition of methane (Shen and Lua 2015). Catalytic methane decomposition (CMD) produces clean hydrogen and associated carbon oxides formed with conventional reforming of methane are eliminated in the in the CMD process (Toebes *et al.* 2002). Despite these advantages, the CMD process has not been fully commercialized due to unavailability of a suitable catalyst system. In order to commercialize the process, studies on several metal catalysts and supports have been investigated extensively (Al-Fatesh *et al.* 2016). The overall performance of the catalysts for CMD process depends on all the catalyst components namely; the metals, the support and the promoters.

2.7.4 Reaction kinetics

According to (Snoeck *et al.* 1997), the CMD reaction proceeds as follows on the active site S:

$$CH_4 + nS \leftrightarrow CH_4\,Sn \quad (26)$$

$$CH_4\,Sn \leftrightarrow CH_3Sn + HS \leftrightarrow \ldots\ldots\ldots \leftrightarrow CS_{n-4} + 4HS \quad (27)$$

$$C\,S_{n-4} \leftrightarrow C + (n-4)S \quad (28)$$

$$HS \leftrightarrow \frac{1}{2}H_2 + S \quad (29)$$

The Langmuir-Hinshelwood type rate equation was obtained as follows;

$$(1 + K_H {p_{H_2}}^{0.5}) \quad (30)$$

$$r = \left(\frac{k(pCH4 - p^2 H_2)/Ke}{(1 + K_H {p_{H_2}}^{0.5})^n}\right) \quad (31)$$

Assumption; C-H bond dissociation is considered as the rate determining step

Where r is the reaction rate, K is the rate constant of CNF growth, K_e is the equilibrium constant of hydrogen adsorption,p_{CH4} the partial pressure of methane and H_2 is the partial pressure of H_2.

When n equals to 7, this model fits the experimental data well and results in activation energy of 88.2kJ/mol. The kinetic model was built based on the effect of reaction condition on the decay of the activity in which the deactivation rate increases with an increase in reaction temperature and it is proportional to p_{CH4}/p_{H2}(,p_{CH4}kpa). Removal of the first hydrogen atom constitutes the rate determining step in this model and consequently, a methyl group is formed.

$$r = \frac{k^{+}M.KCH_{4.-}(K_M K_r).pH_2}{(1+\left(\frac{1}{K_r}\right).P^{\frac{3}{2}}H_2+K_{CH4}.p_{CH4})} \quad (32)$$

In which,

$$K^{-}{}_M = K^{-}{}_M.K^{1/2}{}_M \quad (33)$$

$$K''{}_r = \frac{K_3 K_4 K_5}{K_H{}^{3/2} K_C C_{C,(Ni,f)}} \quad (34)$$

In these equations p_i, represents partial pressure of i, $c_{C,(Ni,f)}$,(mol C/m^3 Ni) is the concentration of carbon dissolved in nickel at the face of the particle, just below the selvedge (gas side),$K^{-}{}_M$ and $K^{1/2}{}_M$ are the rate constants for the forward and reverse reactions of the rate determining step and K is a symbol used for the equilibrium coefficient.

Therefore, dissociations of CH_3, CH_2 or CH were found not to be the rate limiting steps and as a result, the C-H bond dissociations could be the rate determining step (Snoeck *et al.* 1997). While using a tapered element oscillating microbalance (TEOM) to study the reaction kinetics on an FC-derived Ni catalyst reaction, (Kvande *et al.* 2008) found out that, the initial reaction rate and the steady state reaction are identified and the activation energy to be 64.6KJ/mol similar to carbon diffusion on the nickel (111) surface estimated by a DFT method.

2.7.5 Decomposition products

Major products of catalytic decomposition of methane are carbon nanomaterial and high purity hydrogen (Dincer and Acar 2015).

2.7.5.1 Hydrogen

Hydrogen is abundantly found on earth and is the major source of raw material in a chemical and petroleum industries. Hydrogen demand is expected to increase because of two reasons namely; major hydrogen production raw materials like water, biogas and biomass are renewable and water is the only by-product during its combustion and oxidation (Demirci and Miele 2013).

In fuel cells, hydrogen and oxygen combine to produce heat, electricity and water. On a larger scale, hydrogen is a possible alternative to conventional fuel due to its widespread production and distribution. The occurrence of hydrogen on earth is mainly in its compounds such as water, biomass or in hydrocarbons. During combustion of hydrogen, the energy produced is 3 times higher than that produced by any other means when evaluated on mass basis (Ashik *et al.* 2015b). The environmentally benign characteristic of hydrogen has led to its huge demand in recent years, especially in industrial applications and merchant uses (Amin *et al.* 2011; Amin *et al.* 2012). Since hydrogen is not a primary fuel, it can be extracted from water, biomass or from any other hydrocarbon without contaminating the environment (Nasir Uddin *et al.* 2013). Gasification of coal, water splitting, and thermochemical cracking of methane are other methods of producing hydrogen. The hydrogen produced by cracking of methane is free of carbonaceous compounds and can thus be directly used in a H_2-O_2 fuel cell and in internal combustion engine. Table 2-5 below shows the higher heating values (HHV) and lower heating values (LHV) of hydrogen and other conventional fossil fuels (Dincer and Acar 2015). From the table, an increase in the amount of HHV and LHV makes hydrogen stand out as a more attractive fuel source, hence a reduction in environmental impact. Therefore, its use is a distinct advantage in reducing carbon emissions into the atmosphere.

Table 2-5 HHV and LHV of hydrogen and common fossil fuels at 25C℃ and 1 atmosphere.

Fuel	HHV (KJ/kg)	LHV(KJ/kg)
Hydrogen	141.9	119.9
Methane	55.5	50.0
Gasoline	47.5	44.5
Diesel	44.8	42.5
Methanol	20.0	18.1

Some of the advantages of using hydrogen are; high energy conversion efficiencies, easily produced from water with no emissions, abundance, flexible storage methods, ease of transportation, and ready transformation to other forms of energy and higher values of (HHV) and (LHV) compared to most fossil fuel sources.

2.7.5.2 Carbon nanomaterial

In an CMD reaction, the following carbon nanomaterial can be obtained; carbon nanotubes (Chen *et al.* 1997), carbon nanofibers (Zhang *et al.* 2001), carbon encapsulated on metal and nanoonions (He *et al.* 2006). From these primary structures, emanates different configurations and different textures of carbon nanomaterial in parallel bundles, self-woven particles and octopus like units.

The build-up of graphene layers at different angles represents 3-d coordinated carbon as proper single walled carbon nanotubes (SWCNTs) and multi walled carbon nanotubes (MWCNTs) as annular concentric cylinders of graphite. The angle $(\propto)$between two graphene layers can also be used to classify carbon nanotubes since the $(\propto)$ of the platelet type carbon nanofiber (CNF) is close to 180° and the angle of the fish-bone type has distinct $(\propto)$values, i.e. $40° < \propto < 160°$. Structures of bamboo shaped CNFs have a periodical replication of hollow CNFs which are formed due to systematic movement of metal particles (Li *et al.* 2002) while carbon onions have graphite structured material and consists of many spherical shells and hollow filled core with minute distance between the graphitic planes in the shell (He *et al.* 2006).

Since reaction conditions determine the physical properties of the CNFs formed, the properties of CNFs formed using a Ni-Cu-Mg-Al catalyst determines the structure of the CNFs and draws its physical properties from the parent metal particles. The rates of carbon diffusion both at low and high reaction temperatures are different and that is why low temperatures favour CNTs growth and elevated temperatures favour the growth of hollow CNFs. Between 773-873K, the catalyst particles are distinct and rigid but above 973K, metal particles are almost in molten state with elongated shape, hence the generation of hollow CNFs (Chen *et al.* 2004).

Herringbone (or fishbone) type of CNFs has been found deposited on a catalyst with nickel as the active component when methane and hydrogen are mixed in the gas feed is at low temperature. According to (Takenaka *et al.* 2003),there are two models for fishbone-type CNFs

which are cup-stack and helical texture. In cup-stack model, the CNFs formed resembles a bowl in shape while in helical model, there is only one continuous layer of graphite. The cup-stack model was favoured because the CNF samples were easy to separate during grinding process but at low shearing energy.

A feed of CH_4:H_2 in the ratio 1:2 respectively (Chen *et al.* 2001) on a Ni-Cu/Al_2O_3 catalyst at 993-1013K generates CNFs which are bamboo-like with well-developed knots. The phenomenon of a jump movement of the metal particle and driving force from the deposited carbon depends on physical properties. According to (Chen *et al.* 2001), there exists a growth mechanism in which two kinds of movement of the metal particles are involved in the formation of bamboo-shaped CNTs; a smooth movement driven by the intersection of new carbon layers at the carbon metal interface leading to the formation of a continuous and uniform wall and curve only when the metal particle is in a quasi-liquid state. Upon formation of a new carbon layer, force builds up on the metal particle towards its axis and growing direction thus accumulating stress. In this case, a jump of the particle only happens when the stress becomes more than the combination force of metal and carbon. Catalyst surface area and porosity determines the amount of carbon diffusion through it and this constitutes reaction determining step.

The shape of carbon nanomaterial can change from spherical to elliptical (Purohit *et al.* 2014) and can continuously deform in order to remain stable until the energy lost from being stretched exceeds the energy gained from being held to the graphine layer. Formation of hollow carbon nanotubes growing away from the particle is attributed to the presence of hemifullerence cap formed on the partially filled carbon-carbon coated particle after the cap is lifted. Results obtained using factorial design of experiment (Kuo *et al.* 2005), established that, the growth of CNFs of diameter 7.0-21.8nm is dependent on CMD reaction temperature, the pressure and the methane flow rate.

2.7.6 Thermodynamic challenges in methane conversion.

Dissociation of a methane molecule into carbon and hydrogen takes place in several steps. These chain reactions yield intermediates which are more reactive than methane itself and therefore, separation and recycling of unconverted methane in the product stream can only be achieved at low conversion levels. High temperatures do favor high syngas production rendering the catalyst

less important due to radical reactions and deactivation of catalysts increases with an increase in temperature. Most methane decomposition processes are operated batch wise due to loss of catalyst life, hence the need to stop the process and regenerate the catalyst.

At temperatures well above 1000℃, the issue of carbon clogging the reactor becomes more pronounced (Keipi *et al.* 2016) and the residence times can be very short. Hardness of deposited carbon increases with temperature which complicates carbon removal from the reactor. In the presence of the catalyst, the methane decomposition process can occur at less than 1000℃,but the main challenge is catalyst becoming deactivated as a result of carbon deposition (Keipi *et al.* 2016).

2.8 Market value of decomposition products.

Presently, the market stock of carbon nanomaterial is projected to be as follows; 8.1-9.4million tons of carbon black, 1.9million tons of activated carbon and 500million tons of metallurgical coke (Keipi *et al.* 2016). The same researchers showed that, the yearly production of carbon nanotubes was 2500 tons in 2010 with a projected increase to 12000 tons in 2016.

From statistics, annual consumption of natural gas was 3.4 trillion m^3 in 2014 and the global annual production of hydrogen was 60 million tons in 2013. Carbon finds its use as building material in building industry, direct carbon cells and soil amendment (Muradov 2001b). Generally, carbon is desired based on its particle size, strength and distribution. On the market front presently, the market value for carbon is estimated to be 1500 $/ ton of activated carbon, carbon black (555-444) $ / ton and the value of metallurgical coke is 150€ per ton. The market value of CNTs research grade is 0.6-10 $/g and that of the industrial grade is 380 $/ ton for a diameter of 10 to 30nm.

The other decomposition product of methane is hydrogen whose commercial value is in the range of 0.0555-0.1111€ per ton of hydrogen from natural gas steam reforming and 0.177-0.333€ per ton for the hydrogen grade that comes from electrolysis. As shown in table 2-6 below, the global market price of hydrogen gas depends on the purity of the hydrogen gas (Y. Li *et al.*2017). The highest purity grade fetches the highest retail price. Some challenges associated with utilization of hydrogen energy are; emission of carbonaceous compounds from major

hydrogen producing technologies and handling and storage challenges due to flammability of the gas.

Table 2-6: Global market price of hydrogen gas of different purities (2017)

Purity of hydrogen gas	Retail price of hydrogen ($/Kg-$H_2$)
99.9%	4.2
99.99%	5.2
99.999%	6.0
99.9999%	6.9

2.9 Basis of research

Despite adequate use of metal catalysts such as nickel, iron, cobalt and molybdenum in catalytic decomposition of methane, their draw backs such as coking, sintering and limited selectivity have not been adequately addressed. A gap still exists in the efficient catalytic decomposition of methane to hydrogen and carbon in that a catalyst that has enhanced performance characteristics still needs to be developed. One such noble idea could be the development and commercialisation of a supported molten metal catalyst which can eliminate draw backs of conventional solid metal catalysts such as sintering, coking and limited selectivity.

Such an invention should develop a catalyst which has;

- ✓ High rates of reaction due to efficient catalyst utilization
- ✓ High catalytic performance due to dispersion owing to thinness
- ✓ Absence of corrosion since the catalyst is confined inside the walls of the refractory support and doesn't meet the walls of the reactor.
- ✓ Deactivation due to sintering is avoided.
- ✓ High rates of reaction due to efficient catalyst utilization.
- ✓ No sophistication required in their preparation.

The development of a supported molten metal catalyst in this work aims at addressing the above deficiencies and can be commercially explored for use in catalytic decomposition of methane on industrial scale.

CHAPTER 3. METHODOLOGY

3.1 Introduction

The method employed in this study is purely experimental. In the present work samples of catalyst precursors have been designated as catalysts because they were found to be reactive in methane decomposition. Therefore, 5 different catalysts with varying amounts of nickel and lithium on a calcium oxide support were synthesized, characterized using XRD, BET, SEM and TEM and the actual catalytic methane decomposition experiment was done in a stainless steel packed bed reactor. The products of methane decomposition were analyzed using a gas chromatograph (Shimadzu-2014).

3.2 Catalyst preparation

3.2.1 Chemicals for catalyst preparation

- Nickel nitrate hexahydrate ($Ni(NO)_3.6H_2O$)
- Lithium hydroxide monohydrate ($LiOH.H_2O$)
- Calcium oxide (CaO)
- Methane gas (99% pure) in the feed ($20\%CH_4$:$80\%N_2$)
- Hydrogen gas (99% pure) in the feed ($10\%H_2$:$90\%N_2$)
- Nitrogen gas for reactor purging.
- Distilled water

3.2.2 Equipment and materials for catalyst preparation

- Pyrex beakers
- Burette
- Porcelain mortars and pestle
- Reagent bottles
- Stirring rods
- Spatula
- Watch/timer
- Oven for catalyst drying
- Furnace for calcination
- Quartz wool
- Custom made stainless steel tube reactor

- Gas bombs
- Gas chromatograph (Shimadzu GC-2014)

3.2.3 Catalyst preparation procedure

The method employed in catalyst preparation was incipient wetness impregnation which entailed admixing of nickel nitrate hexahydrate and lithium hydroxide monohydrate aqueous solutions and depositing the resultant solution on solid calcium oxide, drying, calcining to get rid of the residual moisture from the catalyst and reducing in a hydrogen atmosphere ($10\%H_2$:$90\%N_2$). In this present work, the supported molten metal catalyst was prepared and characterized in the laboratory according to procedures previously done by (Lee *et al.* 2016). The precursor of nickel which is nickel nitrate hexahydrate $Ni(NO_3)_2).6H_2O$ and lithium precursor being lithium hydroxide monohydrate($LiOH.H_2O$) were dissolved in distilled water in exact quantities as shown in Table I-1 in appendix I for each catalyst and the resultant solution added to porous calcium oxide dropwise until incipient wetness was reached. The mixture was stirred for 2hrs at 50℃ and left to dry at 120℃ for 15hrs, after which, it was calcined at 400℃ at heating rate of 5℃ min^{-1} for 5hrs. The calcined catalysts were then characterized by XRD, SEM and BET to ascertain their size, structure, morphology and surface area. The synthesized catalysts were designated based on wt% as shown in Table 3-1 below;

Table 3-1 Catalyst nomenclature and designation

Catalyst	Composition (Wt%)
50%Ni/CaO	50%Ni:50%CaO
37.5%Ni-12.5%Li/CaO	37.5%Ni:12.5%Li:50%CaO
25.0%Ni-25.0%Li/CaO	25%Ni:25%Li:50%CaO
12.5%Ni-37.5%Li/CaO	12.5%Ni:37.5Li%:50%CaO
50%Li/CaO	50%Li:50%CaO

3.3 Catalyst characterization

To obtain information on particle size, shape, surface area and phase composition, the catalysts were characterized by XRD, BET, SEM and TEM

3.3.1 Characterization of the synthesized catalyst

3.3.1.1 XRD-analysis

X-ray diffraction (XRD) analyses of fresh catalysts were carried out sing an XRD instrument (BRUKER AXS-Germany) equipped with a diffractometer (D8 Advance). The measurements were done continuously on a J-J scan in locked coupled mode and the tube was Cu-Ka radiation (lKa_1=1.5406Å). Lynx Eye (Position sensitive detector) at 40kV and 40mA with a V20 variable slit was used. The measurement range was 0.5° to 130° with an increment (D2J: 0.034°) most of the time. Data evaluation was done using EVA software from BRUKER **(**PDF database 1999).

Crystallite size of individual catalyst sizes was calculated using Scherrer equation. The Scherrer equation is given by:

$$B = \frac{k\lambda}{L\cos\theta} \tag{35}$$

Where B = the breadth of half-peak height of an XRD line

L = the size of the crystallites

λ = X-ray wavelength

θ = diffraction angle

K = a constant usually equal to 1

3.3.1.2 SEM analysis

Scanning electron microscopy (SEM) was done using (FEI Nova Nano SEM 230) instrument with a field emission gun to analyse particle size of synthesized catalysts. The samples were imaged using the high-resolution immersion lens. The EDS detector (Oxford X-Max equipped with INCA software Landing E 5.00KeV) and a working distance of HFW 5.97-29.8, Sopt3.5 and WD (5.8-6.7 was used. The samples were prepared by sprinkling a small amount of the sample onto a 12mm aluminium SEM stub covered in carbon glue. The excess sample was blown off with compressed air and the samples were carbon coated before being loaded into the SEM equipment.

3.3.1.3 BET analysis

The specific areas, pore volume and particle size distributions of the catalysts were determined from N_2 adsorption-desorption data at -196℃ using a Micromeritics Tristar II 3020 instrument. For each analysis,0.2g of each catalyst was degassed at 150℃ for 2 hours to remove residual moisture from the catalyst surface and other adsorbed gases before loading the samples on the BET instrument. Specific surface areas were calculated according to B.E.T method and the pore size distributions were obtained according to Barrete Joynere Halenda (BJH) method from the desorption isotherm data.

3.4 Characterization of spent catalyst

To analyze the particle size, shape and morphology of deposited carbon nanomaterial on the catalyst, Transmission Electron Microscopy (TEM) analysis was used.

3.4.1 TEM analysis

The instrument used in TEM analysis was (JEOL JEM-1010-South Korea, equipped with a high-resolution camera). Before the test, 5mg of each catalyst was prepared by ultrasonic dispersion in isopropyl alcohol and sonicated for 10mins. After sonication, a drop of each catalyst was deposited on a carbon supported film and dried for 15mins before putting the sample in the TEM machine. Statistical data on particle size, shape and morphology was then generated using the inbuilt software in the instrument.

3.5 Catalyst performance

Actual catalytic decomposition of methane experiment was performed in a straight stainless steel packed bed reactor (ID 9.5mm, OD 13mm, 450mm long). Before the CMD reaction, the reactor was purged with nitrogen for 30mins. The performance of each catalyst was evaluated in terms of methane conversion, hydrogen yield, hydrogen purity and carbon yield.

3.5.1 Experimental procedure.

For each decomposition run, a stainless steel packed bed reactor was weighed at 25℃, placed in the heating zone of the furnace equipped with a thermocouple (J-type), purged with nitrogen at 50 ml/min for 30mins and loaded with 0.4g of catalyst. The catalyst was held in the middle of the reactor using 0.4g of Quartz wool as a catalyst bed support. The quartz wool was also weighed and recorded. Heating was adjusted manually until the desired temperature was

attained. Then methane/nitrogen gas feed (20%CH_4:80%N_2) was let into the reactor at a metered flowrate from the top of the reactor and the gaseous products exited from the bottom of the reactor for analysis. Gas sampling was done at an interval of 18 mins up to 90 mins using potable gas bombs attached to reactor product stream. Every decomposition run was done for 90mins. After each run, the reactor was allowed to cool in air up to ambient temperature and its final weight determined to establish microscopic weight changes on the catalyst due to coke deposition.

3.5.2 Methane Conversion

The conversion of methane was determined by measuring the volume of methane into and out of the reactor after one complete run.

The formula below was used;

$$CH_4 \text{ Conversion } (\%) = \frac{CH4\ in - CH4\ out}{CH4\ in} \text{ x } 100 \quad (36)$$

3.5.3 Hydrogen yield and purity

The hydrogen yield was determined by measuring the total volume of hydrogen out of the reactor after one complete run. Peak areas under hydrogen TCD signals were used to determine its composition relative to other gases in the product stream. The formula below was used;

$$\text{Hydrogen yield } (\%) = \frac{H2\ out}{2\ X\ CH4\ (in)} \text{ x } 100 \quad (37)$$

3.5.4 Carbon yield

To determine the actual amount of deposited coke on each catalyst, the following procedure was adopted. A reactor with 0.4g of catalyst and 0.4g of quartz wool was weighed at 25℃ and its weight recorded. Then the reactor was put into the furnace for the reaction to take place at 650℃ for 90 mins after which it was left to cool in air up to ambient temperature and weighed again. The difference in weight was taken as the amount of deposited carbon on the catalyst. Carbon yield (%) was calculated using equation (38) below;

$$\text{Carbon yield } (\%) = \frac{No.\ of\ moles\ of\ deposited\ carbon}{No.\ of\ moles\ of\ methane\ in\ feed\ x\ 1} \text{ x } 100 \quad (38)$$

3.6 Block flow diagram for catalytic methane decomposition

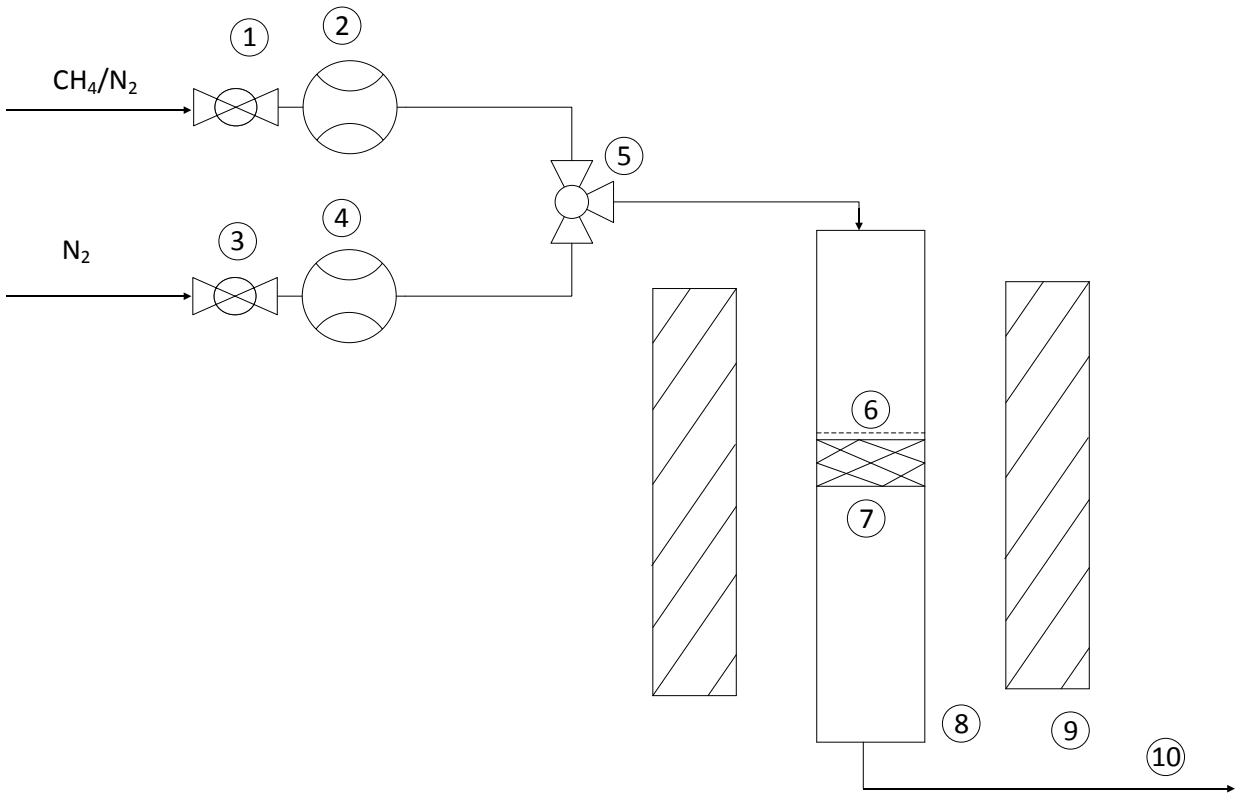

Fig 3-1 Process flow diagram for methane decomposition

1-Ball valve, 2-Flow meter, 3-Ball valve, 4-Flow meter, 5-3way plug valve, 6-Catalyst, 7-Quartz wool, 8-Reactor, 9-Furnace, 10-Gaseous products.

3.7 CMD reaction operating conditions

- Reactor temperature regions were; 500℃, 550℃, 600℃, 650℃ and 700℃.
- GHSVs; (2, 3 and 4) $Lg^{-1}{}_{cat}h^{-1}$
- Reactor pressure: Atmospheric pressure
- Ambient temperature

3.8 Analytical equipment Operating conditions

Figure 3-2 below shows the photograph of the analytical instrument which was used to analyze CMD gaseous products.

Fig 3-2 Photograph of Gas chromatograph used in the analysis

Gaseous products of CMD reaction were determined by TCD analysis using a gas chromatograph equipped with a Porapark column. During the analysis, instrument operating parameters were maintained as follows;

- Carrier gas used-nitrogen
- Detector temperature; 250℃
- Injector temperature; 180℃
- Current; 50 mA
- Hold time;9999.9mins
- Flow rate 12ml/min
- Inlet pressure 60KPa

CHAPTER 4. RESULTS AND DISCUSSION

4.1 Catalyst characterization

Fresh synthesized catalysts and spent catalysts after the CMD reaction were characterised using various techniques to ascertain their structural properties. Structural properties of fresh catalysts had a bearing on catalyst performance while the morphological properties of the spent catalyst gave an insight into the size and nature of deposited carbon nanomaterial.

4.1.1 XRD-Patterns of the synthesized catalyst

XRD analyses of fresh synthesized catalyst was done using an XRD instrument and Match software was used to interpret the results. From the results, the XRD patterns of 50%Ni/CaO catalyst as shown in Figure 4-1 shows the presence of three distinct phases namely; NiO, CaO and $Ca(OH)_2$. Peaks for NiO at 2θ =38°, 44°, 63°, 77°, and 80° correspond to (111), (200) and (220) crystal planes which are in agreement with that in JCPDS file (4-0835) and in other reports (Dharmaraj *et al.* 2006). The peaks for $Ca(OH)_2$ at 2θ =17°, 28°, 32° and 46° are identified as portlandite in JCPDS file (72-0156) and also in other reports (López-Arce *et al.* 2011). The third phase corresponds to CaO whose peaks at 2θ=31°, 34°, 38°, 54°, 63° and 67° and is similar to (111), (200), (220) and (311) crystal planes in standard JCPDS file (82-1691) and in other reports (Balázsi *et al.* 2007).

Catalyst 50%Ni/CaO is less crystalline due to formation of complex intermediates of the nickel nitrate decomposition process hexahydrate ((Brockner *et al.* 2007). The intermediates such as; HNO_3, NO, NO_2, Ni_2O_3 and $Ni(NO)_2.2H_2O$ formed adversely affect the catalyst crystal lattice. This is the reason why the crystallites in the catalyst are seen in lumps heaped on each other. Table 4-1 below shows the size of crystallites calculated manually using Scherrer equation. Sample calculations of crystallite sizes using Scherrer equation are illustrated in appendix B.

Table 4-1 Crystallite size of each catalyst determined Debye Scherer equation (Equation 35)

Catalyst	Average crystallite diameter (nm)
37.5%Ni-12.5%Li/CaO	5.35
50%Ni/CaO	6.10
12.5%Ni-37.5Li%/CaO	7.25
50%Li/CaO	7.5
25%Ni-25%Li/CaO	7.65

XRD profile for different crystallite sizes of the synthesized catalysts are as shown below;

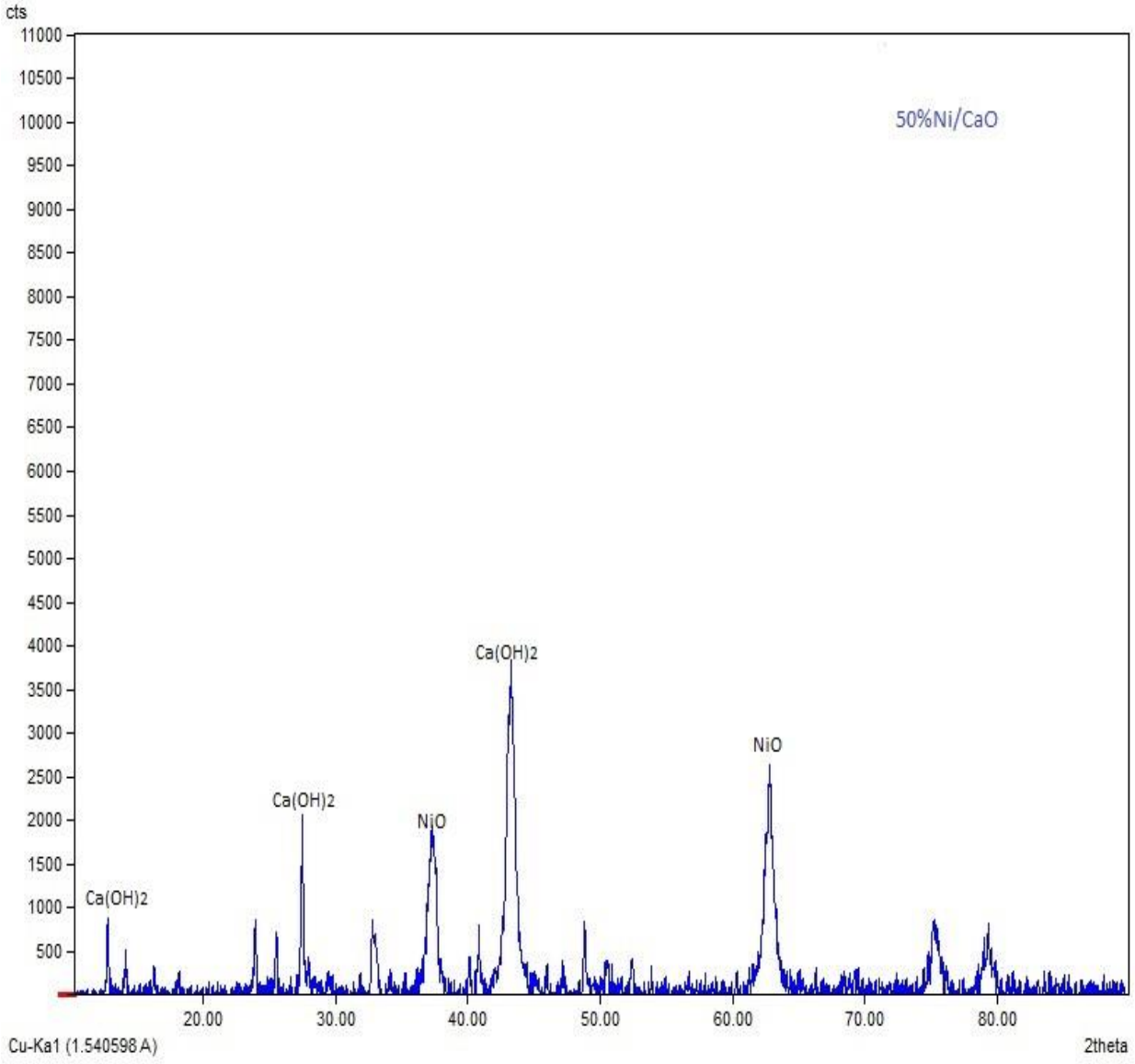

Fig 4-1 XRD pattern for 50%Ni/CaO catalyst

Catalysts 37.5%Ni-12.5%Li/CaO, 25.0%Ni-25.0%Li/CaO as shown in Figure 4-2, Figure 4-3 and Figure 4-4 respectively, shows the presence of three phases namely; NiO whose peaks at 2θ =38°, 44°, 63°, 77°, and 80°, $Ca(OH)_2$ whose peaks at 2θ =17°, 28°, 32° and 46° and LiOH whose peaks at 2θ =17°, 21°, 26°, 30°, 32° , 36° , 37° and 38°. The peaks for LiOH correspond to those in JCPDS file (25-486) and in other reports (Kiat *et al.* 1998). Apart from positive identification of the peaks in these catalysts, the intensity of LiOH peaks increases as the amount of lithium increases in the catalyst.

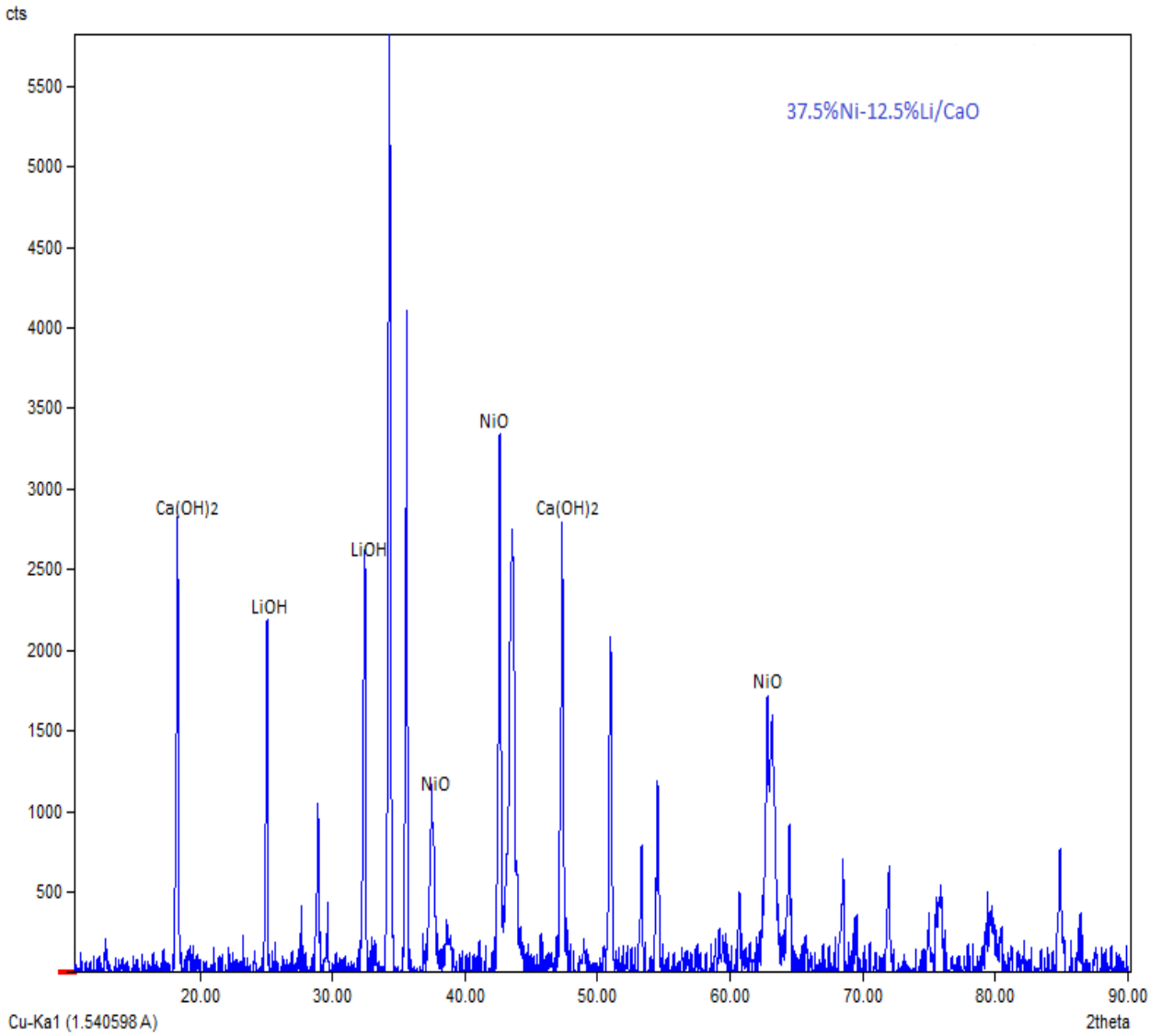

Fig 4-2 XRD pattern for 37.5%Ni-12.5%Li/CaO catalyst

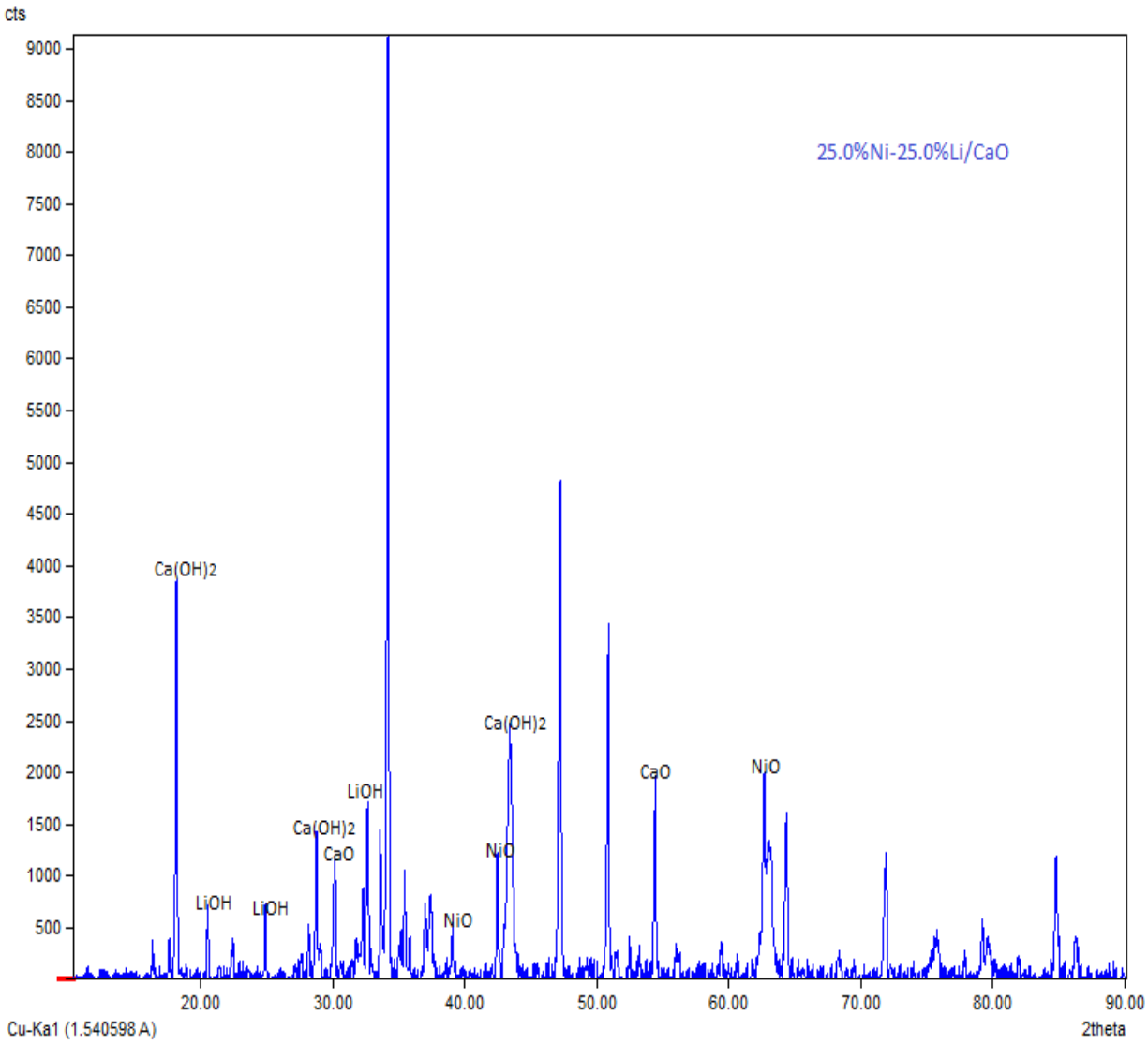

Fig 4-3 XRD pattern for 25.0%Ni-25.0%Li/CaO catalyst

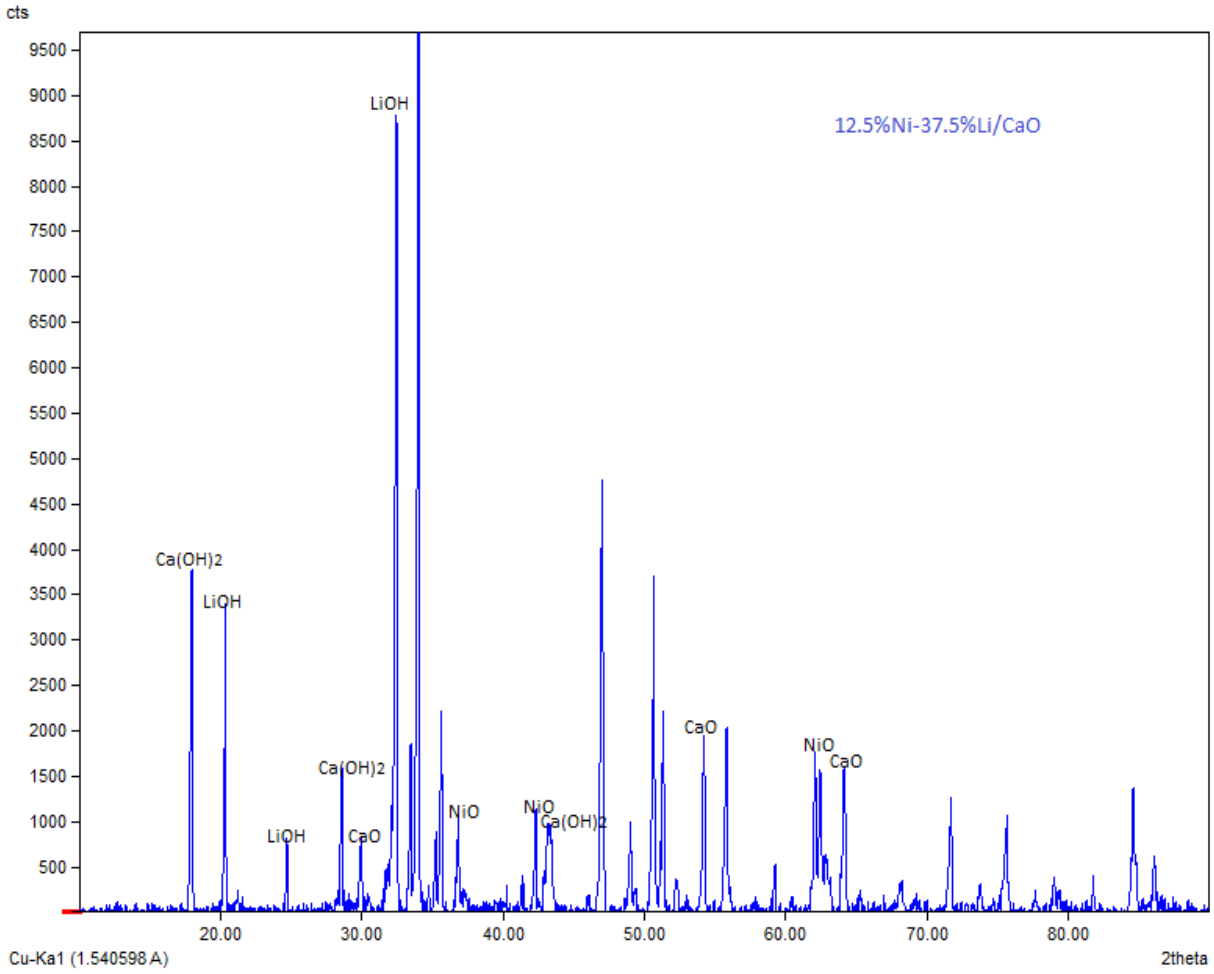

Fig 4-4 XRD pattern for 12.5%Ni-37.5%Li/CaO catalyst

Figure4-5 below shows the XRD patterns of catalyst 50%Li/CaO. In this catalyst, only two phases namely; $Ca(OH)_2$ whose peaks at 2θ =17°, 28°, 32° and 46° and LiOH whose peaks at 2θ =17°, 21°, 26°, 30°, 32°, 36°, 37° and 38° manifest themselves. Strong intensity of the peaks shows that the structural lattice of the catalyst is crystalline

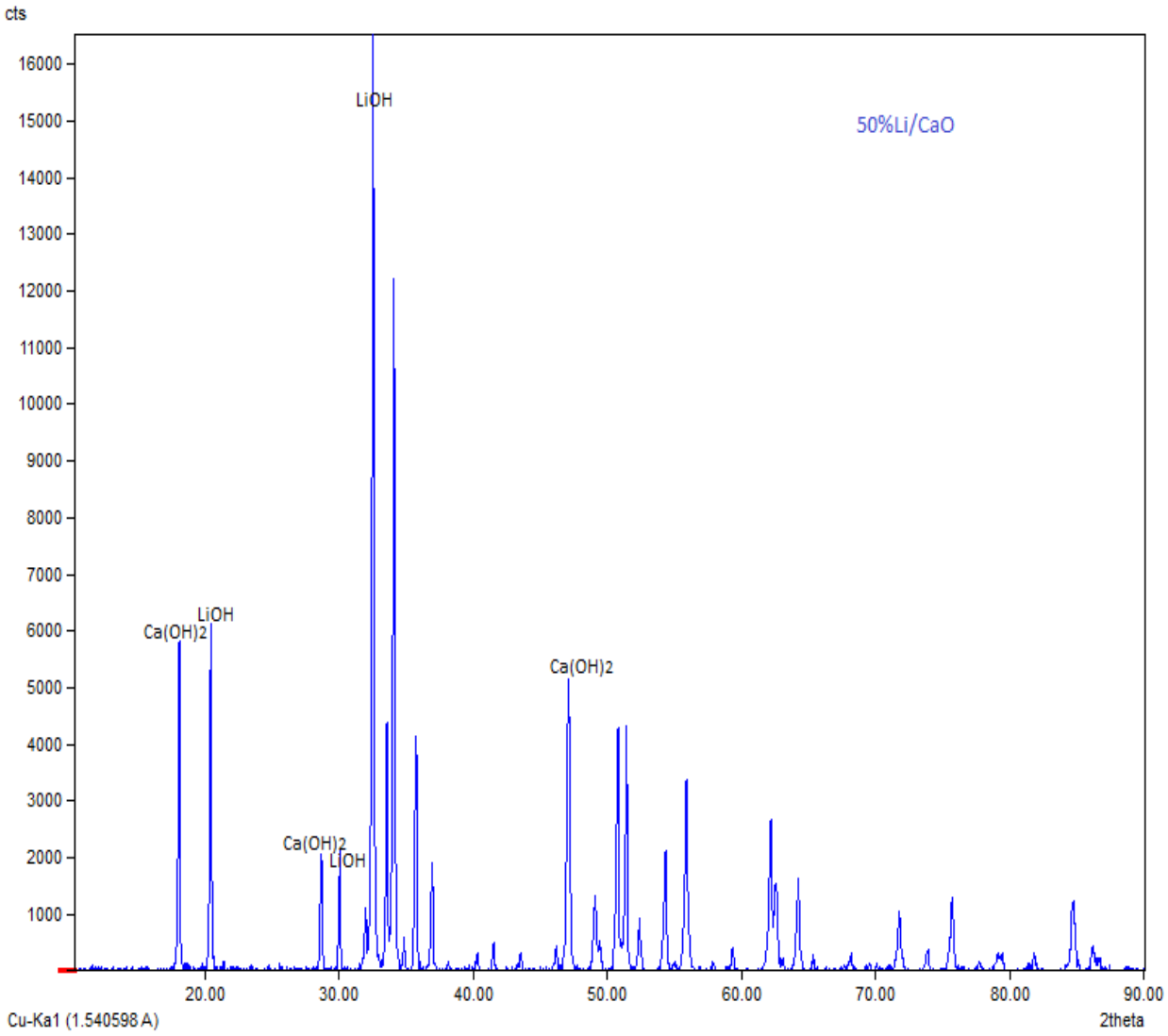

Fig 4-5 XRD pattern for 50%Li/CaO catalyst

From Figure 4-6 below, the intensity of LiOH peaks increases with an increase in LiOH content from catalyst 37.5%Ni-12.5%Li/CaO to catalyst 50%Li/CaO. Conspiqously, CaO peaks in catalyst 50%Ni/CaO are not clearly visible due to the presence of nickel nitrate hexahydrate intermediates which affected its crystalline structure.

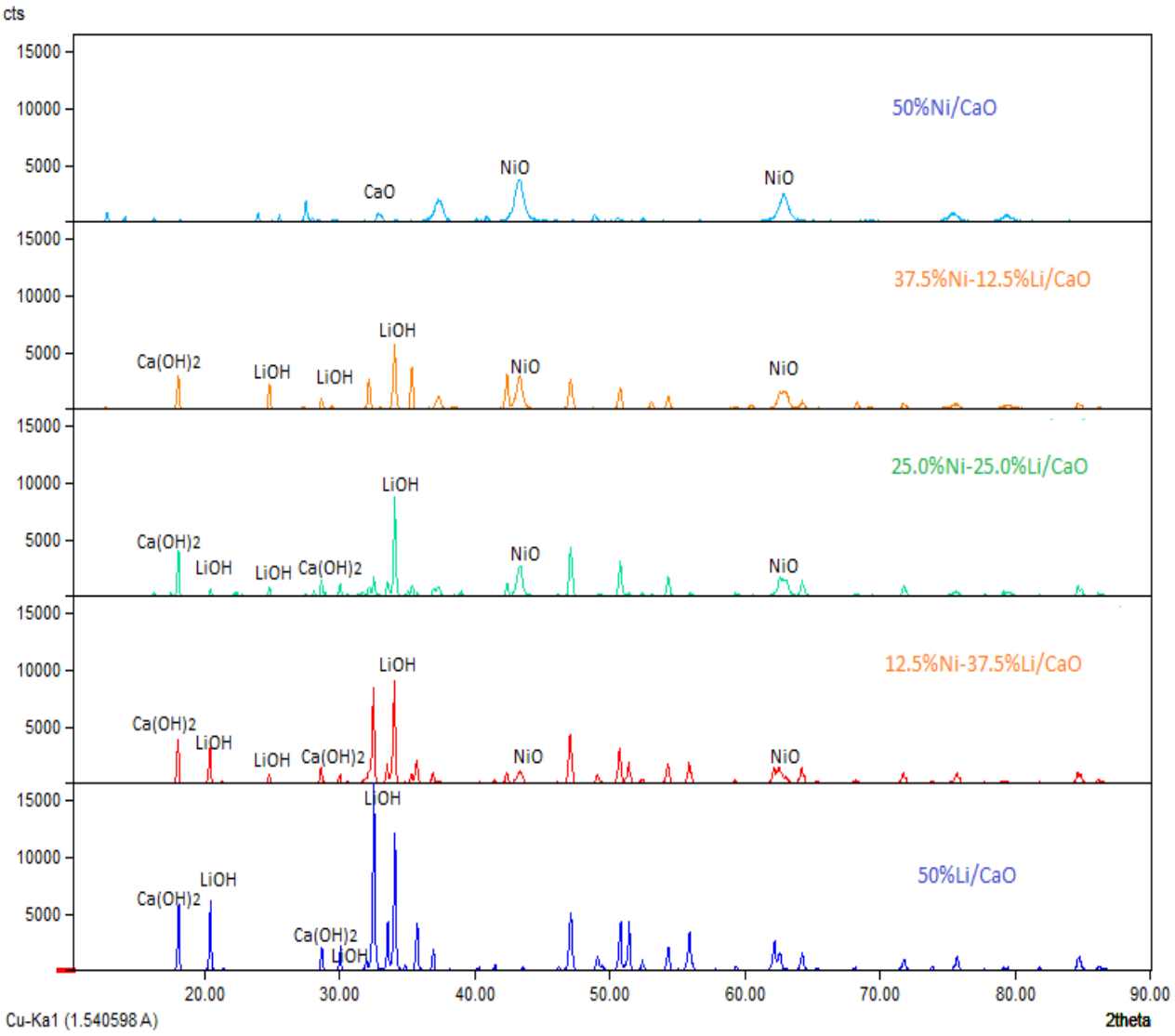

Fig 4-6 Combined XRD patterns for 50%Ni/CaO, 37.5%Ni-12.5%Li/CaO, 25.0%Ni-25.0%Li/CaO, 12.5%Ni-37.5%Li/CaO and 50%Li/CaO catalyst

4.1.2 SEM analysis

Surface properties and particle size of the synthesized catalysts were analyzed using a scanning electron microscope (SEM). To obtain fine details about particle size and particle size distribution, Image-J software was used to analyze the results. Table 4-2 below shows the average particle of each catalyst using a software (Image-J). Introduction of 12.5%,25.0% and 37.5% lithium to Ni/CaO matrix, improves the crystallinity of 37.5%Ni-12.5%Li/CaO, 25.0%Ni-25.0%Li/CaO and 12.5%Ni-37.5%Li/CaO catalysts. The smallest particles were

found in catalyst 37.5%Ni-12.5%Li/CaO while the big particles were found in catalyst 50%/Li/CaO. Therefore, incorporation of LiOH in the Ni/CaO Matrix led to a slight increase in particle size due to agglomeration caused by the hydroxide component.

Table 4-2 Average particle size of each catalyst using Image-J software.

Catalyst Name	Average particle diameter (nm)
37.5%Ni-12.5%Li/CaO	3.09
50%Ni/CaO	3.32
12.5%Ni-37.5Li%/CaO	3.86
50%Li/CaO	5.56
25%Ni-25%Li/CaO	6.56

SEM image of catalyst 50%Ni/CaO catalyst in Figure 4-7 shows an orderly pack of very fine nanoparticles. There is homogeneous distribution of NiO on the catalyst surface and the particles are spherical nanoclusters due to the agglomeration process. The amorphous characteristic of the 50%Ni/CaO catalyst is attributed to the presence of several intermediate oxides of nickel during thermal decomposition of nickel nitrate hexahydrate (Brockner *et al.* 2007). When metal nitrates decompose, various intermediates such as HNO_3,NO,NO_2 and hydroxide nitrate hydrates are formed (Ehrhardt *et al.* 2005).

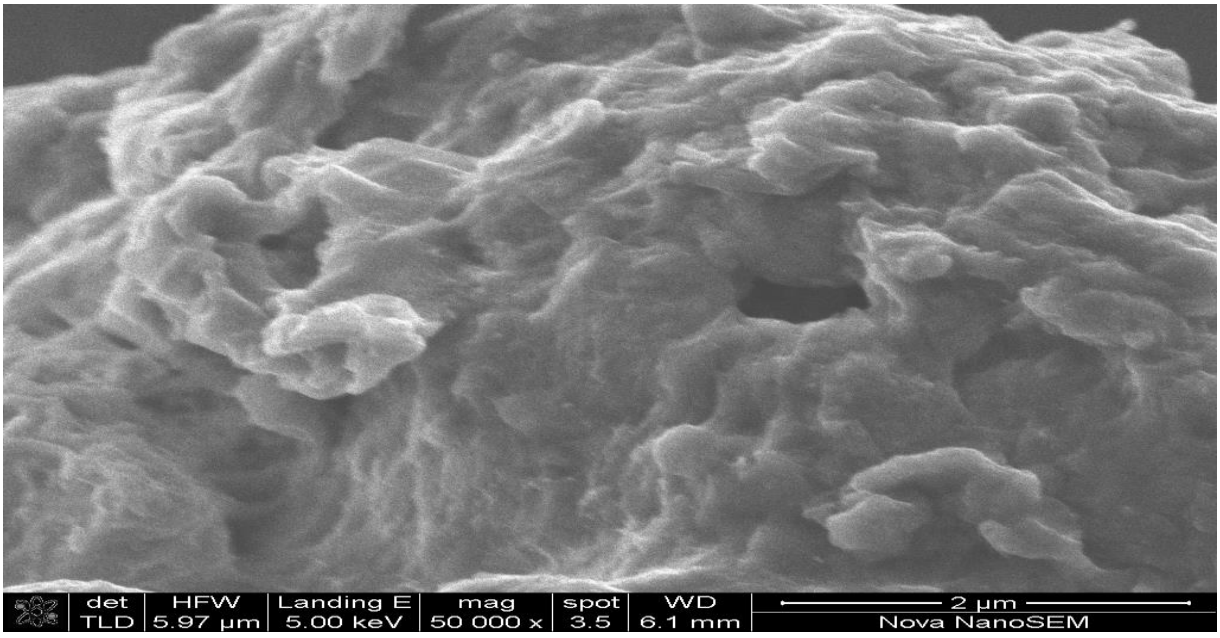

Fig 4-7 SEM image of 50%Ni/CaO catalyst

SEM images of catalyst 37.5%Ni-12.5%Li/CaO in Figure 4-8 below shows aggloromates of well-defined tetrahedral shaped nanoparticles which are closely packed. Cubic structures of nanoparticles are also seen stacked neatly on top of each other in a regular pattern. The presence of few spherical nanoparticles confirms that, introduction of lithium into Ni/CaO matrix does not alter its spherical structure entirely. This new structure can be linked to $Ca(OH)_2$ when LiOH reacts Ni/CaO.

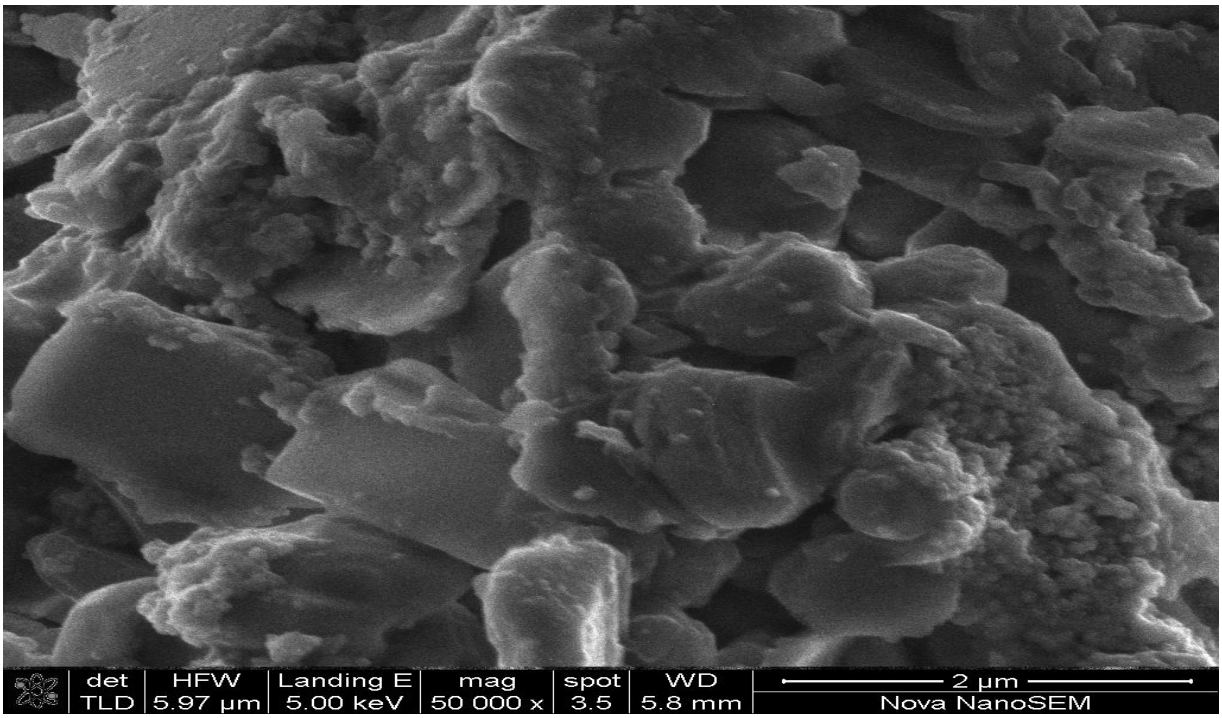

Fig 4-8 SEM image of 37.5%Ni-12.5Li/CaO catalyst

SEM images of catalyst 25.0%Ni-25.0%Li/CaO in Figure 4-9 show aggloromates of irregular shaped nanoparticles which are closely packed. This shows that equal amounts of nickel and lithium loading both on CaO support results into an amorphous catalyst. Few uniform spherical nanoparticles are seen scattered all over the catalyst surface.

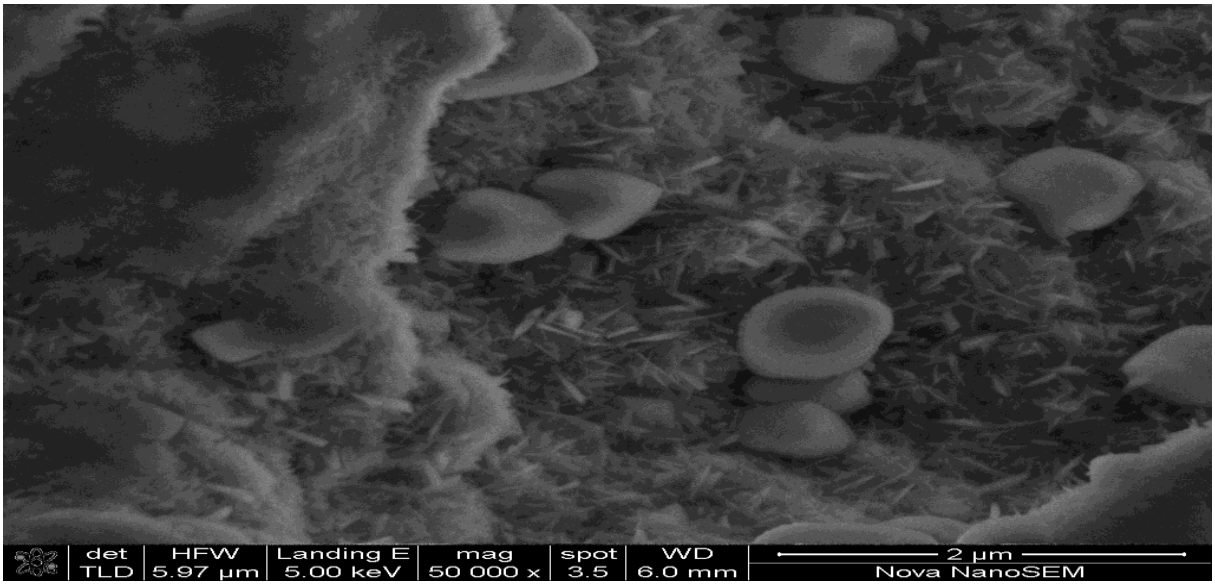

Fig 4-9 SEM image of 25.0%Ni-25.0%Li/CaO catalyst

SEM images of catalyst 12.5%Ni-37.5%Li/CaO in Figure 4-10 and catalyst 50%Li/CaO in Figure 4-11 show definite structures nano material which are neatly packed. The shapes of these particles conform to both tri lobes and Quadra lobes. Therefore, a higher lithium loading in the catalyst destructs the Ni/CaO matrix by lumping together spherical particles into well-defined tri lobes and Quadra lobes.

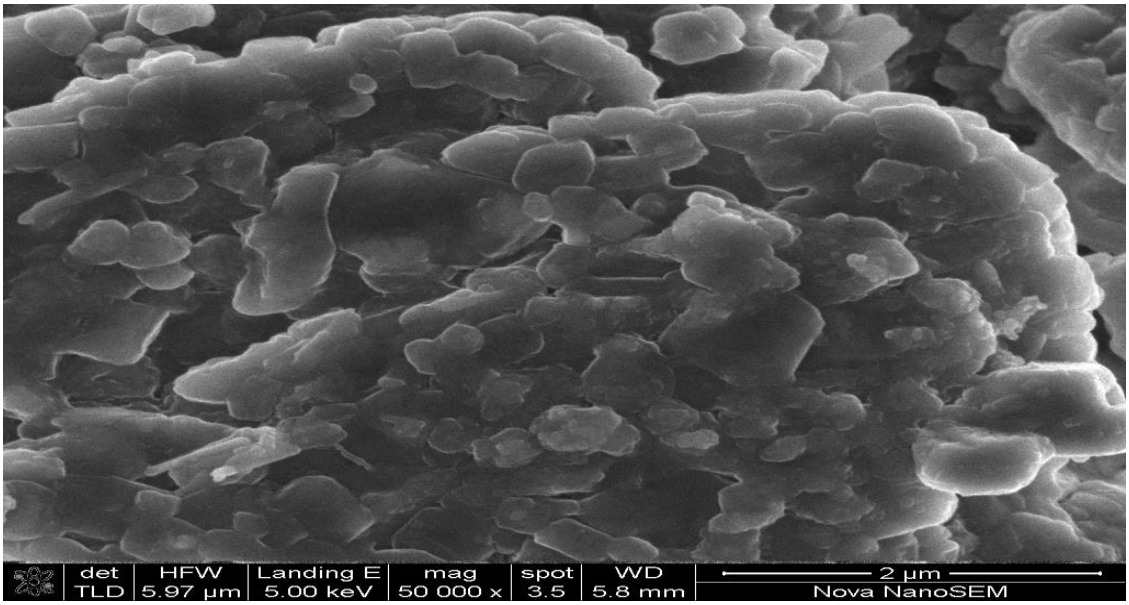

Fig 4-10 SEM image of 12.5%Ni-37.5Li/CaO catalyst

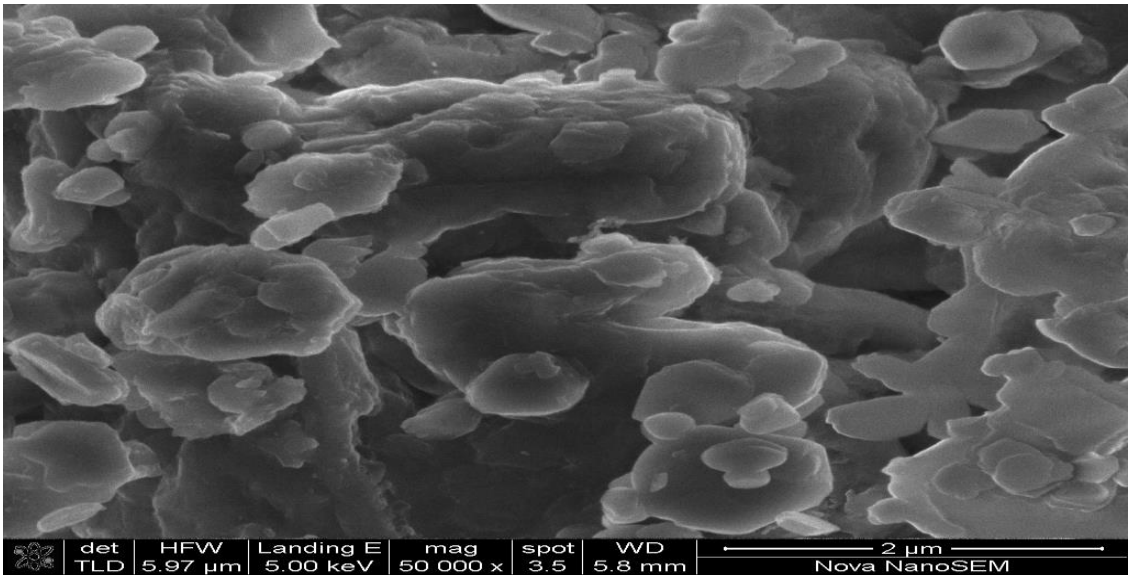

Fig 4-11 SEM image of 50%Li/CaO catalyst.

Figure 4-12 below shows particle size distributions in catalyst 50%Ni/CaO by using Image -J. In that catalyst, the particle size ranged from 1.95nm to 5.29nm with 50 of the particles falling between 2.1nm to 3.0nm. The mean particle size in this catalyst was 3.02nm with a standard deviation of 0.83.

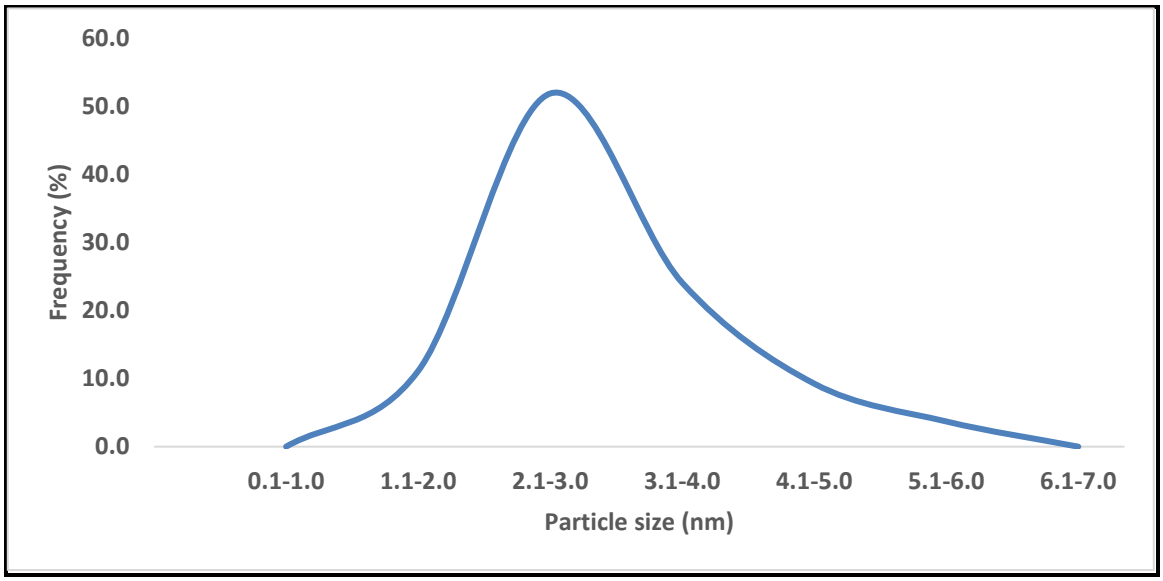

Fig 4 -12 Particle size distribution of 50%Ni/CaO catalyst

Figure 4-13 below shows particle size distributions in catalyst 37.5%Ni-12.5%Li/CaO by using Image -J. In that catalyst, the particle size ranged from 1.95nm to 3.91nm with 60% of the

particles falling between 2.1nm to 3.0nm. The mean particle size in this catalyst was 2.64nm with a standard deviation of 0.50.

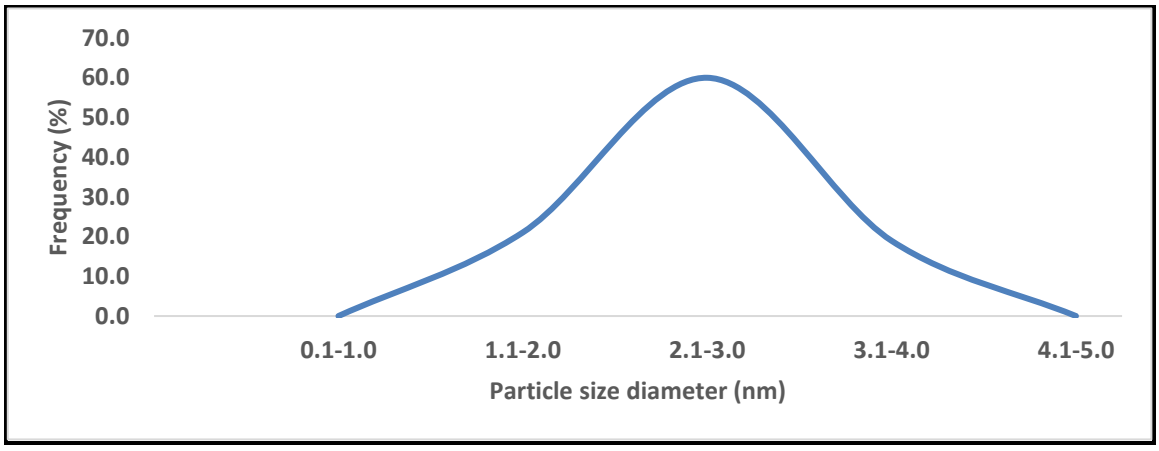

Fig 4 -13 Particle size distribution of 37.5Ni-12.5%Li/CaO catalyst

Figure 4-14 below shows particle size distributions in catalyst 25.0%Ni-25.0%Li/CaO by using Image -J. In that catalyst, the particle size ranged from 3.91nm to 7.98nm with 55% of the particles falling between 5.01nm to 6.0nm. The mean particle size in this catalyst was 5.48nm with a standard deviation of 1.05.

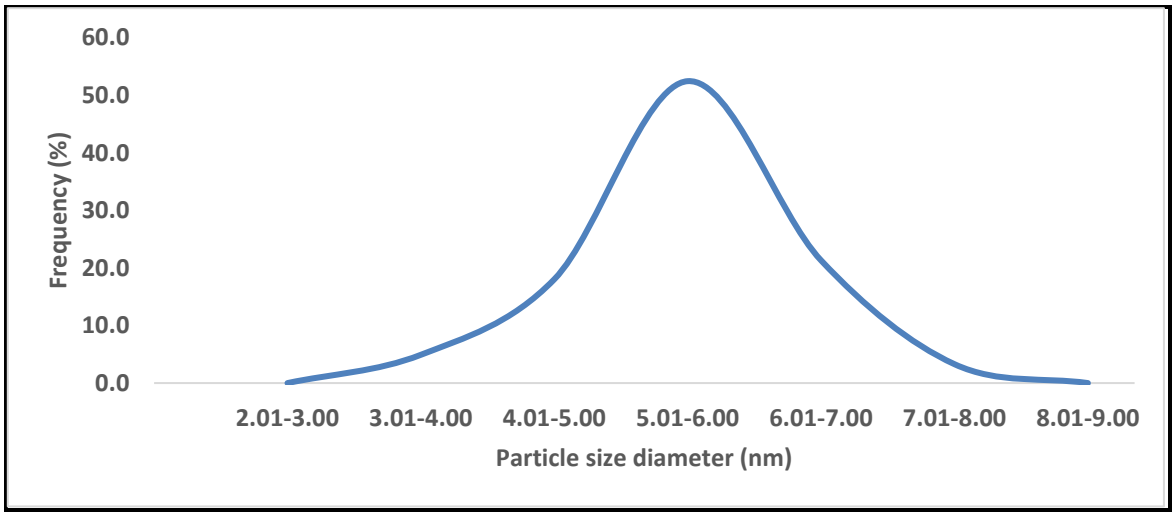

Fig 4 -14 Particle size distribution of 25.0Ni%-25.0%Li/CaO catalyst

Figure 4-15 below shows particle size distributions in catalyst 12.5%Ni-37.5%Li/CaO by using Image -J. In that catalyst, the particle size ranged from 1.95nm to 6.18nm with 45% of the

particles falling between 3.1nm to 4.0nm. The mean particle size in this catalyst was 3.54nm with a standard deviation of 0.91.

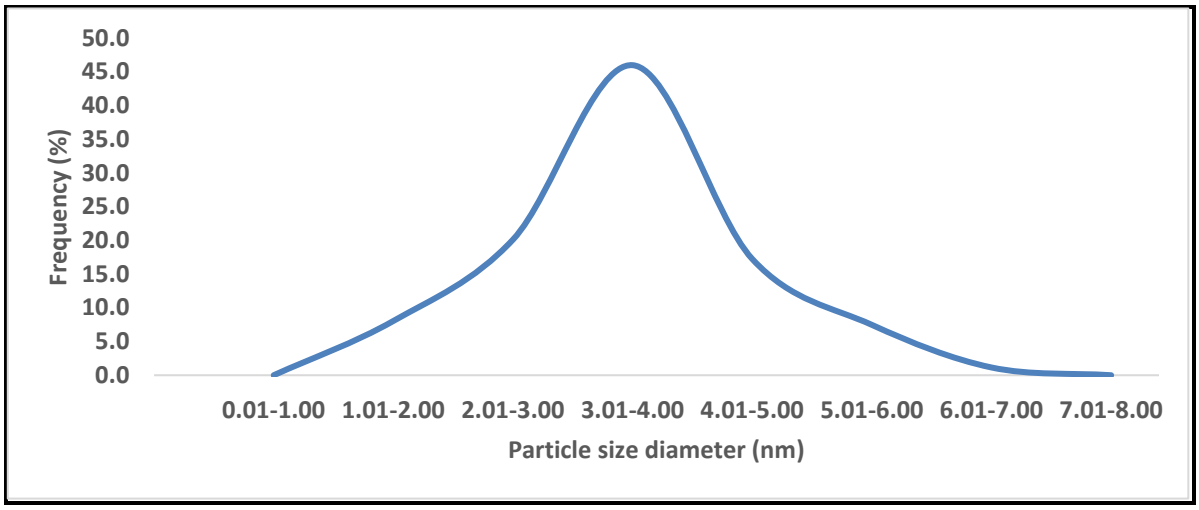

Fig 4-15 Particle size distribution of 12.5Ni%- 37.5%Li/CaO catalyst

Figure 4-16 below shows particle size distributions in catalyst 50%Li/CaO by using Image -J. In that catalyst, the particle size ranged from 1.95nm to 7.74nm with 43% of the particles falling between 3.1nm to 4.0nm. The mean particle size in this catalyst was 3.73nm with a standard deviation of 1.05.

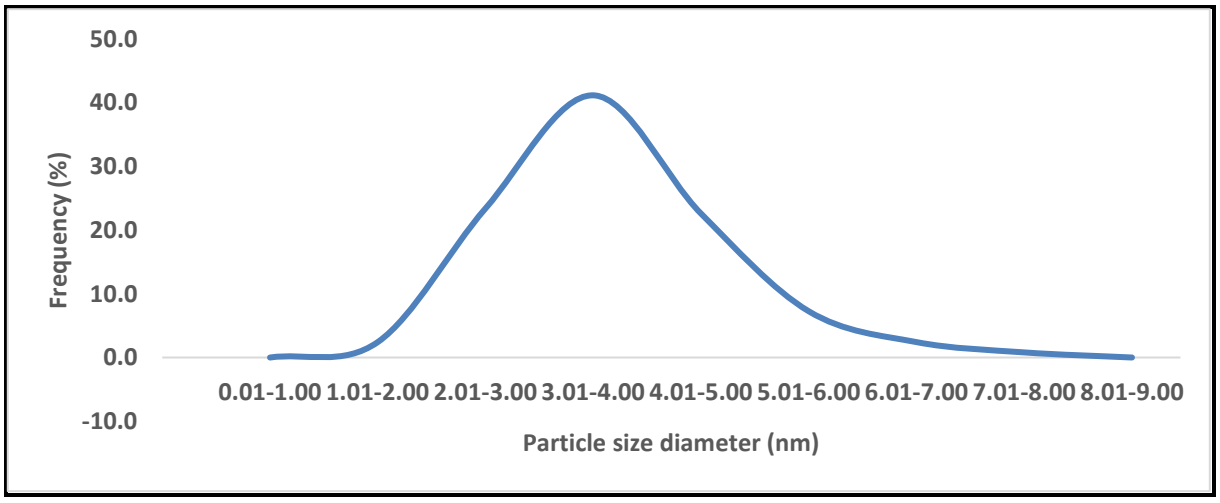

Fig 4-16 Particle size distribution of 50%Li/CaO catalyst

4.1.1.3 BET analysis

The specific areas, pore volume and pore size distributions of the catalysts were determined from N_2 adsorption-desorption data at -196℃ by use of Brunauer-Emmett-teller (B.E.T)

equipment (Micromeritics Tristar II 3020). For each analysis, 0.2g of catalyst was degassed at 150℃ for 2 hours to remove residual moisture from the catalyst surface and other adsorbed gases.

From table 4-3 below, all the catalysts are mesoporous with pore sizes ranging from 20.1nm to 45.3nm. Introduction of LiOH to Ni/CaO generates mesoporous structures by destructing the lattices of the CaO structure during the formation of Ni-Li/CaO species. Increasing the lithium content in Ni/CaO catalyst increases the pore size but reduces the overall surface area due to the presence of the hydroxide which inhibits further liquid nitrogen absorption. These irregular pores play avery important role in the CMD reaction in that a methane molecule travels to cover a distance greater than the granule size when passing through the catalyst granule pores because the tortuosity factor will be high. The surface area and pore volume show a particular trend from catalyst 50%Ni/CaO to catalyst 12.5%Ni-37.5%Li/CaO with an exception of catalyst 50%Li/CaO. From this trend, it can be concluded that catalyst surface area and pore volume is directly proportional to nickel loading.The higher the nickel content the higher the surface area due to exposed pores.

Table 4-3 Catalyst surface area, pore volume and pore size

Catalyst Name	BET Surface area (m^2/g)	Pore volume (cm^3/g)	Pore size (Å)
50%Ni/CaO	5.169	0.0260	201.374
37.5%Ni-12.5%Li/50%CaO	2.934	0.0160	186.493
25.0%Ni-25.0%Li/CaO	0.203	0.0020	424.882
12.5%Ni-37.5%Li/CaO	0.186	0.0021	453.287
50%Li/CaO	0.2950	0.0138	130.541

Porous solids have a higher surface area as compared to their external surface area because of the contribution of pore walls.Most common catalysts have a specific area of 1-1000m^2g^{-1}, while their external surface area is in the range of 0.1-10m^2g^{-1} (Leofanti *et al.* 1998). Since catalytic processes take place on the surface of the catalyst and also through the porous system, the surface area strongly affects catalytic activity. Mass transfer processes taking place inside the granules depends on pore size (bulk diffusion in macropores, knudsen diffusion in micropores) and the tortuosity factor. Pore size also affects catalyst deactivation because carbon deposition blocks catalyst pore mouths (Zhang *et al.* 2007).

4.2 Catalyst performance

The performance of each catalyst was evaluated in terms of methane conversion, hydrogen yield and carbon yield. Table 4-4 below shows a sample calculation for methane conversion and hydrogen yield. Values for methane conversion and hydrogen yield were calculated using equations (33) and (34) respectively. According to Avogadro's law, one mole of a gas at stp has a volume of 22.4 litres. Methane mixture used in this present study was (20%CH_4: 80%N_2) by volume. In this case therefore, one run with time on stream (TOS) of 90 minutes at GHSV consumed 1.35litres of methane mixture which translates to 0.27 litres of pure methane. Like in the case of catalyst 50%Ni/CaO, deposited carbon nanomaterial on the catalyst after 90mins TOS was 0.087g.

From mass balance, the mass of feed should be equal to the mass of products assuming no losses. Therefore, the mass of methane feed should be equal to the mass of the gaseous products minus the mass of deposited carbon nanomaterial. Using a gas chromatograph, we established the composition of the gaseous products and calculated the mass of individual gases. Knowledge of individual mass of the gaseous products was very handy in applying the above equations to calculate methane conversion and hydrogen yield in all cases. Calculations for methane conversion and hydrogen yield in this study were done based on deposited carbon.

Table 4-4 Results showing methane conversion and hydrogen yields at 650℃ and GHSV of 2

CATALYST	CH4 Feed (moles)	Deposited carbon (moles)	Evolved H_2 (moles)	Unreacted CH4 (moles)	CH_4 conversion (%)	Hydrogen Yield (%)
50%Ni/CaO	0.01205	0.00725	0.00518	0.00480	60.2	35.7
37.5%Ni-12.5%Li/CaO	0.01205	0.00792	0.00606	0.00414	65.7	38.3
25.0%Ni-25.0%Li/CaO	0.01205	0.00775	0.00564	0.00430	64.3	36.4
12.5%Ni-37.5%Li/CaO	0.01205	0.00767	0.00533	0.00439	63.6	34.8
50%Li/CaO	0.01205	0.00758	0.00556	0.00447	62.9	35.9

4.2.1 Effect of reaction temperature on methane conversion and hydrogen yield

Actual catalytic decomposition experiments were carried out at 500℃,550℃,600℃,650℃ and 700℃ at atmospheric pressure. Prior the experiment, the reactor was pacified with nitrogen for 30 minutes before feeding in methane (20%CH_4:80%N_2). In each run, a catalyst mass of 0.4g was used and time on stream was 90mins.

The results of each catalyst in terms of methane conversion and hydrogen yield followed a common trend. In that trend, the initial methane conversion was low at 500℃ and kept on increasing up to 650℃ after which, a conversion started to decrease. During catalyst synthesis, reduction of nickel oxide to metallic nickel was not complete due to the presence of lithium hydroxide whose melting point is 456℃. Therefore, during the first 30-40mins, methane reacted with NiO to produce hydrogen, CO and metallic nickel according to the equation;

$$CH_4 + NiO \rightarrow Ni + CO + 2H_2 \quad (39)$$

Part of the produced hydrogen was also used in the nickel oxide to metallic nickel reduction process, hence low hydrogen yields. The presence of surface oxygen completed further oxidation of the process CO into CO_2 which was positively identified at 18mins and 36mins product sampling intervals. As the reaction temperature increased, the catalyst became more stable due to expulsion of moisture and availability of active nickel sites which were evenly distributed in the molten lithium hydroxide until 650℃.

Nickel catalyst is active within a narrow range of temperature; 350-550℃ within which a maximum conversion level of up to 60% can be achieved. At temperatures higher than 650℃, nickel loses its stability because the coke formed during the reaction tends to grow on the metal (encapsulating carbon) which drastically reduces the active sites of the catalyst (Lægsgaard Jørgensen *et al.* 1995). Above 650℃, hydrogen yield starts to decline partly due to coke deposition on the molten catalyst surface and near decomposition temperature of lithium hydroxide which starts at 780℃. At this point, the catalyst ceases to function as a supported molten metal catalyst.

The results of catalyst activity in terms of methane conversion and hydrogen yield are presented in Figure 4-17 and Figure 4-18. Although all the five catalysts had high methane conversion and

hydrogen yields, catalyst 37.5%Ni-12.5%Li/CaO displayed outstanding results at almost all temperature regions. Methane conversion was 65.7% and hydrogen yield was 38.3% at 650℃ and gas hourly space velocity (GHSV) of 2. This was attributed to the presence of high nickel metal content and high surface area as can be adduced by having the smallest crystallites which were evenly dispersed in the molten lithium hydroxide. This aided surface reaction and chemisorption unlike catalyst 50%Ni/CaO which had 60.3%methane conversion and 35.7% hydrogen yield under the same conditions. In this catalyst, the molten component was missing, and life of metallic nickel reduced tremendously due to coke deposition. Loss of alkali ions above 700℃ can be attributed to their inability to enter the CaO lattice as decomposition temperature of LiOH into Li_2O begins at 780℃.

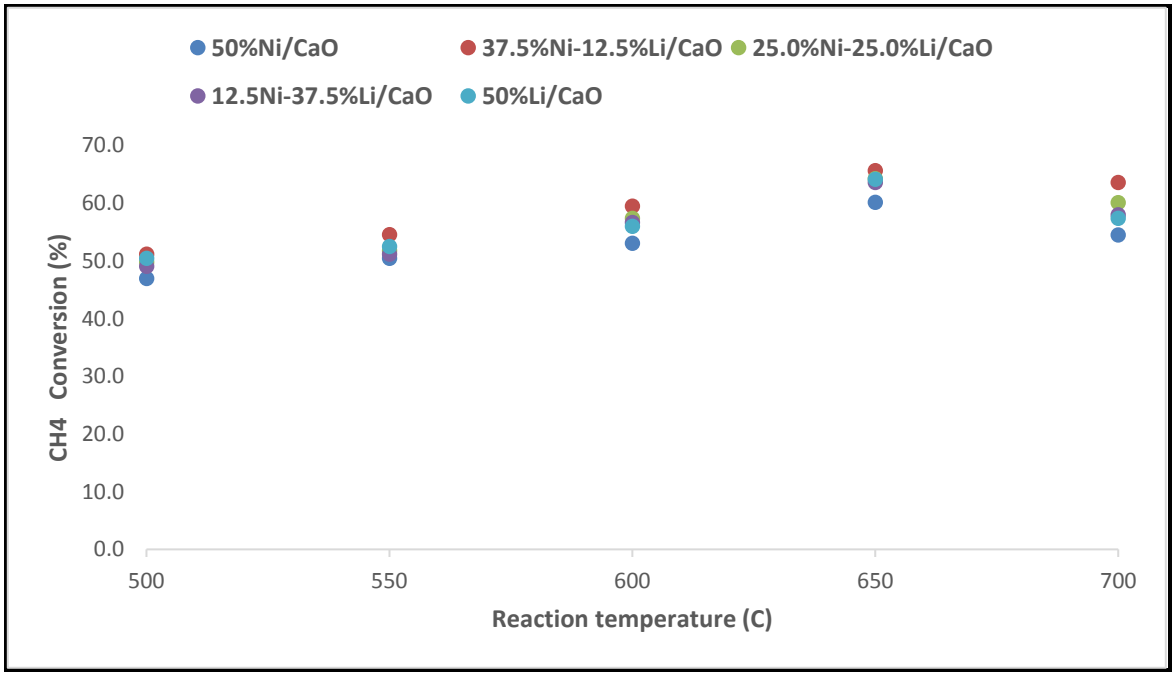

Figure 4-17 Effect of reaction temperature on methane conversion

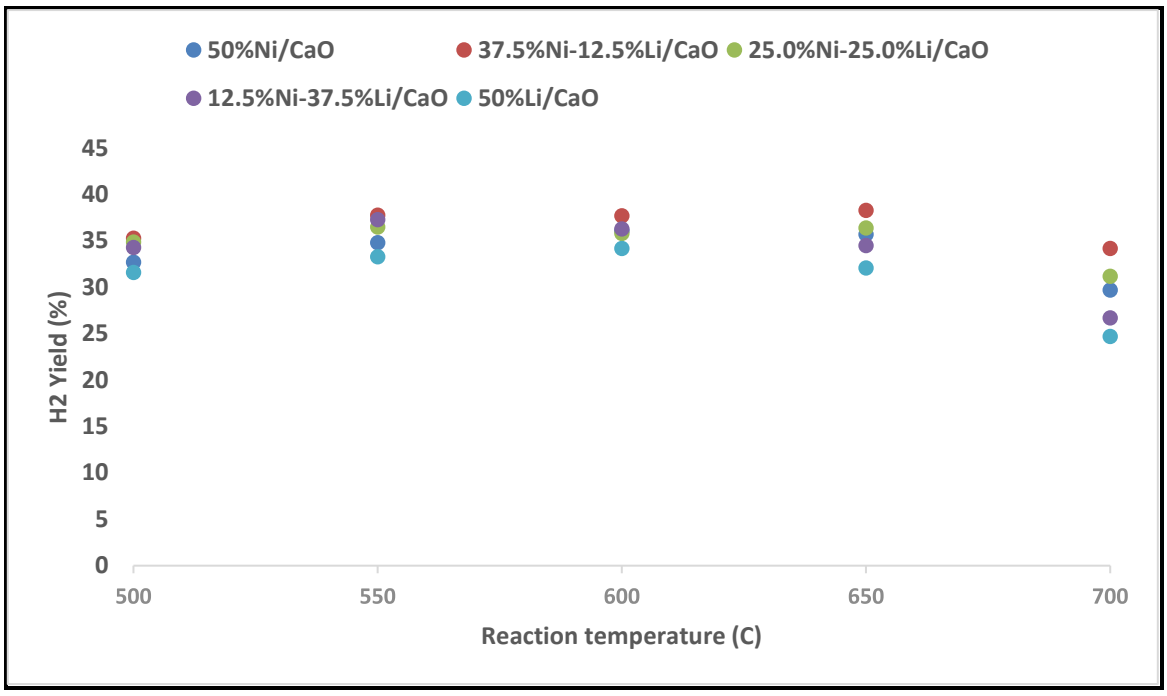

Figure 4-18 Effect of reaction temperature on hydrogen yield.

4.2.2 Effect of activation time on methane conversion and hydrogen yield

Decomposition reactions of catalyst precursors taking place gives birth to various reactions which have a bearing on catalyst performance during the initial stages of CMD reaction.

4.2.2.1 Thermal decomposition of nickel nitrate hexahydrate

Thermal decomposition of nickel(II) nitrate hexahydrate proceeds in various steps forming tetra and dihydrates if the formation of a hydrate melt is prevented (Elmasry *et al.* 1998; Małecki *et al.* 2000; Estellé *et al.* 2003). Apart from this, there is notable (Tiernan *et al.* 2001) existence of the controversial intermediate nickel nitrate salt ($Ni(NO_3)_2.5.5H_2O$ (Metz *et al.* 2004). A single phase of $Ni_3(NO_3)_2(OH)_4$ which is a homogeneous phase corresponds to hydrolysis of nickel nitrate and releases HNO_3 according to the equation 39 below;

$$3Ni(NO_3)_2.2H_2O=Ni_3(NO_3)_2(OH)_4+4HNO_3+2H_2O \quad (40)$$

4.2.2.2 Overview of CaO/LiOH interaction

The protons in the $Ca(OH)_2$ are not rigidly fixed due to the covalent character of the metal hydroxyl bond, hence dehydration of $Ca(OH)_2$ starts at 300℃ and completes at 450℃.

Dehydration of $Ca(OH)_2$ (Gonçalves *et al.* 2017) occurs through a combination of mobile protons with neighbouring OH^- sites while the other possibility being the direct transfer of OH^- ions from LiOH to CaO matrix through the newly created vacant sites in the CaO particles where the OH^-ions can be readily converted into O^{2-} ions by dehydration of the hydroxyl ions.

The increase in concentration of basic ionic sites of the CaO matrix after calcination can be considered as an indication for the incorporation of Li^+ ions. Ionic radius of Ca^{2+}=0.99Å while that of Li^+=0.68Å and therefore limited inclusion of Li^+ into $Ca(OH)_2$ which could not restrict any appreciable change in lattice parameter values since the ionic radius of CaO (a=4.817Å) and LiOH (a=4.815Å). From electron spin resonance (ESR), Li^+ and O^- ions form in the Centre of the CaO matrix (Yoshinaga *et al.* 1997). Catalytic activity measurements for decomposition of methane (Gonçalves *et al.* 2017), indicate that catalysts consisting of alkali and alkaline earth compounds resulted in Selectivities of up to 76% for the formation Ca^+ hydrocarbons which is higher than that for CaO alone.

The doping of alkali ions into the alkaline earth oxide (CaO) produces many low coordinate sites on which heterolytic activation of methane can occur more effectively. During CMD reaction, sampling to ascertain product composition was done at intervals of 18mins between 0-90mins at 650℃ and GHSV of 2. From figure 4-19 below, the initial values of methane conversion and hydrogen yield were low, but steadily rose to peak values at 54mins and slightly dropped after 90minutes time on stream. At the onset of methane decomposition, the synthesized catalyst underwent decomposition before stability after 20-30 mins. This is demonstrated by the presence of moisture and carbon dioxide during the first two-18minutes-sample collection time intervals.

Figure 4-19 and 4-20 below shows the effect of activation time on catalyst performance at 650℃. In all cases, catalyst 37.5%Ni/CaO had the highest methane conversions;44.3% at 18mins, 56.4% at 36mins, 59.5% at 54mins, 64.9% at 72mins and 65.7% at 90mins. Using the same catalyst, a hydrogen yield of; 45.5% at 18mins, 40.7% at 36mins, 38.8% at 54mins, 39.3% at 72mins and 38.3% at 90mins. Dismal performance was registered by catalyst 50%Ni/CaO which had methane a conversion of; 42.2% at 18mins, 53.2% at 36mins, 56.0% at 54mins, 59.5% at 72 mins and 60.2 at 90mins. In terms of hydrogen yield, the same catalyst had; 45.0% at 18mins, 39.1% at 36mins, 37.2.0% at 54mins, 37.1% at 72mins and 35.7% at 90 mins. This

dismal performance is attributed to coking of the nickel catalyst whose active sites increasingly became blocked by deposited carbon nanomaterial.

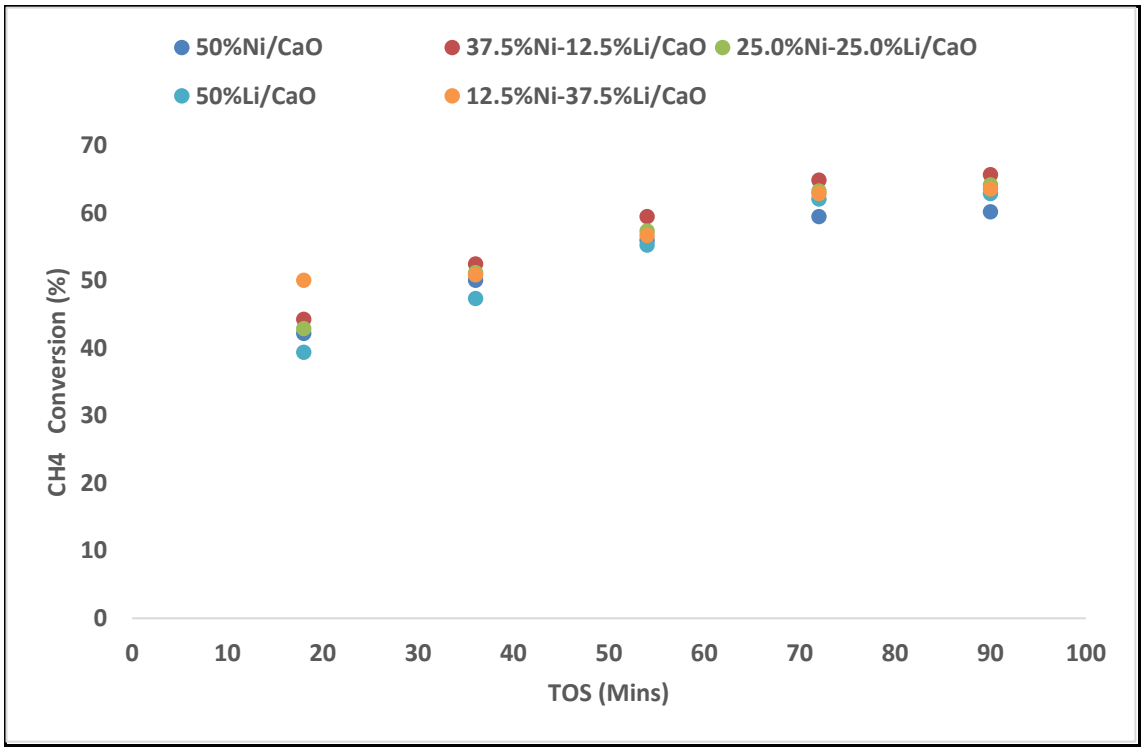

Figure 4-19 Effect of activation time on methane conversion at 650℃ and GHSV 2

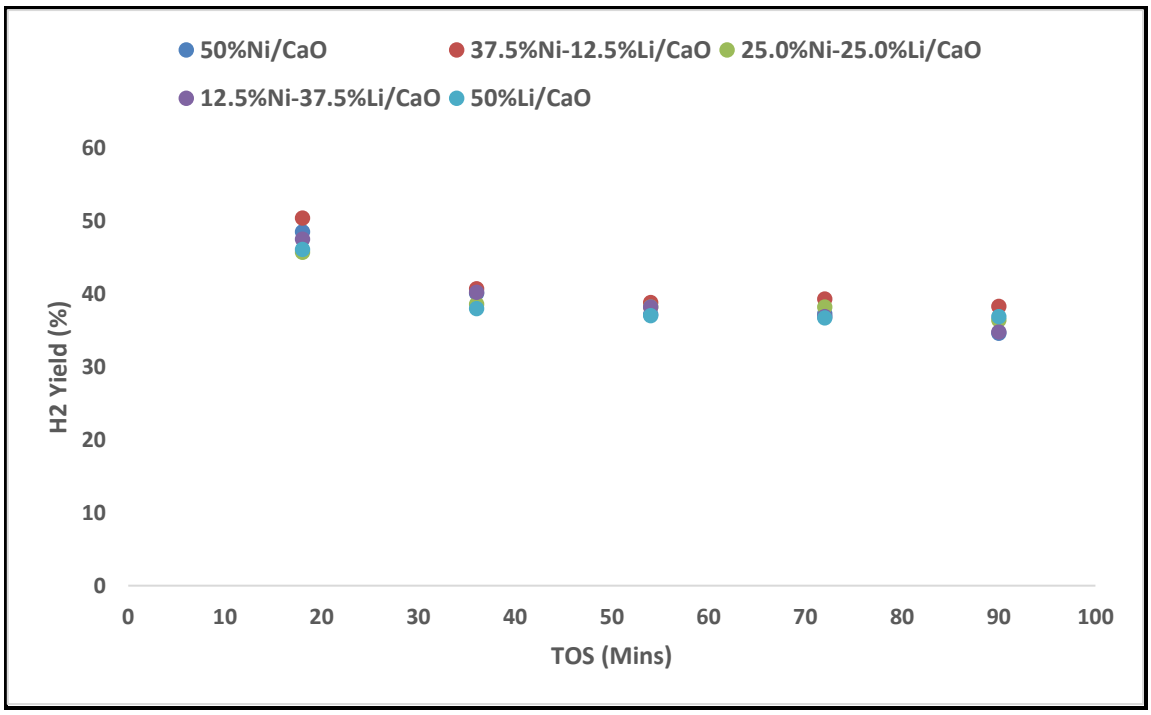

Figure 4-20 Effect of activation time on hydrogen yield at 650℃ at GHSV 2

4.2.3 Effect of GHSV on CH_4 conversion and H_2 yield

To study the effect of GHSV, a catalyst mass of 0.4g supported on 0.4g quartz wool was used in each case and the best performing catalyst 37.5%Ni/CaO at 650℃ was used. Three GHSV $2Lg^{-1}_{cat}h^{-1}$, $3Lg^{-1}_{cat}h^{-1}$ and $4Lg^{-1}_{cat}h^{-1}$ were used to observe methane conversion and hydrogen yield. The results for methane conversion and hydrogen yield under these GHSVs are presented in Figure 4-21 and Figure 4-22. Catalyst 37.5%Ni/CaO showed a decline in methane conversion from 65.7% at $2Lg^{-1}_{cat}h^{-1}$ to 60.2% at $4Lg^{-1}_{cat}h^{-1}$ and a decline in hydrogen yield from 38.3% at $2Lg^{-1}_{cat}h^{-1}$ to 32.2% at $4Lg^{-1}_{cat}h^{-1}$.

It has been reported in literature (Al-Fatesh *et al.* 2016) that an increase in GHSV decreases the contact time between the reactants and the catalyst surface thus reducing catalyst activity and vice versa. In this case, better results for each catalyst were recorded at $2Lg^{-1}_{cat}h^{-1}$. Since GHSV is the ratio of feed flow rate to catalyst mass, a suitable combination is required to provide maximum contact time between the catalyst and the reactant. From previous studies (Chai *et al.* 2011), a catalyst can only accommodate a certain amount of methane flow rate, above which methane molecules will cause formation of encapsulating carbon which leads to catalyst deactivation.

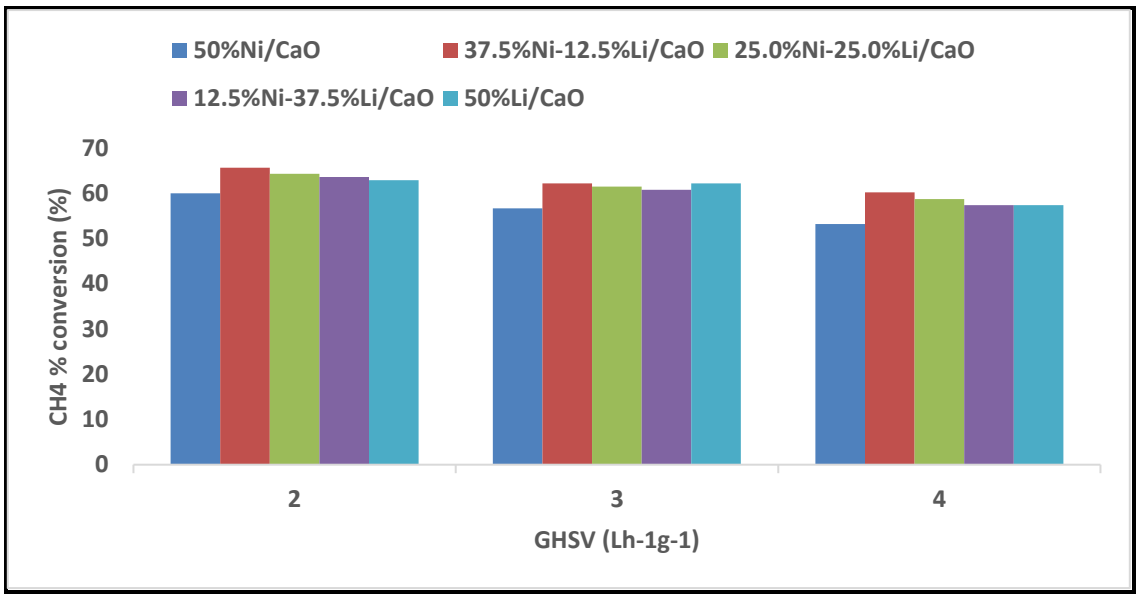

Figure 4-21 Effect of GHSV on methane conversion at 650℃

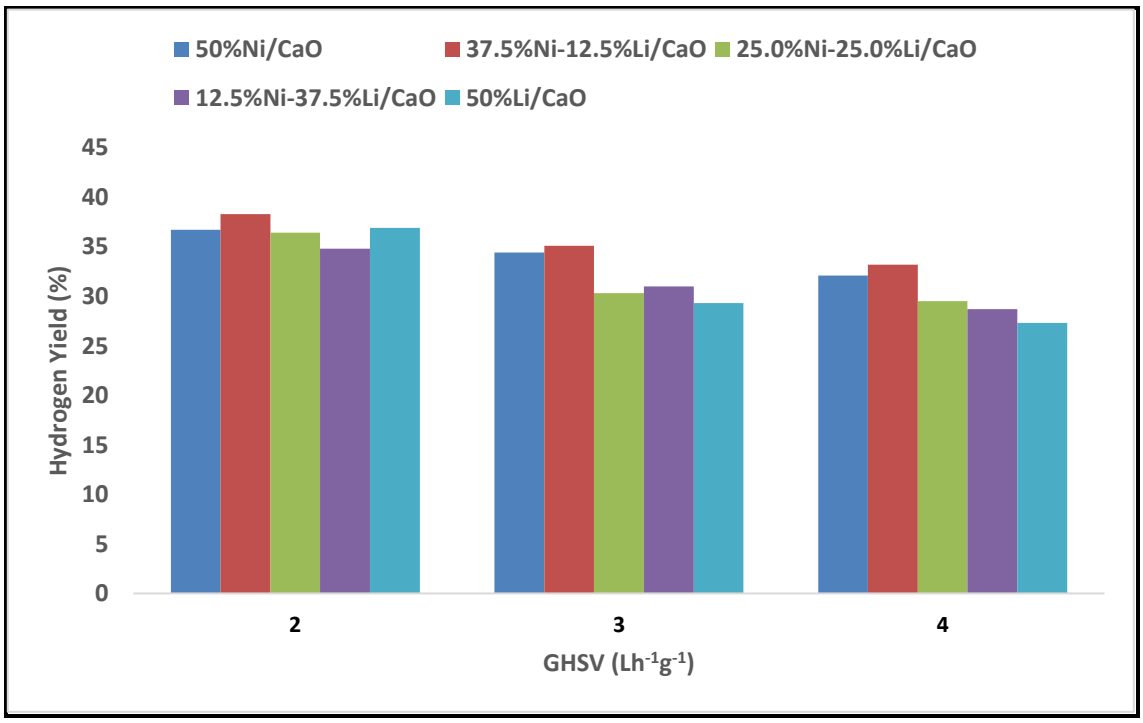

Figure 4-22 Effect of GHSV on hydrogen yield at 650℃

4.2.4 Effect of catalyst type on carbon yield

From table 4-6 below, 50%Ni/CaO catalyst recorded the highest amount of deposited coke as compared to 50%Li/CaO. This is because, the highly dispersed and individual nickel metal

particles are believed to have facilitated the diffusion of methane to the catalyst surface and thus favoring coke formation. This coke formation is in agreement with previous studies on catalyst deactivation by coking (Li *et al.* 2002). This shows a trend in which a catalyst with the amount of nickel loading is directly proportional to carbon yield.

Table 4-5 Amount of coke deposited on each catalyst after 90 mins time on stream.

Catalyst Name	Amount of deposited coke (mg/g catalyst)	Carbon Yield (%)	Temperature (℃)	Time on stream (Minutes)
50%Ni/CaO	217.5	21.8	650	90
37.5%Ni-12.5%Li/50%CaO	237.5	23.8	650	90
25.0%Ni-25.0%Li/CaO	232.5	23.3	650	90
12.5%Ni-37.5%Li/CaO	230.0	23	650	90
50%Li/CaO	227.5	22.8	650	90

4.3 Characterization of spent catalyst

4.3.1 TEM Analysis

From the micrographs of these catalysts in Figure 4-23 and Figure 4-24, it can be seen clearly that the growth pattern followed both growth mechanisms i.e., tip growth and base growth since the metal particles were found on both tips and inside carbon nanofibers providing the platform for growth of carbon particles (Li *et al.* 2011). This is attributed to increased presence of Lithium hydroxide which is more crystalline hence, less agglomeration of the catalyst particles to inhibit methane diffusion. The carbon nano material structure depends on the metal-graphite interface on which graphene layers form particles (Li *et al.* 2002). From table 4-7 below, minimum and maximum values of particle sizes for 50%Ni/CaO, 37.5%Ni-12.5Li/CaO and 25.0%Ni%-25.0%Li/CaO catalysts decrease respectively while the minimum and maximum length of the carbon nanofibers similar to those reported by (Zhang *et al.* 2001) for catalyst 12.5%Ni-37.5%Li/CaO begin to increase respectively. From this particle size distribution, a higher nickel loading in the catalyst favours the formation of carbon nanotubes while higher lithium hydroxide loading favours the formation of carbon fibres (CF). Low CF yield (Li *et al.* 2016) from methane decomposition on unsupported Ni catalyst in 50%Ni/CaO was attributed

to the presence of large Ni particles with low index planes. The low index planes were incapable of dissociating the unreactive methane molecule.

Table 4-6 Particle size distribution of deposited carbon nanomaterial on each catalyst in (nm)

Catalyst	Count	Min	Max	Mean	Standard Deviation
50%Ni/CaO	36	22.52	98.76	61.62	16.94
37.5%Ni-12.5%LiCaO	42	19.97	97.13	60.96	21.43
25.0%Ni-25.0%Li/CaO	25	19.52	55.0	35.20	8.39
12.5%Ni-37.5%Li/CaO	22	23.68	154.96	58.25	32.03
50%Li/CaO	27	145.67	487.14	249.96	90.57

TEM micrographs of catalyst 50%Ni/CaO, 37.5%Ni-12.5%Li/CaO and 25.0%Ni-25.0%Li/CaO spent catalysts in CMD reaction at 650℃ and GHSV 2 are shown in Figures 4-23, 4-24 and 4-25 respectively. From TEM images of the three catalysts, deposited carbon nano material share some similarities in that the Ni metal particles are found inside and at the tip of carbon nanotubes produced. The carbon products all over the catalysts are multi-walled nanotubes (MWCNTs) with hollow cores like those reported by (Chen *et al.* 1997) . In figure 4-24, more uniform carbon nanotubes with smooth external surfaces are found in the 37.5%Ni-12.5%Li/CaO catalyst because, the highly dispersed and individual nickel metal particles are believed to facilitate the diffusion of methane to the catalyst surface and thus favor the formation of uniform carbon nanotubes (Li *et al.* 2002). Conversely, long and short length MWCNTs are formed in denseness on 50%Ni/CaO catalyst indicating low hydrogen yields and subsequent formation of MWCNTs. This is attributed to formation of various nickel oxide species and other intermediate products during reduction of nickel oxide to nickel metal from thermal decomposition of nickel nitrate hexahydrate.

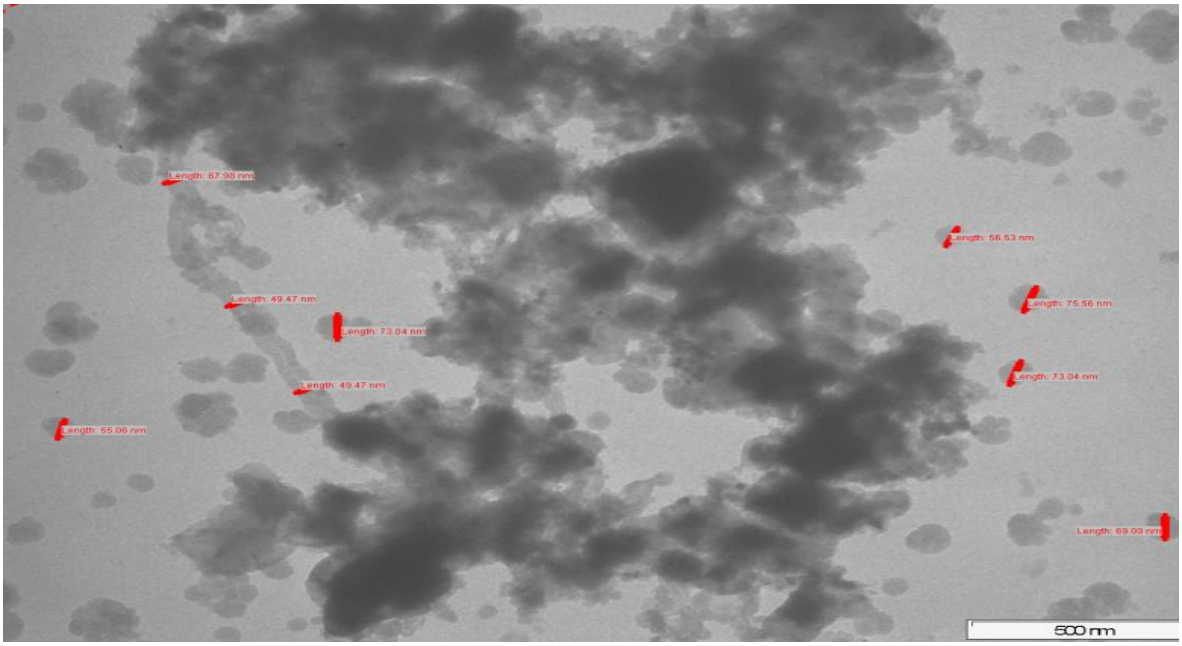

Figure 4-23 TEM image of 50%Ni/CaO spent catalyst

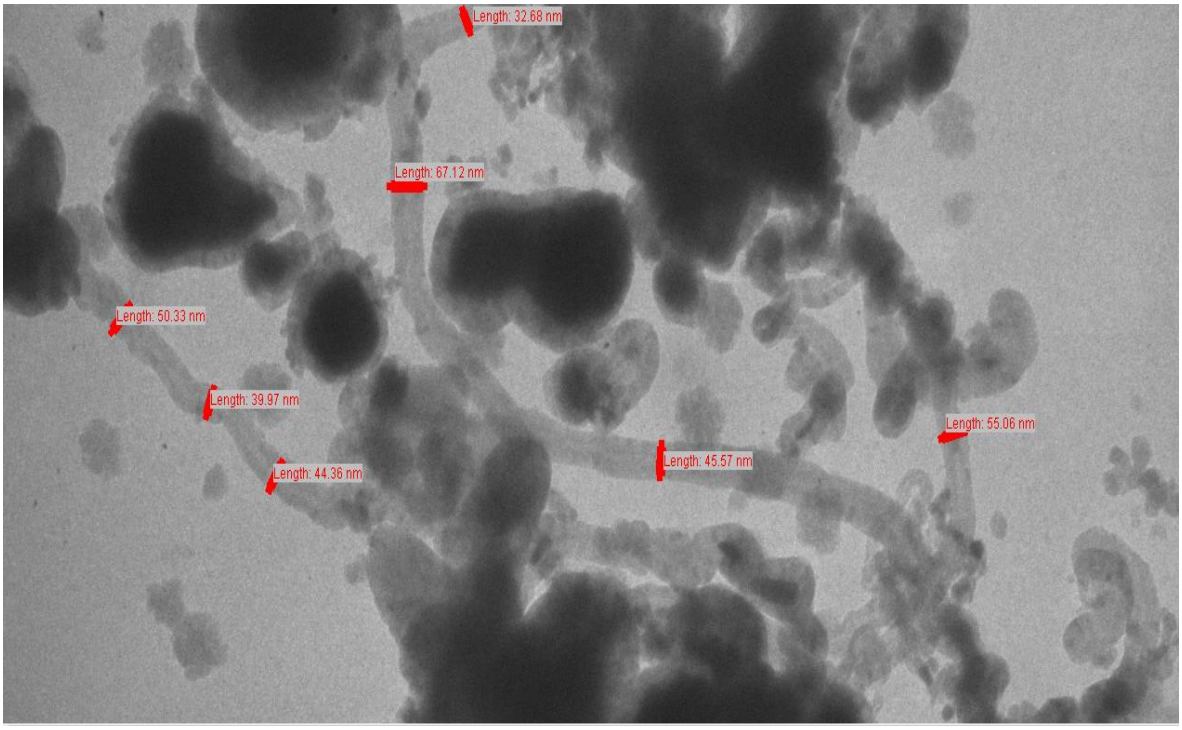

Fig 4-24 TEM image of 37.5%Ni-12.5Li/CaO spent catalyst

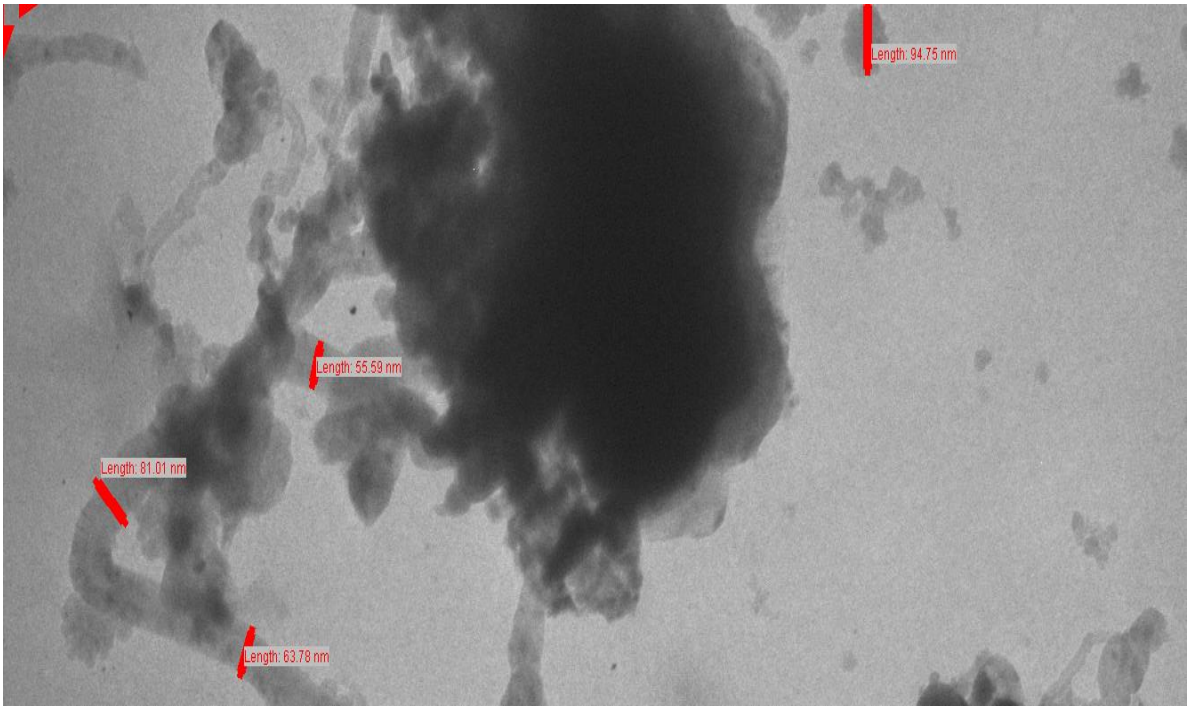

Fig 4-25 TEM image of 25.0%Ni-25.0%Li/CaO spent catalyst

From Figure 4-26 and 4-27, TEM images of carbon fibers are seen deposited on catalyst 12.5%Ni-37.5%Li/CaO and on catalyst 50%Li/CaO. Different carbon nanofibers (CNFs) including chain-like CNFs, CNFs having tips containing metal particles, open and closed ended CNFs are formed on catalysts. This shows that higher lithium content in the catalyst favors the formation of carbon fibers than carbon nanotubes during CMD reaction.

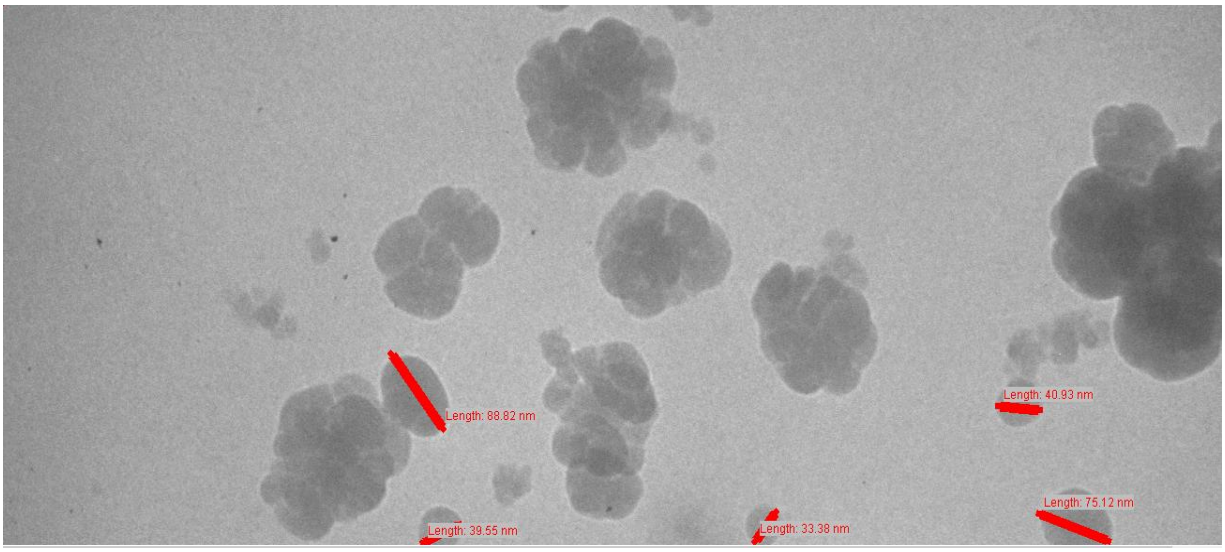

Fig 4-26 TEM image of 12.5%Ni-37.5Li/CaO spent catalyst

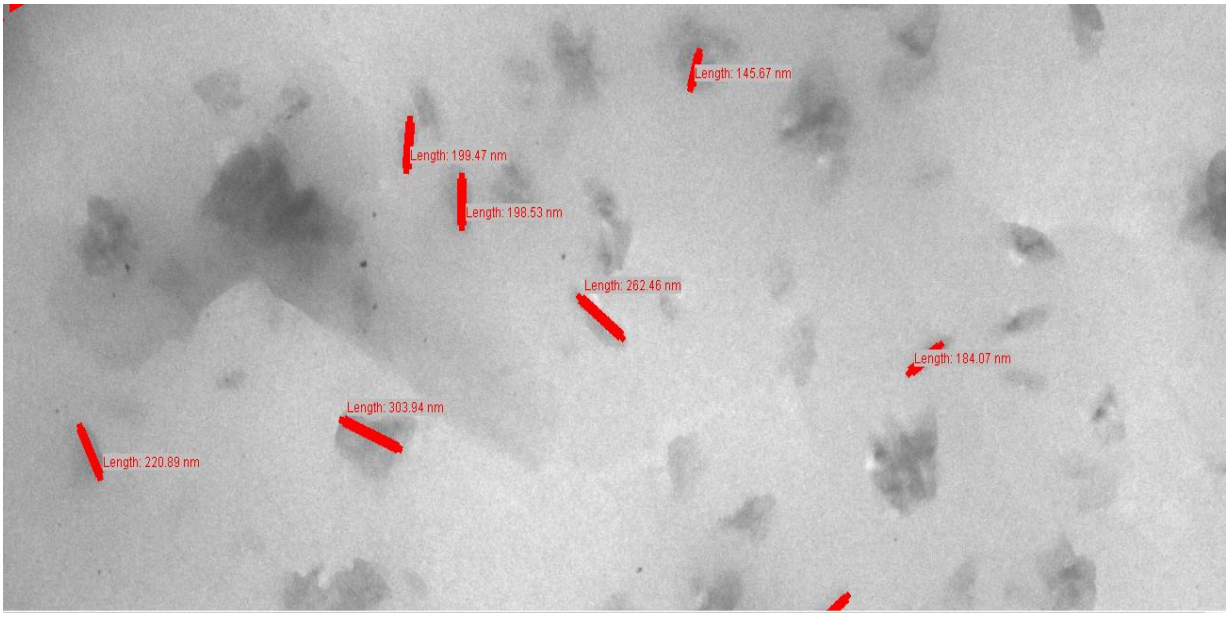

Fig 4-27 TEM image of 50%Li/CaO spent catalyst.

CHAPTER 5. CONCLUSIONS AND RECOMMENDATIONS

From this present study, conclusions based on findings and recommendations for further research in this area are hereby documented.

CONCLUSIONS

Catalytic decomposition of methane is one of the best alternatives to producing pure hydrogen. Solid nickel catalysts have been widely used in methane decomposition, but they readily undergo deactivation due to coking and sintering. Several metal oxides such as; Al_2O_3, MgO and SiO_2, Al_2O_3 have been used as supports to increase its surface area but of greater interest, is the use of CaO which has catalytic activity. From the set of temperatures used in this study, 650℃ was taken as the optimum operating temperature because every catalyst recorded peak performance at this point. Catalyst 50%Ni/CaO showed a 60.2% methane conversion and 35.7% hydrogen at 650℃ and GHSV of 2. Introduction of lithium to Ni/CaO catalyst improved its performance tremendously and all catalysts in the molten environment showed close values since their major component was the support at 50%. Activity results revealed that catalyst 37.5%Ni-12.5%Li/CaO displayed outstanding results among all the catalysts by having 65.7% methane conversion and 38.3% hydrogen yield at 650℃ and GHSV of $2Lg^{-1}{}_{cat}h^{-1}$. This confirms the objective of this present work, which was to develop a stable and active supported molten metal catalyst for CMD reaction. The supported molten metal catalyst recorded better performance than the unsupported catalyst because the CMD reaction took place by surface reaction and chemisorption. By this, the molten environment aided the catalyst activity by 9.1%. Under those conditions the life of the supported catalyst was extended due to less pronounced coking. This shows promise to more application and commercialization of the catalyst for use in catalytic decomposition of methane to produce carbon and clean hydrogen.

RECOMMENDATIONS

Considering current demand for pure hydrogen and an envisioned increase in number of its uses, a suitable process based on CMD reaction needs to be developed with special emphasis on hydrogen yield, purity of hydrogen and carbon nanomaterial as determining factors. Decomposition of methane using an active and stable catalyst is an attractive option to producing high purity hydrogen. Conventional catalysts such as nickel, iron, activated carbon, cobalt and carbon black have been widely used in CMD reaction. The major challenge of this catalytic

process is rapid loss of catalyst life due to coking by carbon nanomaterial and difficulty in regenerating the spent catalyst. Significance advances have been made in regenerating the spent catalyst by introducing other higher hydrocarbons in the methane feed i.e. inclusion of 40% ethanol to methane feed improves the yield of hydrogen by 10times. Spent catalysts can be effectively regenerated using oxygen, though other methods employing steam can be used as well. Operating conditions like temperature, pressure, CH_4/H_2 conversion, feed composition and flowrate need to be studied further to improve catalytic methane decomposition process.

In the present work, good performance of Ni-Li/CaO catalyst in terms of methane conversion and hydrogen yield has been claimed but to commercialize the catalyst, further research is open to interested researchers to explore the following aspects which were not covered in this work. Such studies can focus on;

- Regeneration of the spent catalyst
- The actual time taken for the Ni-Li/CaO catalyst be completely deactivated.
- To use the same Ni-Li catalyst on different metal oxide supports

REFERENCES

Abbas, H. F. and Baker, I. F. 2011. Thermocatalytic decomposition of methane using activated carbon: Studying the influence of process parameters using factorial design. *International Journal of Hydrogen Energy*, 36 (15): 8985-8993.

Abbas, H. F. and Wan Daud, W. M. A. 2010. Hydrogen production by methane decomposition: A review. *International Journal of Hydrogen Energy*, 35 (3): 1160-1190.

Abd Hamid, S. B., Ambursa, M. M., Sudarsanam, P., Voon, L. H. and Bhargava, S. K. 2017. Effect of Ti loading on structure-activity properties of Cu-Ni/Ti-MCM-41 catalysts in hydrodeoxygenation of guaiacol. *Catalysis Communications*, 94: 18-22.

Acar, C. and Dincer, I. 2014. Comparative assessment of hydrogen production methods from renewable and non-renewable sources. *International Journal of Hydrogen Energy*, 39 (1): 1-12.

Aiello, R., Fiscus, J. E., zur Loye, H.-C. and Amiridis, M. D. 2000. Hydrogen production via the direct cracking of methane over Ni/SiO2: catalyst deactivation and regeneration. *Applied Catalysis A: General*, 192 (2): 227-234.

Al-Fatesh, A. S., Fakeeha, A. H., Khan, W. U., Ibrahim, A. A., He, S. and Seshan, K. 2016. Production of hydrogen by catalytic methane decomposition over alumina supported mono-, bi- and tri-metallic catalysts. *International Journal of Hydrogen Energy*, 41 (48): 22932-22940.

Alcheikhhamdon, Y. and Hoorfar, M. 2016. Natural gas quality enhancement: A review of the conventional treatment processes, and the industrial challenges facing emerging technologies. *Journal of Natural Gas Science and Engineering*, 34: 689-701.

Aljundi, I. H. 2011. Effect of dry hydrocarbons and critical point temperature on the efficiencies of organic Rankine cycle. *Renewable Energy*, 36 (4): 1196-1202.

Allouhi, A., Zamzoum, O., Islam, M. R., Saidur, R., Kousksou, T., Jamil, A. and Derouich, A. 2017. Evaluation of wind energy potential in Morocco's coastal regions. *Renewable and Sustainable Energy Reviews*, 72: 311-324.

Amin, A. M., Croiset, E., Constantinou, C. and Epling, W. 2012. Methane cracking using Ni supported on porous and non-porous alumina catalysts. *International Journal of Hydrogen Energy*, 37 (11): 9038-9048.

Amin, A. M., Croiset, E. and Epling, W. 2011. Review of methane catalytic cracking for hydrogen production. *International Journal of Hydrogen Energy*, 36 (4): 2904-2935.

Arena, F., Italiano, G., Barbera, K., Bonura, G., Spadaro, L. and Frusteri, F. 2009. Basic evidences for methanol-synthesis catalyst design. *Catalysis Today*, 143 (1–2): 80-85.

Ashik, U., Daud, W. W. and Abbas, H. F. 2015a. Production of greenhouse gas free hydrogen by thermocatalytic decomposition of methane–a review. *Renewable and Sustainable Energy Reviews*, 44: 221-256.

Ashik, U. P. M., Wan Daud, W. M. A. and Abbas, H. F. 2015b. Production of greenhouse gas free hydrogen by thermocatalytic decomposition of methane – A review. *Renewable and Sustainable Energy Reviews*, 44: 221-256.

Ashok, J., Raju, G., Reddy, P. S., Subrahmanyam, M. and Venugopal, A. 2008. Catalytic decomposition of CH4 over Ni-Al2O3-SiO2 catalysts: Influence of pretreatment conditions for the production of H2. *Journal of Natural Gas Chemistry*, 17 (2): 113-119.

Atilgan, B. and Azapagic, A. 2015. Life cycle environmental impacts of electricity from fossil fuels in Turkey. *Journal of Cleaner Production*, 106: 555-564.

Bai, Z., Chen, H., Li, B. and Li, W. 2007. Methane decomposition over Ni loaded activated carbon for hydrogen production and the formation of filamentous carbon. *International Journal of Hydrogen Energy*, 32 (1): 32-37.

Baiker, A. 1987. Catalysis and surface properties of liquid metals and alloys. *Applied Catalysis*, 35 (2): 416-417.

Balázsi, C., Wéber, F., Kövér, Z., Horváth, E. and Németh, C. 2007. Preparation of calcium–phosphate bioceramics from natural resources. *Journal of the European Ceramic Society*, 27 (2): 1601-1606.

Bayat, N., Meshkani, F. and Rezaei, M. 2016. Thermocatalytic decomposition of methane to COx-free hydrogen and carbon over Ni–Fe–Cu/Al2O3 catalysts. *International Journal of Hydrogen Energy*, 41 (30): 13039-13049.

Baykara, S. Z. 2004. Experimental solar water thermolysis. *International Journal of Hydrogen Energy*, 29 (14): 1459-1469.

Bilgili, M., Ozbek, A., Sahin, B. and Kahraman, A. 2015. An overview of renewable electric power capacity and progress in new technologies in the world. *Renewable and Sustainable Energy Reviews*, 49: 323-334.

Borghei, M., Karimzadeh, R., Rashidi, A. and Izadi, N. 2010. Kinetics of methane decomposition to COx-free hydrogen and carbon nanofiber over Ni–Cu/MgO catalyst. *International Journal of Hydrogen Energy*, 35 (17): 9479-9488.

Brockner, W., Ehrhardt, C. and Gjikaj, M. 2007. Thermal decomposition of nickel nitrate hexahydrate, Ni(NO3)2·6H2O, in comparison to Co(NO3)2·6H2O and Ca(NO3)2·4H2O. *Thermochimica Acta*, 456 (1): 64-68.

Carstens, J. N. and Bell, A. T. 1996. Methane Activation and Conversion to Higher Hydrocarbons on Supported Ruthenium. *Journal of Catalysis*, 161 (1): 423-429.

Castaldo, V. L., Coccia, V., Cotana, F., Pignatta, G., Pisello, A. L. and Rossi, F. 2015. Thermal-energy analysis of natural "cool" stone aggregates as passive cooling and global warming mitigation technique. *Urban Climate*, 14, Part 2: 301-314.

Chai, S.-P., Seah, C.-M. and Mohamed, A. R. 2011. A parametric study of methane decomposition into carbon nanotubes over 8Co-2Mo/Al2O3 catalyst. *Journal of Natural Gas Chemistry*, 20 (1): 84-89.

Chai, S.-P., Zein, S. H. S. and Mohamed, A. R. 2007a. The effect of reduction temperature on Co-Mo/Al2O3 catalysts for carbon nanotubes formation. *Applied Catalysis A: General*, 326 (2): 173-179.

Chai, S.-P., Zein, S. H. S. and Mohamed, A. R. 2007b. Synthesizing carbon nanotubes and carbon nanofibers over supported-nickel oxide catalysts via catalytic decomposition of methane. *Diamond and Related Materials*, 16 (8): 1656-1664.

Chari, V. D., Sharma, D. V. S. G. K., Prasad, P. S. R. and Murthy, S. R. 2013. Methane hydrates formation and dissociation in nano silica suspension. *Journal of Natural Gas Science and Engineering*, 11: 7-11.

Chen, D., Christensen, K. O., Ochoa-Fernández, E., Yu, Z., Tøtdal, B., Latorre, N., Monzón, A. and Holmen, A. 2005. Synthesis of carbon nanofibers: effects of Ni crystal size during methane decomposition. *Journal of Catalysis*, 229 (1): 82-96.

Chen, J., He, M., Wang, G., Li, Y. and Zhu, Z. J. 2009a. Production of hydrogen from methane decomposition using nanosized carbon black as catalyst in a fluidized-bed reactor. *International Journal of Hydrogen Energy*, 34 (24): 9730-9736.

Chen, J., Li, Y., Li, Z. and Zhang, X. 2004. Production of COx-free hydrogen and nanocarbon by direct decomposition of undiluted methane on Ni–Cu–alumina catalysts. *Applied Catalysis A: General*, 269 (1–2): 179-186.

Chen, J., Li, Y., Ma, Y., Qin, Y. and Chang, L. 2001. Formation of bamboo-shaped carbon filaments and dependence of their morphology on catalyst composition and reaction conditions. *Carbon*, 39 (10): 1467-1475.

Chen, J., Ma, Q., Rufford, T. E., Li, Y. and Zhu, Z. 2009b. Influence of calcination temperatures of Feitknecht compound precursor on the structure of Ni–Al2O3 catalyst and the corresponding catalytic activity in methane decomposition to hydrogen and carbon nanofibers. *Applied Catalysis A: General*, 362 (1–2): 1-7.

Chen, P., Zhang, H. B., Lin, G. D., Hong, Q. and Tsai, K. R. 1997. Growth of carbon nanotubes by catalytic decomposition of CH4 or CO on a Ni□MgO catalyst. *Carbon*, 35 (10): 1495-1501.

Cherubini, F. and Strømman, A. H. 2011. Life cycle assessment of bioenergy systems: State of the art and future challenges. *Bioresource Technology*, 102 (2): 437-451.

Chesnokov, V. V. and Chichkan, A. S. 2009. Production of hydrogen by methane catalytic decomposition over Ni–Cu–Fe/Al2O3 catalyst. *International Journal of Hydrogen Energy*, 34 (7): 2979-2985.

Cho, Y. H., Aminorroaya, S., Liu, H. K. and Dahle, A. K. 2011. The effect of transition metals on hydrogen migration and catalysis in cast Mg–Ni alloys. *International Journal of Hydrogen Energy*, 36 (8): 4984-4992.

Choudhary, V. R., Banerjee, S. and Rajput, A. M. 2001. Continuous Production of H2 at Low Temperature from Methane Decomposition over Ni-Containing Catalyst Followed by Gasification by Steam of the Carbon on the Catalyst in Two Parallel Reactors Operated in Cyclic Manner. *Journal of Catalysis*, 198 (1): 136-141.

Choudhary, V. R., Banerjee, S. and Rajput, A. M. 2002. Hydrogen from step-wise steam reforming of methane over Ni/ZrO2: factors affecting catalytic methane decomposition and gasification by steam of carbon formed on the catalyst. *Applied Catalysis A: General*, 234 (1–2): 259-270.

Cunha, A. F., Órfão, J. J. M. and Figueiredo, J. L. 2009a. Methane decomposition on Fe–Cu Raney-type catalysts. *Fuel Processing Technology*, 90 (10): 1234-1240.

Cunha, A. F., Órfão, J. J. M. and Figueiredo, J. L. 2009b. Methane decomposition on Ni–Cu alloyed Raney-type catalysts. *International Journal of Hydrogen Energy*, 34 (11): 4763-4772.

Das, D. and Veziroglu, T. N. 2008. Advances in biological hydrogen production processes. *International Journal of Hydrogen Energy*, 33 (21): 6046-6057.

de la Casa-Lillo, M. A., Moore, B. C., Cazorla-Amorós, D. and Linares-Solano, A. 2002. Molecular sieve properties obtained by cracking of methane on activated carbon fibers. *Carbon*, 40 (13): 2489-2494.

de_Richter, R. K., Ming, T., Caillol, S. and Liu, W. 2016. Fighting global warming by GHG removal: Destroying CFCs and HCFCs in solar-wind power plant hybrids producing renewable energy with no-intermittency. *International Journal of Greenhouse Gas Control*, 49: 449-472.

Demirci, U. B. and Miele, P. 2013. Overview of the relative greenness of the main hydrogen production processes. *Journal of Cleaner Production*, 52: 1-10.

Dhankhar, M., Pal Singh, O. and Singh, V. N. 2014. Physical principles of losses in thin film solar cells and efficiency enhancement methods. *Renewable and Sustainable Energy Reviews*, 40: 214-223.

Dharmaraj, N., Prabu, P., Nagarajan, S., Kim, C. H., Park, J. H. and Kim, H. Y. 2006. Synthesis of nickel oxide nanoparticles using nickel acetate and poly(vinyl acetate) precursor. *Materials Science and Engineering: B*, 128 (1): 111-114.

Dincer, I. and Acar, C. 2015. Review and evaluation of hydrogen production methods for better sustainability. *International Journal of Hydrogen Energy*, 40 (34): 11094-11111.

Ding, C., Ai, G., Zhang, K., Yuan, Q., Han, Y., Ma, X., Wang, J. and Liu, S. 2015. Coking resistant Ni/ZrO2@SiO2 catalyst for the partial oxidation of methane to synthesis gas. *International Journal of Hydrogen Energy*, 40 (21): 6835-6843.

Dragomir, G., Șerban, A., Năstase, G. and Brezeanu, A. I. 2016. Wind energy in Romania: A review from 2009 to 2016. *Renewable and Sustainable Energy Reviews*, 64: 129-143.

Dufour, A., Celzard, A., Fierro, V., Martin, E., Broust, F. and Zoulalian, A. 2008. Catalytic decomposition of methane over a wood char concurrently activated by a pyrolysis gas. *Applied Catalysis A: General*, 346 (1–2): 164-173.

Dunker, A. M., Kumar, S. and Mulawa, P. A. 2006. Production of hydrogen by thermal decomposition of methane in a fluidized-bed reactor—Effects of catalyst, temperature, and residence time. *International Journal of Hydrogen Energy*, 31 (4): 473-484.

Echegoyen, Y., Suelves, I., Lázaro, M. J., Sanjuán, M. L. and Moliner, R. 2007. Thermo catalytic decomposition of methane over Ni–Mg and Ni–Cu–Mg catalysts: Effect of catalyst preparation method. *Applied Catalysis A: General*, 333 (2): 229-237.

Egeberg, R. C., Ullmann, S., Alstrup, I., Mullins, C. B. and Chorkendorff, I. 2002. Dissociation of CH4 on Ni(1 1 1) and Ru(0 0 0 1). *Surface Science*, 497 (1–3): 183-193.

Ehrhardt, C., Gjikaj, M. and Brockner, W. 2005. Thermal decomposition of cobalt nitrato compounds: Preparation of anhydrous cobalt(II)nitrate and its characterisation by Infrared and Raman spectra. *Thermochimica Acta*, 432 (1): 36-40.

Elitzur, S., Rosenband, V. and Gany, A. 2016. Combined energy production and waste management in manned spacecraft utilizing on-demand hydrogen production and fuel cells. *Acta Astronautica*, 128: 580-583.

Elmasry, M., Gaber, A. and Khater, E. 1998. Thermal decomposition of Ni (II) and Fe (III) nitrates and their mixture. *Journal of thermal analysis and calorimetry*, 52 (2): 489-495.

Ermakova, M. A. and Ermakov, D. Y. 2002. Ni/SiO2 and Fe/SiO2 catalysts for production of hydrogen and filamentous carbon via methane decomposition. *Catalysis Today*, 77 (3): 225-235.

Ermakova, M. A., Ermakov, D. Y. and Kuvshinov, G. G. 2000. Effective catalysts for direct cracking of methane to produce hydrogen and filamentous carbon: Part I. Nickel catalysts. *Applied Catalysis A: General*, 201 (1): 61-70.

Estellé, J., Salagre, P., Cesteros, Y., Serra, M., Medina, F. and Sueiras, J. 2003. Comparative study of the morphology and surface properties of nickel oxide prepared from different precursors. *Solid State Ionics*, 156 (1): 233-243.

Fakeeha, A. H., Khan, W. U., Al-Fatesh, A. S., Ibrahim, A. A. and Abasaeed, A. E. 2016. Production of hydrogen from methane over lanthanum supported bimetallic catalysts. *International Journal of Hydrogen Energy*, 41 (19): 8193-8198.

Faramawy, S., Zaki, T. and Sakr, A. A. E. 2016. Natural gas origin, composition, and processing: A review. *Journal of Natural Gas Science and Engineering*, 34: 34-54.

Forzatti, P. and Lietti, L. 1999. Catalyst deactivation. *Catalysis Today*, 52 (2–3): 165-181.

Frusteri, F., Italiano, G., Espro, C. and Arena, F. 2011. CH4 decomposition on Ni and Co thin layer catalysts to produce H2 for fuel cell. *Catalysis Today*, 171 (1): 60-66.

Fu, T. and Li, Z. 2015. Review of recent development in Co-based catalysts supported on carbon materials for Fischer–Tropsch synthesis. *Chemical Engineering Science*, 135: 3-20.

Fukada, S., Nakamura, N., Monden, J. and Nishikawa, M. 2004. Experimental study of cracking methane by Ni/SiO2 catalyst. *Journal of Nuclear Materials*, 329–333, Part B: 1365-1369.

Fulcheri, L., Probst, N., Flamant, G., Fabry, F., Grivei, E. and Bourrat, X. 2002. Plasma processing: a step towards the production of new grades of carbon black. *Carbon*, 40 (2): 169-176.

Gatica, J. M., Gómez, D. M., Harti, S. and Vidal, H. 2013. Monolithic honeycomb design applied to carbon materials for catalytic methane decomposition. *Applied Catalysis A: General*, 458: 21-27.

Gaurav, N., Sivasankari, S., Kiran, G. S., Ninawe, A. and Selvin, J. 2017. Utilization of bioresources for sustainable biofuels: A Review. *Renewable and Sustainable Energy Reviews*, 73: 205-214.

Gawande, V. B., Dhoble, A. S. and Zodpe, D. B. 2014. Effect of roughness geometries on heat transfer enhancement in solar thermal systems – A review. *Renewable and Sustainable Energy Reviews*, 32: 347-378.

Ghandehariun, S., Rosen, M. A. and Naterer, G. F. 2016. Direct contact heat transfer from molten salt droplets in a thermochemical water splitting process of hydrogen production. *International Journal of Heat and Mass Transfer*, 96: 125-131.

Gonçalves, A. M., Lima-Corrêa, R. A. B., Assaf, J. M. and Nogueira, A. R. A. 2017. Lithium and calcium based perovskite type oxides for ethylic transesterification. *Catalysis Today*, 279: 177-186.

Guevara, J. C., Wang, J. A., Chen, L. F., Valenzuela, M. A., Salas, P., García-Ruiz, A., Toledo, J. A., Cortes-Jácome, M. A., Angeles-Chavez, C. and Novaro, O. 2010. Ni/Ce-MCM-41 mesostructured catalysts for simultaneous production of hydrogen and nanocarbon via methane decomposition. *International Journal of Hydrogen Energy*, 35 (8): 3509-3521.

Guil-Lopez, R., Botas, J. A., Fierro, J. L. G. and Serrano, D. P. 2011. Comparison of metal and carbon catalysts for hydrogen production by methane decomposition. *Applied Catalysis A: General*, 396 (1–2): 40-51.

He, C., Zhao, N., Du, X., Shi, C., Ding, J., Li, J. and Li, Y. 2006. Low-temperature synthesis of carbon onions by chemical vapor deposition using a nickel catalyst supported on aluminum. *Scripta Materialia*, 54 (4): 689-693.

Ho, W. W. S., Ng, H. K., Gan, S. and Tan, S. H. 2014. Evaluation of palm oil mill fly ash supported calcium oxide as a heterogeneous base catalyst in biodiesel synthesis from crude palm oil. *Energy Conversion and Management*, 88: 1167-1178.

Hornés, A., Bera, P., Fernández-García, M., Guerrero-Ruiz, A. and Martínez-Arias, A. 2012. Catalytic and redox properties of bimetallic Cu–Ni systems combined with CeO2 or Gd-doped CeO2 for methane oxidation and decomposition. *Applied Catalysis B: Environmental*, 111–112: 96-105.

Hussain, A., Arif, S. M. and Aslam, M. 2017. Emerging renewable and sustainable energy technologies: State of the art. *Renewable and Sustainable Energy Reviews*, 71: 12-28.

Jawahar, C. P. and Michael, P. A. 2017. A review on turbines for micro hydro power plant. *Renewable and Sustainable Energy Reviews*, 72: 882-887.

Jin, L., Si, H., Zhang, J., Lin, P., Hu, Z., Qiu, B. and Hu, H. 2013. Preparation of activated carbon supported Fe–Al2O3 catalyst and its application for hydrogen production by catalytic methane decomposition. *International Journal of Hydrogen Energy*, 38 (25): 10373-10380.

Jones, A. M. E., Bridges, M., Bones, A. M., Cole, R. and Rossiter, J. T. 2001. Purification and characterisation of a non-plant myrosinase from the cabbage aphid Brevicoryne brassicae (L.). *Insect Biochemistry and Molecular Biology*, 31 (1): 1-5.

Karakaya, C. and Kee, R. J. 2016. Progress in the direct catalytic conversion of methane to fuels and chemicals. *Progress in Energy and Combustion Science*, 55: 60-97.

Keipi, T., Tolvanen, K. E. S., Tolvanen, H. and Konttinen, J. 2016. Thermo-catalytic decomposition of methane: The effect of reaction parameters on process design and the utilization possibilities of the produced carbon. *Energy Conversion and Management*, 126: 923-934.

Kępiński, L., Stasińska, B. and Borowiecki, T. 2000. Carbon deposition on Ni/Al2O3 catalysts doped with small amounts of molybdenum. *Carbon*, 38 (13): 1845-1856.

Kiat, J. M., Boemare, G., Rieu, B. and Aymes, D. 1998. Structural evolution of LiOH: evidence of a solid–solid transformation toward Li2O close to the melting temperature. *Solid State Communications*, 108 (4): 241-245.

Kim, M. H., Lee, E. K., Jun, J. H., Kong, S. J., Han, G. Y., Lee, B. K., Lee, T.-J. and Yoon, K. J. 2004. Hydrogen production by catalytic decomposition of methane over activated carbons: kinetic study. *International Journal of Hydrogen Energy*, 29 (2): 187-193.

Kuchtanin, V., Kleščíková, L., Šoral, M., Fischer, R., Růžičková, Z., Rakovský, E., Moncoľ, J. and Segľa, P. 2016. Nickel(II) Schiff base complexes: Synthesis, characterization and catalytic activity in Kumada–Corriu cross-coupling reactions. *Polyhedron*, 117: 90-96.

Kuo, C.-S., Bai, A., Huang, C.-M., Li, Y.-Y., Hu, C.-C. and Chen, C.-C. 2005. Diameter control of multiwalled carbon nanotubes using experimental strategies. *Carbon*, 43 (13): 2760-2768.

Kuras, M., Zimmermann, Y. and Petit, C. 2008. Reactivity of perovskite-type precursor in MWCNTs synthesis. *Catalysis Today*, 138 (1–2): 55-61.

Kvande, I., Chen, D., Yu, Z., Rønning, M. and Holmen, A. 2008. Optimization and scale-up of CNF production based on intrinsic kinetic data obtained from TEOM. *Journal of Catalysis*, 256 (2): 204-214.

Kyriakis, S. A. and Younger, P. L. 2016. Towards the increased utilisation of geothermal energy in a district heating network through the use of a heat storage. *Applied Thermal Engineering*, 94: 99-110.

Kyriakopoulos, G. L. and Arabatzis, G. 2016. Electrical energy storage systems in electricity generation: Energy policies, innovative technologies, and regulatory regimes. *Renewable and Sustainable Energy Reviews*, 56: 1044-1067.

Lægsgaard Jørgensen, S., Nielsen, P. E. H. and Lehrmann, P. 1995. Steam reforming of methane in a membrane reactor. *Catalysis Today*, 25 (3): 303-307.

Lee, E. K., Lee, S. Y., Han, G. Y., Lee, B. K., Lee, T.-J., Jun, J. H. and Yoon, K. J. 2004a. Catalytic decomposition of methane over carbon blacks for CO2-free hydrogen production. *Carbon*, 42 (12–13): 2641-2648.

Lee, G., Kang, J. Y., Yan, N., Suh, Y.-W. and Jung, J. C. 2016. Simple preparation method for Mg–Al hydrotalcites as base catalysts. *Journal of Molecular Catalysis A: Chemical*, 423: 347-355.

Lee, K. C. 2001. Classification of geothermal resources by exergy. *Geothermics*, 30 (4): 431-442.

Lee, K. K., Han, G. Y., Yoon, K. J. and Lee, B. K. 2004b. Thermocatalytic hydrogen production from the methane in a fluidized bed with activated carbon catalyst. *Catalysis Today*, 93–95: 81-86.

Lemus, R. G. and Martínez Duart, J. M. 2010. Updated hydrogen production costs and parities for conventional and renewable technologies. *International Journal of Hydrogen Energy*, 35 (9): 3929-3936.

Leofanti, G., Padovan, M., Tozzola, G. and Venturelli, B. 1998. Surface area and pore texture of catalysts. *Catalysis Today*, 41 (1): 207-219.

Levin, D. B. and Chahine, R. 2010. Challenges for renewable hydrogen production from biomass. *International Journal of Hydrogen Energy*, 35 (10): 4962-4969.

Li, J., Dong, L., Xiong, L., Yang, Y., Du, Y., Zhao, L., Wang, H. and Peng, S. 2016. High-loaded NiCuSiO2 catalysts for methane decomposition to prepare hydrogen and carbon filaments. *International Journal of Hydrogen Energy*, 41 (28): 12038-12048.

Li, Y., Chen, J. and Chang, L. 1997. Catalytic growth of carbon fibers from methane on a nickel-alumina composite catalyst prepared from Feitknecht compound precursor. *Applied Catalysis A: General*, 163 (1): 45-57.

Li, Y., Chen, J., Chang, L. and Qin, Y. 1998. The Doping Effect of Copper on the Catalytic Growth of Carbon Fibers from Methane over a Ni/Al2O3Catalyst Prepared from Feitknecht Compound Precursor. *Journal of Catalysis*, 178 (1): 76-83.

Li, Y., Li, D. and Wang, G. 2011. Methane decomposition to COx-free hydrogen and nano-carbon material on group 8–10 base metal catalysts: A review. *Catalysis Today*, 162 (1): 1-48.

Li, Y., Zhang, B., Tang, X., Xu, Y. and Shen, W. 2006. Hydrogen production from methane decomposition over Ni/CeO2 catalysts. *Catalysis Communications*, 7 (6): 380-386.

Li, Z., Chen, J., Zhang, X., Li, Y. and Fung, K. K. 2002. Catalytic synthesized carbon nanostructures from methane using nanocrystalline Ni. *Carbon*, 40 (3): 409-415.

Liu, H., Yao, L., Hadj Taief, H. B., Benzina, M., Da Costa, P. and Gálvez, M. E. Natural clay-based Ni-catalysts for dry reforming of methane at moderate temperatures. *Catalysis Today*,

Liu, Q., Tian, Y., Li, H., Jia, L., Xia, C., Thompson, L. T. and Li, Y. 2010. High efficiency chemical energy conversion system based on a methane catalytic decomposition reaction and two fuel cells: Part I. Process modeling and validation. *Journal of Power Sources*, 195 (19): 6539-6548.

Llorente García, I., Álvarez, J. L. and Blanco, D. 2011. Performance model for parabolic trough solar thermal power plants with thermal storage: Comparison to operating plant data. *Solar Energy*, 85 (10): 2443-2460.

López-Arce, P., Gómez-Villalba, L. S., Martínez-Ramírez, S., Álvarez de Buergo, M. and Fort, R. 2011. Influence of relative humidity on the carbonation of calcium hydroxide nanoparticles and the formation of calcium carbonate polymorphs. *Powder Technology*, 205 (1): 263-269.

Luo, S. and Feng, Y. 2016. The production of hydrogen-rich gas by wet sludge pyrolysis using waste heat from blast-furnace slag. *Energy*, 113: 845-851.

Mahela, O. P. and Shaik, A. G. 2016. Comprehensive overview of grid interfaced wind energy generation systems. *Renewable and Sustainable Energy Reviews*, 57: 260-281.

Malafeh, S. and Sharp, B. 2015. Role of royalties in sustainable geothermal energy development. *Energy Policy*, 85: 235-242.

Malaika, A. and Kozłowski, M. 2009. Influence of ethylene on carbon-catalysed decomposition of methane. *International Journal of Hydrogen Energy*, 34 (6): 2600-2605.

Małecki, A., Gajerski, R., Łabuś, S., Prochowska-Klisch, B. and Wojciechowski, K. 2000. Mechanism of thermal decomposition of d-metals nitrates hydrates. *Journal of thermal analysis and calorimetry*, 60 (1): 17-23.

Mancino, G., Cimino, S. and Lisi, L. 2016. Sulphur poisoning of alumina supported Rh catalyst during dry reforming of methane. *Catalysis Today*, 277, Part 1: 126-132.

Meher Kotay, S. and Das, D. 2008. Biohydrogen as a renewable energy resource—Prospects and potentials. *International Journal of Hydrogen Energy*, 33 (1): 258-263.

Meng, T., Xu, Q.-Q., Li, Y.-T., Chang, J.-L., Ren, T.-Z. and Yuan, Z.-Y. 2015. Nickle nanoparticles highly dispersed on reduced graphene oxide for ammonia decomposition to hydrogen. *Journal of Industrial and Engineering Chemistry*, 32: 373-379.

Metz, R., Machado, C., Tenu, R., Elkhatib, M., Letoffe, J. and Delalu, H. 2004. Possible evidence of the nickel nitrate salt Ni (NO $ _3 $) $ _2 $. 5.5 H $ _2 $ O. In: Proceedings of *Journal de Physique IV (Proceedings)*. EDP sciences, 139-142.

Moliner, R., Suelves, I., Lázaro, M. J. and Moreno, O. 2005. Thermocatalytic decomposition of methane over activated carbons: influence of textural properties and surface chemistry. *International Journal of Hydrogen Energy*, 30 (3): 293-300.

Moriarty, P. and Honnery, D. 2007. Intermittent renewable energy: The only future source of hydrogen? *International Journal of Hydrogen Energy*, 32 (12): 1616-1624.

Moury, R., Petit, J. F., Demirci, U. B., Ichikawa, T. and Miele, P. 2015. Pure hydrogen-generating "doped" sodium hydrazinidoborane. *International Journal of Hydrogen Energy*, 40 (24): 7475-7482.

Muradov, N. 2001a. Catalysis of methane decomposition over elemental carbon. *Catalysis Communications*, 2 (3–4): 89-94.

Muradov, N. 2001b. Hydrogen via methane decomposition: an application for decarbonization of fossil fuels. *International Journal of Hydrogen Energy*, 26 (11): 1165-1175.

Muradov, N., Smith, F., Huang, C. and T-Raissi, A. 2006. Autothermal catalytic pyrolysis of methane as a new route to hydrogen production with reduced CO2 emissions. *Catalysis Today*, 116 (3): 281-288.

Muradov, N., Smith, F. and T-Raissi, A. 2005. Catalytic activity of carbons for methane decomposition reaction. *Catalysis Today*, 102–103: 225-233.

Muradov, N. Z. and Veziroğlu, T. N. 2005. From hydrocarbon to hydrogen–carbon to hydrogen economy. *International Journal of Hydrogen Energy*, 30 (3): 225-237.

Nakomcic-Smaragdakis, B., Stajic, T., Cepic, Z. and Djuric, S. 2012. Geothermal energy potentials in the province of Vojvodina from the aspect of the direct energy utilization. *Renewable and Sustainable Energy Reviews*, 16 (8): 5696-5706.

Nasir Uddin, M., Daud, W. M. A. W. and Abbas, H. F. 2013. Potential hydrogen and non-condensable gases production from biomass pyrolysis: Insights into the process variables. *Renewable and Sustainable Energy Reviews*, 27: 204-224.

Nasir Uddin, M., Wan Daud, W. M. A. and Abbas, H. F. 2014. Kinetics and deactivation mechanisms of the thermal decomposition of methane in hydrogen and carbon nanofiber Co-production over Ni-supported Y zeolite-based catalysts. *Energy Conversion and Management*, 87: 796-809.

Ni, L., Kuroda, K., Zhou, L.-P., Kizuka, T., Ohta, K., Matsuishi, K. and Nakamura, J. 2006a. Kinetic study of carbon nanotube synthesis over Mo/Co/MgO catalysts. *Carbon*, 44 (11): 2265-2272.

Ni, M., Leung, M. K. H., Sumathy, K. and Leung, D. Y. C. 2006b. Potential of renewable hydrogen production for energy supply in Hong Kong. *International Journal of Hydrogen Energy*, 31 (10): 1401-1412.

Nicoletti, G., Arcuri, N., Nicoletti, G. and Bruno, R. 2015. A technical and environmental comparison between hydrogen and some fossil fuels. *Energy Conversion and Management*, 89: 205-213.

Nikolaidis, P. and Poullikkas, A. 2017. A comparative overview of hydrogen production processes. *Renewable and Sustainable Energy Reviews*, 67: 597-611.

Nithyadharseni, P., Reddy, M. V., Ozoemena, K. I., Balakrishna, R. G. and Chowdari, B. V. R. 2015. Low temperature molten salt synthesis of Y2Sn2O7 anode material for lithium ion batteries. *Electrochimica Acta*, 182: 1060-1069.

Ntona, E., Arabatzis, G. and Kyriakopoulos, G. L. 2015. Energy saving: Views and attitudes of students in secondary education. *Renewable and Sustainable Energy Reviews*, 46: 1-15.

Panwar, N. L., Kaushik, S. C. and Kothari, S. 2011. Role of renewable energy sources in environmental protection: A review. *Renewable and Sustainable Energy Reviews*, 15 (3): 1513-1524.

Pendyala, V. R. R., Jacobs, G., Bertaux, C., Khalid, S. and Davis, B. H. 2016. Fischer–Tropsch synthesis: Effect of ammonia on supported cobalt catalysts. *Journal of Catalysis*, 337: 80-90.

Piao, L., Li, Y., Chen, J., Chang, L. and Lin, J. Y. S. 2002. Methane decomposition to carbon nanotubes and hydrogen on an alumina supported nickel aerogel catalyst. *Catalysis Today*, 74 (1–2): 145-155.

Ping, D., Wang, C., Dong, X. and Dong, Y. 2016. Co-production of hydrogen and carbon nanotubes on nickel foam via methane catalytic decomposition. *Applied Surface Science*, 369: 299-307.

Pinilla, J. L., Suelves, I., Lázaro, M. J., Moliner, R. and Palacios, J. M. 2010. Parametric study of the decomposition of methane using a NiCu/Al2O3 catalyst in a fluidized bed reactor. *International Journal of Hydrogen Energy*, 35 (18): 9801-9809.

Purohit, R., Purohit, K., Rana, S., Rana, R. S. and Patel, V. 2014. Carbon Nanotubes and Their Growth Methods. *Procedia Materials Science*, 6: 716-728.

Qian, W., Liu, T., Wei, F., Wang, Z., Wang, D. and Li, Y. 2003. Carbon nanotubes with large cores produced by adding sodium carbonate to the catalyst. *Carbon*, 41 (13): 2683-2686.

Rahman, S. M. and Khondaker, A. N. 2012. Mitigation measures to reduce greenhouse gas emissions and enhance carbon capture and storage in Saudi Arabia. *Renewable and Sustainable Energy Reviews*, 16 (5): 2446-2460.

Ruiz, J. A. C., Fraga, M. A. and Pastore, H. O. 2007. Methane combustion over Pd supported on MCM-41. *Applied Catalysis B: Environmental*, 76 (1–2): 115-122.

Saito, M., Sakurai, S., Iwai, H. and Yoshida, H. 2017. Description of reaction rate for steam methane reforming throughout a channel in combination with diffusion in a porous catalytic wall: Extension to concentration variation along flow direction. *International Journal of Hydrogen Energy*, 42 (5): 3027-3035.

Salam, M. A. and Abdullah, B. 2017. Catalysis mechanism of Pd-promoted γ-alumina in the thermal decomposition of methane to hydrogen: A density functional theory study. *Materials Chemistry and Physics*, 188: 18-23.

Salipira, K., Coville, N. J. and Scurrell, M. S. 2016. Carbon produced by the catalytic decomposition of methane on nickel: Carbon yields and carbon structure as a function of catalyst properties. *Journal of Natural Gas Science and Engineering*, 32: 501-511.

Salmones, J., Wang, J. A., Valenzuela, M. A., Sánchez, E. and Garcia, A. 2009. Pore geometry influence on the deactivation behavior of Ni-based catalysts for simultaneous production of hydrogen and nanocarbon. *Catalysis Today*, 148 (1–2): 134-139.

Saraswat, S. K. and Pant, K. K. 2011. Ni–Cu–Zn/MCM-22 catalysts for simultaneous production of hydrogen and multiwall carbon nanotubes via thermo-catalytic decomposition of methane. *International Journal of Hydrogen Energy*, 36 (21): 13352-13360.

Saraswat, S. K. and Pant, K. K. 2013. Synthesis of hydrogen and carbon nanotubes over copper promoted Ni/SiO2 catalyst by thermocatalytic decomposition of methane. *Journal of Natural Gas Science and Engineering*, 13: 52-59.

Serrano, D. P., Botas, J. A., Fierro, J. L. G., Guil-López, R., Pizarro, P. and Gómez, G. 2010. Hydrogen production by methane decomposition: Origin of the catalytic activity of carbon materials. *Fuel*, 89 (6): 1241-1248.

Serrano, D. P., Botas, J. A. and Guil-Lopez, R. 2009. H2 production from methane pyrolysis over commercial carbon catalysts: Kinetic and deactivation study. *International Journal of Hydrogen Energy*, 34 (10): 4488-4494.

Shen, Y. and Lua, A. C. 2015. Synthesis of Ni and Ni–Cu supported on carbon nanotubes for hydrogen and carbon production by catalytic decomposition of methane. *Applied Catalysis B: Environmental*, 164: 61-69.

Shin, Y.-H., Cho, J., Lee, J., Ju, H., Sohn, S., Kim, Y., Noh, H. and Hwang, I. S. 2017. Experimental studies and computational benchmark on heavy liquid metal natural circulation in a full height-scale test loop for small modular reactors. *Nuclear Engineering and Design*, 316: 26-37.

Shinkarev, V. V., Glushenkov, A. M., Kuvshinov, D. G. and Kuvshinov, G. G. 2010. Nanofibrous carbon with herringbone structure as an effective catalyst of the H2S selective oxidation. *Carbon*, 48 (7): 2004-2012.

Snoeck, J. W., Froment, G. F. and Fowles, M. 1997. Kinetic Study of the Carbon Filament Formation by Methane Cracking on a Nickel Catalyst. *Journal of Catalysis*, 169 (1): 250-262.

Su, Y., Zhao, B. and Deng, W. 2015. NO reduction by methane over iron oxides: Characteristics and mechanisms. *Fuel*, 160: 80-86.

Suelves, I., Lázaro, M. J., Moliner, R., Echegoyen, Y. and Palacios, J. M. 2006. Characterization of NiAl and NiCuAl catalysts prepared by different methods for hydrogen production by thermo catalytic decomposition of methane. *Catalysis Today*, 116 (3): 271-280.

Suelves, I., Lázaro, M. J., Moliner, R., Pinilla, J. L. and Cubero, H. 2007. Hydrogen production by methane decarbonization: Carbonaceous catalysts. *International Journal of Hydrogen Energy*, 32 (15): 3320-3326.

Suelves, I., Pinilla, J. L., Lázaro, M. J., Moliner, R. and Palacios, J. M. 2009. Effects of reaction conditions on hydrogen production and carbon nanofiber properties generated by methane decomposition in a fixed bed reactor using a NiCuAl catalyst. *Journal of Power Sources*, 192 (1): 35-42.

Suleman, F., Dincer, I. and Agelin-Chaab, M. 2016. Comparative impact assessment study of various hydrogen production methods in terms of emissions. *International Journal of Hydrogen Energy*, 41 (19): 8364-8375.

Takenaka, S., Kobayashi, S., Ogihara, H. and Otsuka, K. 2003. Ni/SiO2 catalyst effective for methane decomposition into hydrogen and carbon nanofiber. *Journal of Catalysis*, 217 (1): 79-87.

Takenaka, S., Ogihara, H., Yamanaka, I. and Otsuka, K. 2001. Decomposition of methane over supported-Ni catalysts: effects of the supports on the catalytic lifetime. *Applied Catalysis A: General*, 217 (1–2): 101-110.

Takenaka, S., Serizawa, M. and Otsuka, K. 2004. Formation of filamentous carbons over supported Fe catalysts through methane decomposition. *Journal of Catalysis*, 222 (2): 520-531.

Tanksale, A., Beltramini, J. N. and Lu, G. M. 2010. A review of catalytic hydrogen production processes from biomass. *Renewable and Sustainable Energy Reviews*, 14 (1): 166-182.

Tiernan, M., Fesenko, E., Barnes, P. A., Parkes, G. and Ronane, M. 2001. The application of CRTA and linear heating thermoanalytical techniques to the study of supported cobalt oxide methane combustion catalysts. *Thermochimica acta*, 379 (1): 163-175.

Toebes, M. L., Bitter, J. H., van Dillen, A. J. and de Jong, K. P. 2002. Impact of the structure and reactivity of nickel particles on the catalytic growth of carbon nanofibers. *Catalysis Today*, 76 (1): 33-42.

Toklu, E. 2017. Biomass energy potential and utilization in Turkey. *Renewable Energy*, 107: 235-244.

Ummadisingu, A. and Soni, M. S. 2011. Concentrating solar power – Technology, potential and policy in India. *Renewable and Sustainable Energy Reviews*, 15 (9): 5169-5175.

Vella, G., Imoberdorf, G. E., Sclafani, A., Cassano, A. E., Alfano, O. M. and Rizzuti, L. 2010. Modeling of a TiO2-coated quartz wool packed bed photocatalytic reactor. *Applied Catalysis B: Environmental*, 96 (3–4): 399-407.

Villacampa, J. I., Royo, C., Romeo, E., Montoya, J. A., Del Angel, P. and Monzón, A. 2003. Catalytic decomposition of methane over Ni-Al2O3 coprecipitated catalysts: Reaction and regeneration studies. *Applied Catalysis A: General*, 252 (2): 363-383.

Vogelaar, B. M., Eijsbouts, S., Bergwerff, J. A. and Heiszwolf, J. J. 2010. Hydroprocessing catalyst deactivation in commercial practice. *Catalysis Today*, 154 (3–4): 256-263.

Wang, G., Ling, Y., Wang, H., Xihong, L. and Li, Y. 2014. Chemically modified nanostructures for photoelectrochemical water splitting. *Journal of Photochemistry and Photobiology C: Photochemistry Reviews*, 19: 35-51.

Wang, G., Wang, H., Tang, Z., Li, W. and Bai, J. 2009. Simultaneous production of hydrogen and multi-walled carbon nanotubes by ethanol decomposition over Ni/Al2O3 catalysts. *Applied Catalysis B: Environmental*, 88 (1–2): 142-151.

Wang, H. Y. and Lua, A. C. 2014. Deactivation and kinetic studies of unsupported Ni and Ni–Co–Cu alloy catalysts used for hydrogen production by methane decomposition. *Chemical Engineering Journal*, 243: 79-91.

Wang, W., Wang, W. and Chen, S. 2016. The effects of hydrogen dilution, carbon monoxide poisoning for a Pt–Ru anode in a proton exchange membrane fuel cell. *International Journal of Hydrogen Energy*, 41 (45): 20680-20692.

Watwe, R. M., Bengaard, H. S., Rostrup-Nielsen, J. R., Dumesic, J. A. and Nørskov, J. K. 2000. Theoretical Studies of Stability and Reactivity of CHx Species on Ni(111). *Journal of Catalysis*, 189 (1): 16-30.

Wu, Y.-m., Li, S. and Li, C.-y. 2016. Influence of Li loading on the catalytic performance of Li/MgO in the oxidative dehydrogenation of propane to olefins. *Journal of Fuel Chemistry and Technology*, 44 (11): 1334-1340.

Yazici, H. 2016. Energy and exergy based evaluation of the renovated Afyon geothermal district heating system. *Energy and Buildings*, 127: 794-804.

Yoshinaga, Y., Kudo, M., Hasegawa, S. and Okuhara, T. 1997. Active sites of WO3□ZrO2 for metathesis and isomerization of 1-butene characterized by ESR. *Applied Surface Science*, 121: 339-342.

Y.Li, D.W.Chen, M.Liu and R.Z.Wang.2017.Life cycle cost and sensitivity analysis of a hydrogen system using low price electricity in China. *Itnernational Journal of hydrogen energy*, 42(2017) 1899-1911

Zapata, B., Valenzuela, M. A., Palacios, J. and Torres-Garcia, E. 2010. Effect of Ca, Ce or K oxide addition on the activity of Ni/SiO2 catalysts for the methane decomposition reaction. *International Journal of Hydrogen Energy*, 35 (21): 12091-12097.

Zavarukhin, S. G. and Kuvshinov, G. G. 2004. The kinetic model of formation of nanofibrous carbon from CH4–H2 mixture over a high-loaded nickel catalyst with consideration for the catalyst deactivation. *Applied Catalysis A: General*, 272 (1–2): 219-227.

Zhan, W., Guo, Y., Gong, X., Guo, Y., Wang, Y. and Lu, G. 2014. Current status and perspectives of rare earth catalytic materials and catalysis. *Chinese Journal of Catalysis*, 35 (8): 1238-1250.

Zhang, J., Jin, L., He, X., Liu, S. and Hu, H. 2011a. Catalytic methane decomposition over activated carbons prepared from direct coal liquefaction residue by KOH activation with addition of SiO2 or SBA-15. *International Journal of Hydrogen Energy*, 36 (15): 8978-8984.

Zhang, J., Jin, L., Li, Y. and Hu, H. 2013. Ni doped carbons for hydrogen production by catalytic methane decomposition. *International Journal of Hydrogen Energy*, 38 (10): 3937-3947.

Zhang, J., Wang, H. and Dalai, A. K. 2007. Development of stable bimetallic catalysts for carbon dioxide reforming of methane. *Journal of Catalysis*, 249 (2): 300-310.

Zhang, T. and Amiridis, M. D. 1998. Hydrogen production via the direct cracking of methane over silica-supported nickel catalysts. *Applied Catalysis A: General*, 167 (2): 161-172.

Zhang, W., Ge, Q. and Xu, H. 2011b. Influences of reaction conditions on methane decomposition over non-supported Ni catalyst. *Journal of Natural Gas Chemistry*, 20 (4): 339-344.

Zhang, X. X., Li, Z. Q., Wen, G. H., Fung, K. K., Chen, J. and Li, Y. 2001. Microstructure and growth of bamboo-shaped carbon nanotubes. *Chemical Physics Letters*, 333 (6): 509-514.

APPENDIX A: CATALYST PRECURSORS

Table A-1 Composition of each catalyst batch in grams before calcination

Catalyst	Nickel nitrate hexahydrate	Lithium hydroxide	Calcium oxide	**Total (g)**
50%Ni/CaO	19.90	0.0	4.0	**23.9**
37.5%Ni-12.5Li/CaO	14.93	2.54	4.0	**21.47**
25%Ni-25%Li/CaO	9.95	5.07	4.0	**19.02**
12.5%Ni-37.5%Li/CaO	4.98	7.61	4.0	**16.59**
50%Li/CaO	0.0	10.15	4.0	**14.15**
Total (g)	**49.76**	**25.37**	**20.0**	

Elemental composition of catalyst precursors

- **Nickel nitrate hexahydrate**

  Formula ……...$Ni(NO_3)_2.6H_2O$

  Molecular weight…….290.79g

  Elemental composition by mass: Nickel……...20.1%

  : Nitrogen….....9.6%

  : Hydrogen……...4.0%

  : Oxygen …….....66.0%

- **Lithium hydroxide monohydrate**

  Formula……$LiOH.H_2O$

  Molecular weight…….41.96g

  Elemental composition by mass: Lithium……..……..16.54%

  : Hydrogen……..7.21%

  : Oxygen…….…..76.25%

APPENDIX B: CATALYST CRYSTALLITE STRUCTURE

Table B-1 Catalyst crystallite structure

Catalyst	2 Theta	h	k	l	M	Crystal shape
50%Ni/CaO	27.4	1	1	1	4	Monoclinic
	43.4	0	1	1	4	Monoclinic, Orthorhombic
	37.3	0	1	1	4	Monoclinic, Orthorhombic
37.5%Ni-12.5%Li/CaO	18.1	1	1	0	4	Monoclinic, Orthorhombic
	25.1	1	1	1	4	Monoclinic
	34.3	1	1	1	4	Monoclinic
25.0%Ni-25.0%Li/CaO	18.1	1	1	0	4	Monoclinic, Orthorhombic
	34.3	1	1	1	4	Monoclinic
	47.3	1	1	1	4	Monoclinic
12.5%Ni-37.5%Li/CaO	18.1	1	1	0	4	Monoclinic, Orthorhombic
	20.4	1	0	1	2	Monoclinic, Orthorhombic
	32.6	1	1	1	4	Monoclinic
50%Li/CaO	18.1	1	1	0	4	Monoclinic, Orthorhombic
	20.4	1	0	1	2	Monoclinic
	32.6	1	1	1	4	Monoclinic

Table B-2 Size of catalyst crystallites calculated using Scherrer equation

Catalyst type	**50%Ni/CaO**	**37.5%Ni-12.5Li/CaO**	**25.0%Ni-25.0Li/CaO**	**12.5%Ni-37.5Li/CaO**	**50%Li/CaO**
Main Peaks in catalyst (no.)	5	7	13	11	11
2theta at Max intensity (degrees)	23.95	37.57	23.94	36.88	36.93
max intensity (cts)	861.17	928.00	7359.05	1044.79	1906.39
Half intensity (cts)	430.59	464.00	3679.53	522.40	953.20
2theta at half intensity (degrees)	22.40	36.10	22.70	35.70	35.80
B (degrees)	1.55	1.47	1.24	1.18	1.13
B (rad)	0.02706	0.02567	0.02165	0.02060	0.01973
Theta (degrees)	11.98	18.79	11.97	18.44	18.47
Cos[theta] (degrees)	0.83	1.00	0.83	0.92	0.93
Wavelength	0.154	0.154	0.154	0.154	0.154
Constant K	0.89	0.89	0.89	0.89	0.89
Crystalline size -d (nm)	**6.10**	**5.35**	**7.65**	**7.25**	**7.50**

APPENDIX C: SEM RESULTS FOR 50%Ni/CaO USING IMAGE-J SOFTWARE

Table C-1 SEM results for 50%Ni/CaO catalyst using Image-J Software.

	Area	Mean	Min	Max	r2	R	D	Normal				
												%
1	9	255	255	255	2.86	1.69	3.39	0.435		Bin	Frequ.	Frequ.
2	5	255	255	255	1.59	1.26	2.52	0.401		0.1-1.0	0	0
3	7	255	255	255	2.23	1.49	2.99	0.48		1.1-2.0	6	11.1
4	3	255	255	255	0.95	0.98	1.95	0.209		2.1-3.0	28	51.9
5	4	255	255	255	1.27	1.13	2.26	0.316		3.1-4.0	13	24.1
6	3	255	255	255	0.95	0.98	1.95	0.209		4.1-5.0	5	9.3
7	4	255	255	255	1.27	1.13	2.26	0.316		5.1-6.0	2	3.7
8	5	255	255	255	1.59	1.26	2.52	0.401		6.1-7.0	0	0
9	5	255	255	255	1.59	1.26	2.52	0.401			54	100
10	16	255	255	255	5.09	2.26	4.51	0.096				
11	9	255	255	255	2.86	1.69	3.39	0.435			54	100
12	4	255	255	255	1.27	1.13	2.26	0.316	Max	Min	Av.	St.Dev
13	3	255	255	255	0.95	0.98	1.95	0.209	5.29	1.95	3.02	0.83
14	7	255	255	255	2.23	1.49	2.99	0.48				
15	9	255	255	255	2.86	1.69	3.39	0.435				
16	5	255	255	255	1.59	1.26	2.52	0.401				
17	9	255	255	255	2.86	1.69	3.39	0.435				
18	6	255	255	255	1.91	1.38	2.76	0.458				

APPENDIX D: SEM RESULTS FOR 37.5%Ni-12.5%Li/CaO USING IMAGE-J SOFTWARE

Table D-1 SEM Raw results for 37.5%Ni-12.5%Li/CaO catalyst using Image-J Software.

	Area	Mean	Min	Max	r2	R	D	Normal		BIN	Frequ.	% Frequ.
1	5	255	255	255	1.59	1.26	2.52	0.775		0.1-1.0	0	0
2	5	255	255	255	1.59	1.26	2.52	0.775		1.1-2.0	20	21.1
3	3	255	255	255	0.95	0.98	1.95	0.308		2.1-3.0	57	60
4	3	255	255	255	0.95	0.98	1.95	0.308		3.1-4.0	18	18.9
5	6	255	255	255	1.91	1.38	2.76	0.775		4.1-5.0	0	0
6	3	255	255	255	0.95	0.98	1.95	0.308			95	100
7	5	255	255	255	1.59	1.26	2.52	0.775				
8	5	255	255	255	1.59	1.26	2.52	0.775				
9	3	255	255	255	0.95	0.98	1.95	0.308				
10	3	255	255	255	0.95	0.98	1.95	0.308				
11	5	255	255	255	1.59	1.26	2.52	0.775				
12	3	255	255	255	0.95	0.98	1.95	0.308				
13	8	255	255	255	2.55	1.6	3.19	0.436	Max	Min	Av.	St.Dev.
14	5	255	255	255	1.59	1.26	2.52	0.775	3.91	1.95	2.64	0.5
15	5	255	255	255	1.59	1.26	2.52	0.775				
16	3	255	255	255	0.95	0.98	1.95	0.308				
17	7	255	255	255	2.23	1.49	2.99	0.625				
18	3	255	255	255	0.95	0.98	1.95	0.308				

APPENDIX E: SEM RESULTS FOR 25.0%Ni-25.0%Li/CaO USING IMAGE-J SOFTWARE

Table E-1 SEM results for 25.0%Ni-25.0%Li/CaO catalyst using Image-J Software.

	Area	Mean	Min	Max	r2	r	d	Normal		Bin	Frequ.	% Frequ.
1	25	255	255	255	7.96	2.82	5.64	0.38		2.01-3.00	0	0
2	8	255	255	255	2.55	1.6	3.19	0.04		3.01-4.00	6	9.8
3	32	255	255	255	10.2	3.19	6.38	0.26		4.01-5.00	11	18
4	25	255	255	255	7.96	2.82	5.64	0.38		5.01-6.00	30	49.2
5	25	255	255	255	7.96	2.82	5.64	0.38		6.01-7.00	9	14.8
6	25	255	255	255	7.96	2.82	5.64	0.38		7.01-8.00	5	8.2
7	25	255	255	255	7.96	2.82	5.64	0.38		8.01-9.00	0	0
8	14	255	255	255	4.46	2.11	4.22	0.19			61	100
9	25	255	255	255	7.96	2.82	5.64	0.38				
10	25	255	255	255	7.96	2.82	5.64	0.38	Max	Min	Av.	St.Dev
11	16	255	255	255	5.09	2.26	4.51	0.25	7.98	3.19	5.48	1.05
12	25	255	255	255	7.96	2.82	5.64	0.38				
13	25	255	255	255	7.96	2.82	5.64	0.38				
14	25	255	255	255	7.96	2.82	5.64	0.38				
15	25	255	255	255	7.96	2.82	5.64	0.38				
16	25	255	255	255	7.96	2.82	5.64	0.38				
17	32	255	255	255	10.2	3.19	6.38	0.26				
18	32	255	255	255	10.2	3.19	6.38	0.26				
19	25	255	255	255	7.96	2.82	5.64	0.38				
20	25	255	255	255	7.96	2.82	5.64	0.38				
21	25	255	255	255	7.96	2.82	5.64	0.38				
22	18	255	255	255	5.73	2.39	4.79	0.31				
23	25	255	255	255	7.96	2.82	5.64	0.38				
24	27	255	255	255	8.59	2.93	5.86	0.36				
25	25	255	255	255	7.96	2.82	5.64	0.38				

APPENDIX F: SEM RESULTS FOR 12.5%Ni-37.5%Li/CaO USING IMAGE-J SOFTWARE

Table F-1 SEM results for 12.5%Ni-37.5%Li/CaO catalyst using Image-J Software.

	Area	Mean	Min	Max	r2	r	d	Normal		BIN	Frequ.	%Frequ.
1	10	255	255	255	3.18	1.78	3.57	0.438		0.01-1.00	0	0
2	8	255	255	255	2.55	1.6	3.19	0.407		1.01-2.00	14	8
3	13	255	255	255	4.14	2.03	4.07	0.37		2.01-3.00	35	20.1
4	3	255	255	255	0.95	0.98	1.95	0.096		3.01-4.00	80	46
5	25	255	255	255	7.96	2.82	5.64	0.03		4.01-5.00	30	17.2
6	3	255	255	255	0.95	0.98	1.95	0.096		5.01-6.00	13	7.5
7	30	255	255	255	9.55	3.09	6.18	0.007		6.01-7.00	2	1.1
8	16	255	255	255	5.09	2.26	4.51	0.247		7.01-8.00	0	0
9	21	255	255	255	6.68	2.59	5.17	0.088			174	100
10	9	255	255	255	2.86	1.69	3.39	0.432				
11	22	255	255	255	7	2.65	5.29	0.069	Max	Min	Av	St.Dev.
12	3	255	255	255	0.95	0.98	1.95	0.096	6.1	1.95	3.54	0.91
13	3	255	255	255	0.95	0.98	1.95	0.096				
14	12	255	255	255	3.82	1.95	3.91	0.404				
15	8	255	255	255	2.55	1.6	3.19	0.407				
16	10	255	255	255	3.18	1.78	3.57	0.438				
17	14	255	255	255	4.46	2.11	4.22	0.331				
18	3	255	255	255	0.95	0.98	1.95	0.096				
19	3	255	255	255	0.95	0.98	1.95	0.096				
20	11	255	255	255	3.5	1.87	3.74	0.428				
21	16	255	255	255	5.09	2.26	4.51	0.247				
22	15	255	255	255	4.77	2.19	4.37	0.289				
23	11	255	255	255	3.5	1.87	3.74	0.428				
24	9	255	255	255	2.86	1.69	3.39	0.432				
25	11	255	255	255	3.5	1.87	3.74	0.428				
26	8	255	255	255	2.55	1.6	3.19	0.407				
27	11	255	255	255	3.5	1.87	3.74	0.428				

APPENDIX G: SEM RESULTS FOR 50%Li/CaO USING IMAGE-J SOFTWARE

Table G-1 SEM results for 50%Li/CaO catalyst using Image-J Software.

	Area	Mean	Min	Max	r2	r	d	Normal		BIN	Frequ.	%Frequ.
1	10	255	255	255	3.18	1.78	3.57	0.394		0.01-1.00	0	0
2	17	255	255	255	5.41	2.33	4.65	0.261		1.01-2.00	3	2.4
3	11	255	255	255	3.5	1.87	3.74	0.399		2.01-3.00	29	23.4
4	20	255	255	255	6.37	2.52	5.05	0.168		3.01-4.00	51	41.1
5	21	255	255	255	6.68	2.59	5.17	0.141		4.01-5.00	28	22.6
6	14	255	255	255	4.46	2.11	4.22	0.353		5.01-6.00	9	7.3
7	18	255	255	255	5.73	2.39	4.79	0.228		6.01-7.00	3	2.4
8	10	255	255	255	3.18	1.78	3.57	0.394		7.01-8.00	1	0.8
9	10	255	255	255	3.18	1.78	3.57	0.394		8.01-9.00	0	0
10	9	255	255	255	2.86	1.69	3.39	0.376			124	100
11	3	255	255	255	0.95	0.98	1.95	0.082				
12	24	255	255	255	7.64	2.76	5.53	0.079				
13	8	255	255	255	2.55	1.6	3.19	0.345	Max	Min	Av.	St.Dev.
14	3	255	255	255	0.95	0.98	1.95	0.082	7.74	1.95	3.73	1
15	3	255	255	255	0.95	0.98	1.95	0.082				
16	10	255	255	255	3.18	1.78	3.57	0.394				
17	15	255	255	255	4.77	2.19	4.37	0.325				
18	9	255	255	255	2.86	1.69	3.39	0.376				

APPENDIX H: SUMMARY OF METHANE DECOMPOSITION RESULTS

Table H-1 CH_4 conversion (%) at GHSV 2 and different temperatures

50%Ni/CaO	47.0	50.5	53.1	60.2	54.5
37.5%Ni-12.5%Li/CaO	51.2	54.6	59.5	65.7	63.6
37.5%Ni-12.5%Li/CaO	49.8	51.8	57.4	64.3	60.1
12.5%Ni-37.5%Li/CaO	49.1	51.2	56.7	63.6	58.0
50%Li/CaO	50.5	52.5	56.0	64.2	57.4
Temperature (℃)	**500**	**550**	**600**	**650**	**700**

Table H- 2 H_2 Yield (%) at GHSV 2 and different temperatures

50%Ni/CaO	32.7	34.8	37.5	35.7	29.7
37.5%Ni-12.5%Li/CaO	31.0	35.7	35.1	38.3	25.2
25.0%Ni-25.0%Li/CaO	34.9	36.5	35.8	36.4	24.9
12.5%Ni-37.5%Li/CaO	34.3	37.3	36.3	34.5	26.7
50%Li/CaO	32.8	33.3	35.2	36.1	24.7
Temperature (℃)	**500**	**550**	**600**	**650**	**700**

Table H- 3 CH_4 conversion (%) at 650℃ , GHSV 2 and different activation time

50%Ni/CaO	42.2	53.2	56.0	59.5	60.2
37.5%Ni-12.5%Li/CaO	44.3	56.4	59.5	64.9	65.7
25.0%Ni-25.0%Li/CaO	42.9	54.6	57.4	64.3	64.3
12.5%Ni-37.5%Li/CaO	40.1	53.9	56.7	62.9	63.6
50%Li/CaO	39.4	52.5	55.3	63.6	62.9
Activation time (mins)	**18**	**36**	**54**	**72**	**90**

Table H- 4 H_2 yield (%) at 650℃ , GHSV 2 and different activation time

50%Ni/CaO	45.0	39.1	37.2	37.3	35.7
37.5%Ni-12.5%Li/CaO	45.5	40.7	38.8	39.3	38.3
25.0%Ni-25.0%Li/CaO	45.7	38.6	36.8	38.2	36.4
12.5%Ni-37.5%Li/CaO	47.5	40.2	38.2	36.9	34.8
50%Li/CaO	50.4	38.4	38.9	36.7	36.9
Activation time (mins)	**18**	**36**	**54**	**72**	**90**

Table H-5 CH_4 conversion (%) at 650℃ and different GHSVs

50%Ni/CaO	60.2	56.7	53.2
37.5%Ni-12.5%Li/CaO	65.7	62.2	60.2
25.0%Ni-25.0%Li/CaO	64.3	61.5	58.7
12.5 %Ni-37.5%Li/CaO	63.6	60.8	57.0
50%Li/CaO	62.9	62.2	57.4
GHSV ($Lg^{-1}cath^{-1}$)	**2**	**3**	**4**

Table H-6 H_2 yield (%) at 650℃ and different GHSVs

50%Ni/CaO	35.7	34.7	32.1
37.5%Ni-12.5%Li/CaO	38.3	35.1	33.2
25.0%Ni-25.0%Li/CaO	36.4	30.3	29.5
12.5%Ni-37.5%Li/CaO	34.8	30.2	28.7
50%Li/CaO	36.9	30.2	27.3
GHSV ($Lg^{-1}cath^{-1}$)	**2**	**3**	**4**

TITLES OF SUBMITTED MANUSCRIPTS

1. Decomposition of methane to carbon and hydrogen; a catalytic perspective.

2. A novel catalyst system for methane decomposition

3. Hydrogen production via methane decomposition over Ni-Li/CaO catalyst: Effect of Li content and reaction parameters on catalyst performance.